Rainer Rudolf Kulter, BSc

Review of efficient and economic dust separation for medium scale biomass combustion plants

MASTER'S THESIS

to achieve the university degree of

Diplom-Ingenieur

Master's degree programme: Verfahrenstechnik

submitted to

Graz University of Technology

Supervisor

Ass. Prof. Dr. techn. Dipl.-Ing. Stefan Radl

Institute for Process and Particle Engineering

Graz University of Technology

Supported by

Dipl.-Ing. Georg Payer

KBE Kärntner Bioenergie Engineering

and Consulting GmbH

Graz, August 2015

AFFIDAVIT

I declare that I have authored this thesis independently, that I have not used other than the declared sources/resources, and that I have explicitly indicated all material which has been quoted either literally or by content from the sources used. The text document uploaded to TUGRAZonline is identical to the present master's thesis.

20.08.2015
_____

Date

_____

Signature

Abstract

The continuous growth of industry in general causes increasing emissions, which are answered by environmental policies with lower and lower emission limits. Biomass combustion is a renewable energy with a high potential to achieve environmental targets and support industrial growth. At the same time, however, the huge variety of combustion, boiler and fuel types poses big challenges in the field of air pollution control. This thesis deals with dust separation of medium scale biomass combustion and describes the complexity of dust separation including technical and economic aspects. Especially the separation of dust with a small particle size is difficult and only possible with an electrostatic precipitator or a filter. The dust separator combination of a cyclone and an electrostatic precipitator, which is preferred today has proved itself and is one of the most promising and efficient methods for dust separation. Special attention should be paid to a detailed and specific separator design. Emission limits are easy to achieve in the case of a well-defined process and the use of a plant customized separator.

Acknowledgement

Table of contents

List of Figures

List of Tables

1 Introduction

Growth and continuous development in the industry in general are setting new standards for air pollution control. Especially the field of dust removal has been getting more and more attention in recent years. The dedusting technology was originally developed out of economic considerations. Valuable raw materials often occur as dust or fine particles in a process. Dedusting technologies are needed to extract these materials from their carrier phase. The development of dedusting technology has been driven and shaped by amplified environmental measures of the legislature and the demand for clean air[1].

The design of dedusting systems is complex. The most important condition is the knowledge of all processes with their applications, advantages, disadvantages and their chemical and physical basics. Dust is described as solid particles in a carrier gas. Application dependent, a low to high water vapour content in the gas can exist. The multiphase compounds possess certain properties and behaviours that influence the selection of process and design. A successful design can only be developed if all parameters of influence are taken into consideration. Thus, the process can be customized to the properties of certain multiphase systems and applications.

This thesis should review the state of the art concerning dust separation, and should serve as groundwork for the development of a novel dust separator for biomass combustion applications.

1.1 Limit values for dust emissions

Limit values are important for an efficient design process of dust separators. They describe the upper boarder of dust concentration at the emission point (i.e., the outlet of the stack). Limits must be achieved by the dust separator from the plant start-up to the next defined revision. Table 1 shows limit values for dust emissions in the main export countries of Kohlbach Biomass combustion plants. These countries are Austria, Germany, Switzerland and Italy. Dust emission limits vary greatly from country to country, and even may depend on region to biomass plant is installed. In Italy, for example, the dust emission limits are even established by the regional governments.

Table 1: Limit values for dust emissions (basis: 11% O_2 in the off gas)

	<500 [kW]	500-1000 [kW]	1000-2000 [kW]
Austria[2,3]	150 [mg/Nm³]		50 [mg/Nm³]
Germany[4,5]	25 [mg/Nm³]		100 [mg/Nm³]
Switzerland[6]	62.5 [mg/Nm³]	25 [mg/Nm³]	20 [mg/Nm³]
Italy* [7]	30 [mg/Nm³]		10 [mg/Nm³]

*regional variations are possible

Typically, a higher available heat output is associated with a lower dust concentration limit, with the exception of Germany. Plants in Germany with an output of 1000-2000 [kW] are allowed to emit 100 [mg/Nm³] of dust. An identical plant in Italy may only emit 10 [mg/Nm³]. The emitted dust concentration decreases with an increasing plant size. This is because bigger plants have a better regulation of combustion process parameters like flue gas recirculation, velocity and temperature. Future developments are generally driven by legislation, environmental and economic aspects. The ecological sensibility of the general public affects the legislator. Developments can be accelerated by government aid and tighter legislation.

1.2 Goals

This thesis is concerned with efficient and economic dust separation for medium scale biomass combustion. Medium scale biomass combustion plants operate as a stoker-fired furnace, or an underfeed combustion. The output range of these combustions is between 400 and 1500 [kW]. Specifically, the goals of this thesis are:

- Goal 1: State of the art specification of dust separation for biomass combustion.

  In the field of biomass combustion, dry and wet dust separation processes are used. Dry separation processes rely on gravity, centrifugal or electrostatic forces. Filter systems are also typical dry dust separation processes. Wet processes use water droplets for separation. In this thesis, only dry methods are described. At the beginning of a new development, it is important to know all potential processes and their behaviour. One goal of this thesis is to show which separation methods are used and how they work[1].

- Goal 2: Efficiency analyses of dedusting systems and components.

  It is important to know, what are the components that can be optimized as well as the most expensive components of dedusting systems. It is easier to analyze dust separators or dust collecting systems with information about specific costs and the potential of component optimization.

- Goal 3: Development of a customized dust separation process for medium scale biomass combustion plants.

  It is planned to develop a new dust separation process. All information from Goal 1 and Goal 2 form the basis for this development. The new process should be a combination of existing knowledge and new approaches.

1.3 Dust from biomass combustion

Biomass energy can be created out of wood, energy crops, agricultural, municipal or industrial waste. A detailed description is shown in Figure 1.
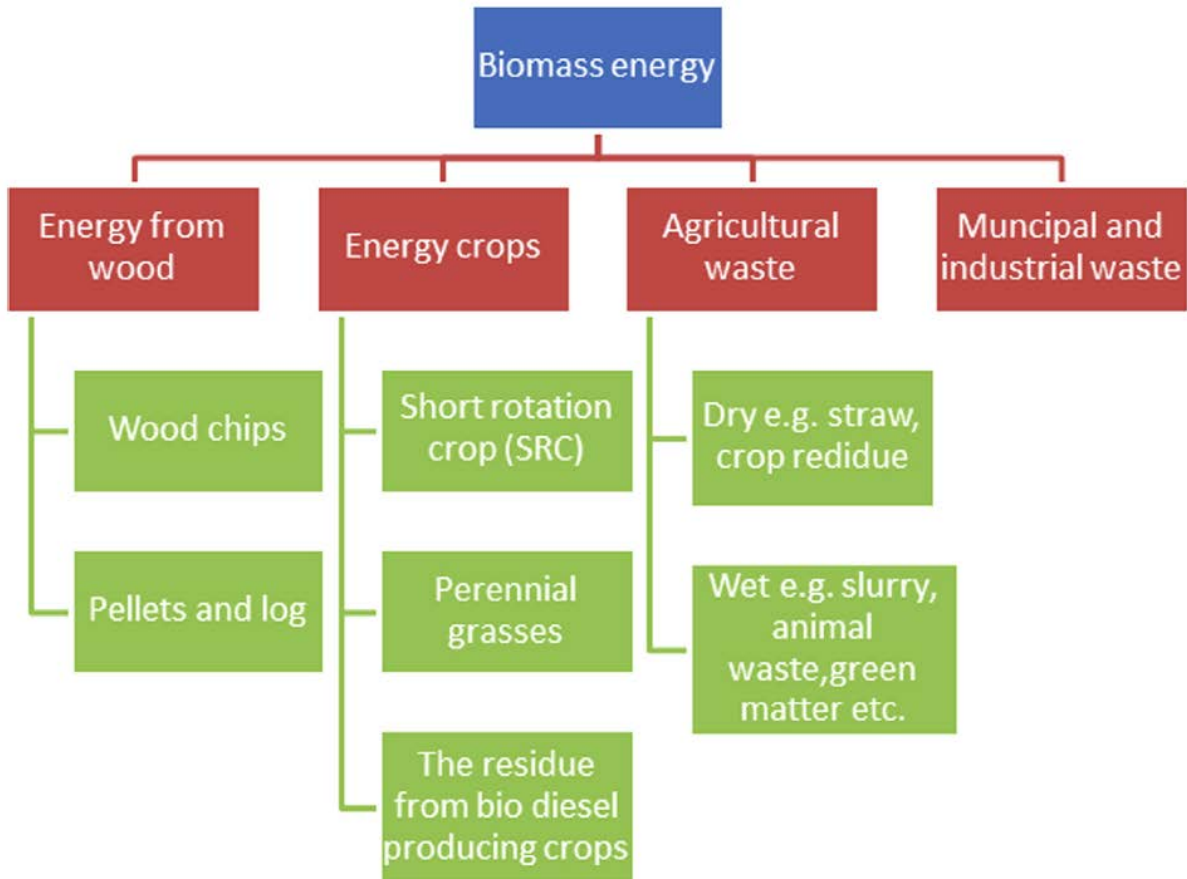
Figure 1: Flow chart for various sources of bioenergy[8]

Flue gas from biomass is a phase mixture between solid particles, water vapour and a carrier gas phase. The carrier gas consists of oxygen, nitrogen, carbon monoxide, carbon dioxide, sulphur oxide and many other components. Typical flue gas compositions are shown in Table 2.

Singh and Shukla[8] list some major sources and associated emissions of biomass in their work. These sources are shown in Table 3.

Table 2: Flue gas composition of a typical biomass combustion plant[9]

Molecule	[Vol.%$_w$]	[Mass.%$_w$]	[Vol.%$_d$]	[Mass.%$_w$]
H_2O	10-22	6-14	-	-
CO_2	9-12	15-17	12.52	18.22
CO	0.012-0.014	0.012-0.014	0.02	0.017
SO_2	0.002	0.004-0.005	0.002	0.005
NO_2	0.014-0.016	0.023-0.025	0.019	0.028
N_2	62-71	63-69	79.43	73.31
O_2	6.2-7.2	7.2-7.9	8	8.4
Cl_2	0.007-0.008	0.017-0.019	0.009	0.02

Wood chips from spruce, fuel water content 10-50 [Mass.%]

Table 3: Some major sources and associated emissions of biomass[8]

type of biomass	source	humidity	density	combustion efficiency	geometry	Emissions	benefits
wood pellets	compacted sawdust by product of sawmilling	low (< 10 [%])		high	regular	NOx, SOx, particulate matter and volatile organic compounds	compact storage
wood chips	wood, recycled wood, sawmill residue, stem wood, logging residue, etc	medium (< 50 [%])	low	medium	irregular		can be compacted into pellets
straw	dry stalks of cereal plants e.g. oats, rice, eye, wheat etc.	low (0-30 [%])	low	high	irregular	polycyclic aromatic hydrocarbons, CO, NOx, SOx, particulate matter and volatile organic compounds	

Brunner et al.[10] described in his work that dust particles in flue gas from biomass combustion consist of fly-ash particles and aerosols. These particles are contaminated with harmful heavy metals like zinc, cadmium and lead. Fly-ash particles are entrained from the fuel bed by the combustion gases and have a particle size > 1 [µm]. Aerosols have a particle size < 1 [µm]. A typical particle size distribution of biomass fly-ashes was provided by Brunner et al.[10]. They used a low-pressure Berner-type cascade impactor to measure the particle size distribution. A pre-separator (i.e., a cyclone) was used to reduce the particle load for the subsequent overflow of the impactor. Machan[11], Christensen[12] and Lind et al.[13] published results of their particle size measurements. The average particle size is larger than 5 [µm], and depends on the combustion technology and the process-control system. Aerosols are produced in the heat exchanger section by condensation of volatile ash-forming compounds. These aerosols also consist of volatile heavy metals that a released during the combustion process. It is now widely accepted that the fuel has the biggest influence on the particle size.
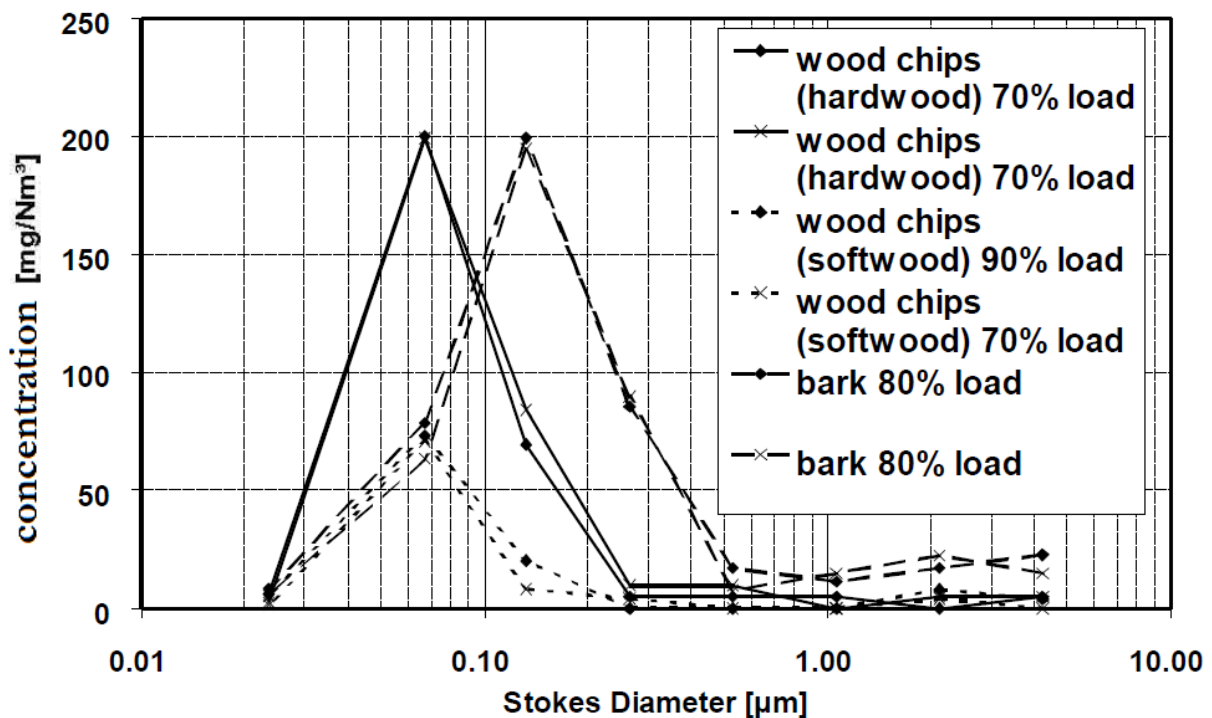
Figure 2: Particle size distribution in wood chip and bark combustion[11]
(13 Vol.%O₂, 16 [µm] pre-separator cyclone cut size)
wood chips: underfeed stoker combustion, 1.4 [MW_th] nominal boiler capacity
bark: moving grate incinerator combustion, 3.0 [MW_th] nominal boiler capacity
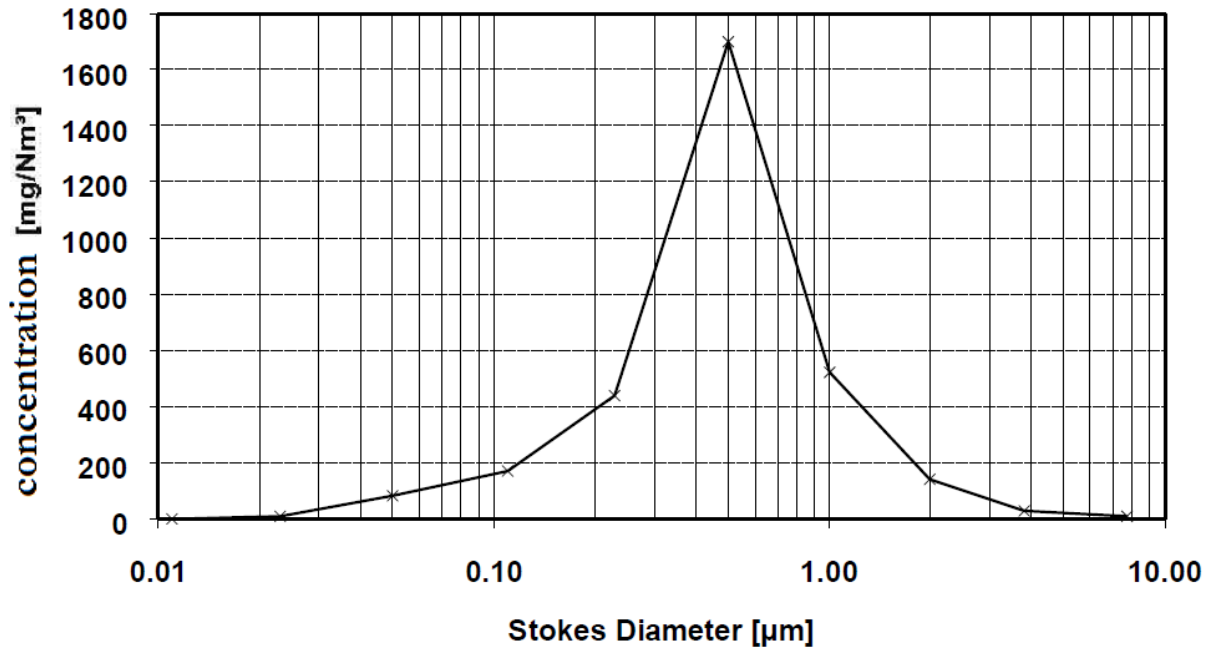
Figure 3: Particle size distribution in straw combustion[12]
(6-8 Vol.%O_2, 16 [µm] pre-separator cyclone cut size)
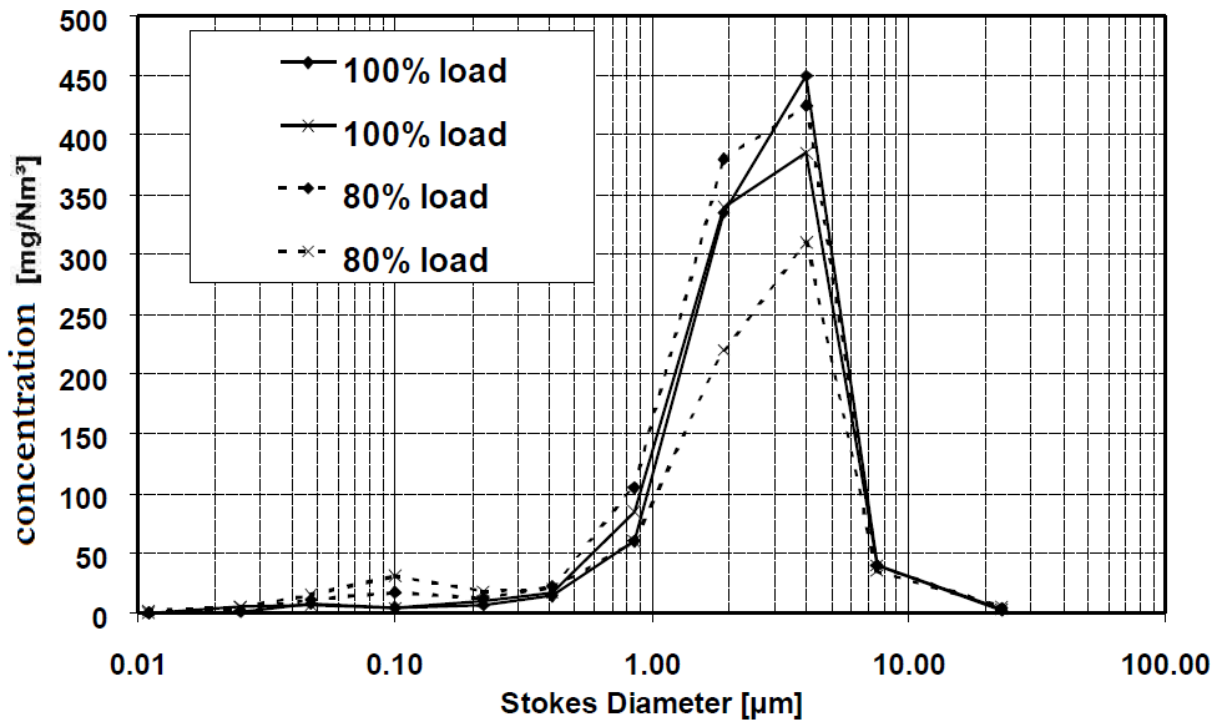
Figure 4: Particle size distribution in wood chips combustion[13]
(3.2 Vol.%O_2, 5 [µm] pre-separator cyclone cut size)

Figure 2, Figure 3 and Figure 4 show typical particle size distributions for grate and fluidized-bed-combustion processes. The significant difference between the diagrams is the peak position. This difference is based on the combustion and the fuel type. Beside this finding, a comparison of Table 1 with the dust limit values shows that dust separators for biomass should separate all dust particles with a diameter larger than 0.03 [µm] to achieve dust emission values below 50 [mg/Nm³] for all fuel types.

Nussbaumer[14] described in his work three dust particle types: salts, soot and condensable organic compounds. These types depend - among other parameters - on the excess air level. Soot is formed at low excess air ratio, specifically in the flame as a by-product of the combustion process. In these situations the flue gas has a high carbon to hydrogen ratio. In contrast, at optimum excess air conditions a complete combustion is can be achieved. In such a situation dust consists of salt particles, and exists with low concentrations and particle sizes. A high overall excess air ratio produces high combustion temperatures, tars during pyrolysis, and condensable organic compounds in the flue gas with a low carbon to hydrogen ratio.

1.4 State of the art in the area of dedusting

Brunner[10] et al. described the multicyclone with a cut diameter of 5 [μm] as the most common particle separation technology for biomass combustion plants with a nominal boiler capacity of 0.5 to 5 [MW_{th}]. Since 1998 a dust limit of 50 [mg/Nm³] (at 13 Vol.% O_2) for biomass combustion plants with a boiler capacity larger than 2 [MW_{th}] exist. Electrostatic and fibrous filters are necessary to achieve these limits, but the costs of these separators are more than twice as high as those of cyclones. Future regulations require dust limits lower than 20 [mg/Nm³] (at 13 Vol.% O_2) and make dust separation more cost-intensive. As a rough guide, cyclones achieve a dust concentration of 100 [mg/Nm³] (at 13 Vol.% O_2) in the clean gas for a typical fuel. Nussbaumer[14] explains that automated biomass combustion plants with a boiler capacity > 200 [kW] exhibit particle emissions of approximately 100 [mg/Nm³] (at 13 Vol.% O_2), depending on the combustion technology and fuel type. The dust of these plants consists of more than 95 [%] of particles with a diameter lower than 10 [μm]. At these conditions electrostatic precipitators or filters are necessary to effectively remove particles. Cyclones achieved a separation to a limit of 150 [mg/Nm³] (at 13 Vol% O_2) and a particle diameter of 20 [μm]. They are used as pre-separators before an electrostatic precipitator or a filter. Electrostatic precipitators have a high separation efficiency, and they are able to separate particles with a diameter of 0.2-0.8 [μm]. These separator are designed for a clean gas concentration of 50 [mg/Nm³] (at 13 Vol% O_2) similar to filters. Both filters and electrostatic separators are often used after a cyclone, because they can be designed smaller and have a higher lifetime due to the lower dust loading. Typical flue gas temperatures are 120 to 180°C at the inlet, depending on the dew point of water and acids.

2 Principles of dedusting

The following subsections of chapter 2 are mainly based on the work of Batel[15] and Robel et al.[16]. These authors published comprehensive knowledge in the field of dust separation. Both works are not very new, but the groundwork is precisely described. More recent publications are cited separately in each sub-chapter.

Dedusting is defined as the removal of solid particles from aero dispersions. The dust particle diameters range between 10^{-3} and 10^{3} µm. The dedusting technology deals with all technical systems, methods and applications for dedusting. Dedusting equipment is called dust separator, or specifically by its physical basis like centrifugal dust separator, bag filter or electrostatic precipitator.

The basic principle of dedusting is to use forces to separate the solid particles from the carrier gas. These forces produce a particle relative motion to the carrier gas, or lead to particles sticking to a surface (e.g., in the case of filtration). Particles accumulate and a separation takes place. A dust separator features two key regions, the separation region and the discharge region. With this description a definition of the discharge chamber, separation chamber and a separation surface is possible. At the separation surface the particles are (theoretically) completely separated from the gas flow.

Gravity, centrifugal and electrostatic forces cause particle-fluid relative motion. Dust separators with these principles are called gravity, centrifugal or electrostatic dust separators. Another method to separate particles from a gas flow is filtration. The gas flows through a porous media with a defined pore diameter. Filtering separators work in three stages: In the first stage particles move due to inertia caused by the redirection of flow, diffusion and electrostatic forces towards the surface of the porous material. Particles stick to the porous media, or to other particles in the second stage. At the third stage particles are removed from the porous media and leave the separator which needs to be done in a discontinuous period.

Table 4: Overview of dust separators[15]**.**
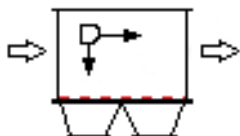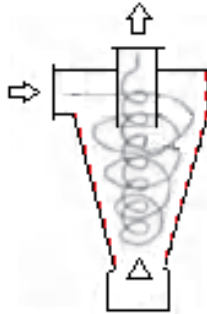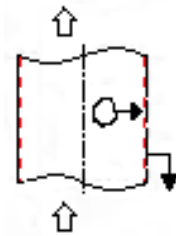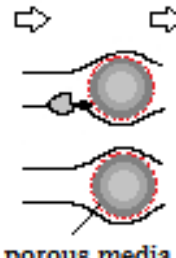
	gravity dust separator	centrifugal dust separator	electrostatic dust separator	filtration dust separator
scheme separation surface -----				porous media
fluid-particle relative motion caused by	gravitational forces	centrifugal forces	electrostatic forces	inertial effects, thermodynamic (diffusion) and electrostatic forces
separation principle	sedimentation	sedimentation	sedimentation	screening and adhesion effects, inertial effects, diffusion
discharge principle	agglomeration	agglomeration	adhesion	adhesion

Table 4 provides an overview of displacement forces, separation principles and cleaning methods of dust separators.

2.1 Separation efficiency

A calculation of the separation efficiency by dust separators is only possible in special cases, so measuring techniques are necessary to verify predictions.

2.1.1 Total separation efficiency

The total separation efficiency indicates what percentage of dust mass is separated.

$$\eta_t = \frac{M_{raw} - M_{clean}}{M_{raw}} = \frac{M_s}{M_{raw}} \tag{2-1}$$

or

$$\eta_t = \frac{c_{raw} - c_{clean}}{c_{raw}} = 1 - \frac{c_{clean}}{c_{raw}} \tag{2-2}$$

Formula (2-2)is based on the following assumptions:

- $V_{raw} = V_{clean} \left[\frac{Nm^3}{s}\right]$

- The dust load is related to the gas volume at standard temperature and pressure (STP,$[Nm^3]$).

2.1.2 Fractional separation efficiency

The fractional separation efficiency provides detailed information about the efficiency of separation for each particle diameters. This parameter indicates the particle size in proportion to the quantity.

$$\eta_f(d_p) = \frac{\frac{\Delta R_{raw}}{\Delta d_p} c_{raw} - \frac{\Delta R_{clean}}{\Delta d_p} c_{clean}}{\frac{\Delta R_{raw}}{\Delta d} c_{raw}} \tag{2-3}$$

or

$$\eta_f(d_p) = \frac{\frac{\Delta R_s}{\Delta d_p}(c_{raw} - c_{clean})}{\frac{\Delta R_{raw}}{\Delta d_p} c_{raw}} = \frac{\frac{\Delta R_s}{\Delta d_p}}{\frac{\Delta R_{raw}}{\Delta d_p}} \eta_t \tag{2-4}$$
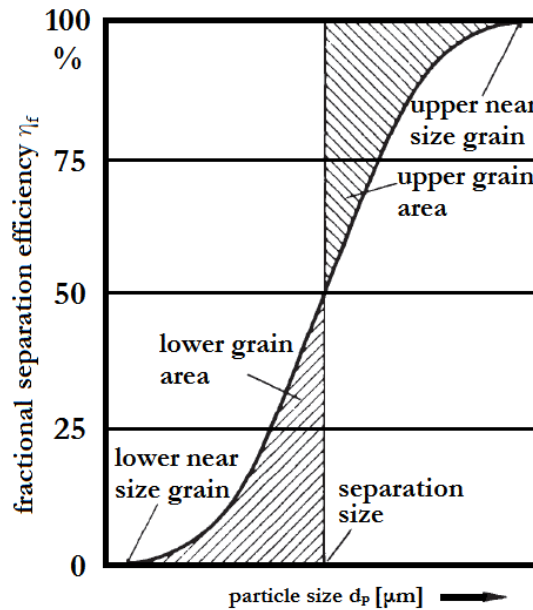
Figure 5: Fractional separation efficiency

In summary the fractional separation efficiency is provided by formula (2-5).

$$\eta_f(d_p) = 1 - (1 - \eta_t)\frac{\Delta R_{clean}}{\Delta R_{raw}} = \frac{\Delta R_s}{\Delta R_{raw}}\eta_t \tag{2-5}$$

2.2 Flow resistance and terminal settling velocity of dust particles

In this chapter the flow resistance and the terminal settling velocity of dust particles is described. Chapter 2.2.1 and 2.2.2 deal with the behaviour of a single particle. Chapter 2.2.3 describes the behaviour of a particle ensemble.

2.2.1 Flow resistance of a single particle

Fluid-particle relative motion is an essential mechanism for dedusting technology. The resistance of a body in a flow depends on the flow resistance, the pressure drop and the flow friction of the medium. The coefficient of flow resistance is a function of the Reynolds number, and can be calculated with the following equations ((2-6)-(2-8)) [17].

$$c_w = \frac{24}{Re_P} \text{ at } Re_P < 0.5 \tag{2-6}$$

$$c_w = \frac{24}{Re_P}\left(1 + 0.15Re_P{}^{0.687}\right) \text{ at } 0.5 < Re_P < 1000 \tag{2-7}$$

$$c_w \approx 0.44 \text{ at } 1000 < Re_P < Re_{crit} \tag{2-8}$$

The flow resistance force is calculated with formula (2-9)[17].

$$F_R = c_w \frac{\pi}{4}d_p{}^2\frac{\rho_g}{2}v_g{}^2 \tag{2-9}$$

Good approximation functions for c_w were developed by Oseen[18], Schiller and Naumann[19], Langmuir and Blodgett[20] and Schytil[21].

In the case of small particles, the continuum hypothesis is no longer valid. Specifically, relative motion between the solid and the gaseous exist, and the previous equations are no longer valid. This happens, if the particle size reached the free path length of the gas molecules. The free path length of air molecules at standard conditions is approximately $0.06 [\mu m]$. For small $\frac{l_p}{d_p}$ ratios a correction factor(2-10) is defined by Cunningham[22].

$$1 - 2A_{Cu}\frac{l_p}{d_p} \approx \frac{1}{1 + 2A_{Cu}\frac{l_p}{d_p}} \qquad \text{(2-10)}$$

The resistance force changes due to the Cunningham correction to formula (2-11).

$$F_{RCu} = \frac{3\pi \cdot \mu \cdot d_p \cdot v_g}{1 + \frac{2 \cdot A_{Cu} \cdot l_p}{d_p}} \qquad \text{(2-11)}$$

The factor A_{Cu} lies between 0.8 and 0.9 for gas at standard conditions. It also follows that the resistance of dust particles with regard of friction is lower than the resistance without it. For larger $\frac{l_p}{d_p}$ ratios, more correlations can be found in the work of Davies[23,24].

2.2.2 Terminal settling velocity of a single particle

The displacement velocity of particles in aero dispersions depends on displacement forces like gravity, centrifugal forces or the buoyancy force. Figure 6 shows the force balance of a single dust particle. The following formulas apply to the gravity field without starting procedures.

$$F_G = F_R + F_B \tag{2-12}$$

$$F_G = m_p \cdot a_p = \frac{\pi \cdot d_p{}^3}{6} \varrho_s \cdot g \tag{2-13}$$

$$F_B = \frac{\pi \cdot d_p{}^3}{6} \rho_g \cdot g \tag{2-14}$$
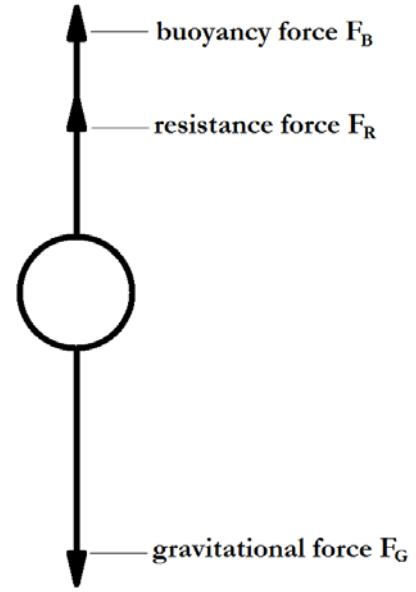
Figure 6: Force balance of a single dust particle

Formula (2-15)defined the settling velocity and is build from the Stokes' law of resistance.

$$w_p = \frac{1}{18 \cdot \mu} g \cdot (\rho_s - \rho_g) \cdot d_p^2 \tag{2-15}$$

With the general resistance law from formula (2-9), formula (2-15) changes to (2-16).

$$w_p = \left(\frac{4}{18 \cdot 3 \cdot c_w \cdot \varrho_g} g \cdot (\varrho_s - \varrho_g) \cdot d_p \right)^{1/2} \tag{2-16}$$

Formula (2-17) is formed by the consideration of the wall friction (2-11).

$$w_p = \frac{1}{18 \cdot \mu} g \cdot (\varrho_s - \varrho_g) \cdot d_p^2 \cdot \left(1 + \frac{2 A_{Cu} \cdot l_{gm}}{d_p} \right) \tag{2-17}$$

The constant A_{Cu} is approximately 0.85 as discussed above. In case centrifugal forces are used for separation, the parameter g turns into the product Z·g for equation (2-15) to (2-17). The Parameter Z multiplies the gravity and describes the performance of the centrifugal field. Formula (2-15) and (2-16) can be used with the resistance coefficient from Oseen[18](2-18). This parameter is also shown in Figure 7.

$$c_w = \frac{24}{Re} \left(1 + \frac{1}{16} Re \right) \tag{2-18}$$
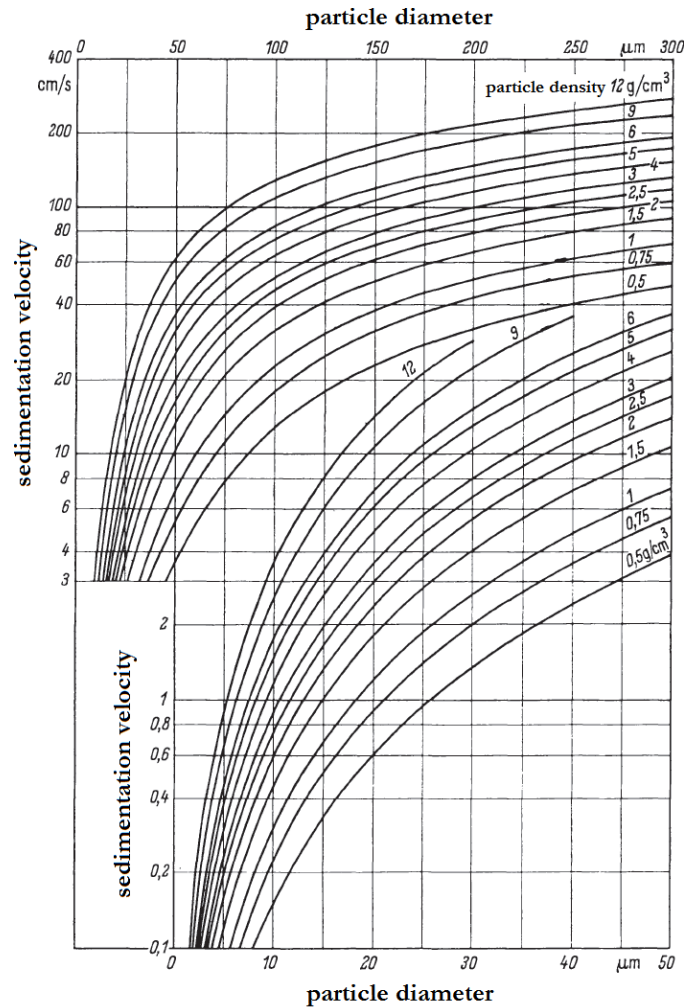
Figure 7: Sedimentation velocity of spherical particles in air (from Equation (2-15) and (2-16))[15]

2.2.3 Sedimentation velocity and resistance of a particle ensemble

Equations of flow resistance for single particles are only considered suitable for a particle ensemble at particle concentrations so low that the particles do not affected each other. The upper bound of concentration is approximately 0.002 (volume concentration, < 2000 [cm³/Nm³]). Dust concentrations above this concentration are rarely found in the field of biomass combustions. Typical concentrations are lower than $10 \cdot 10^3$ [mg/Nm³]. Locally arising concentrations above this value are possible in dust separators. At local high concentrations dust strands or agglomerates can form without an appreciable modification of the flow behaviour. The description of the flow behaviour between the particles is possible with the description for single particles with an adjusted size and density. Approaches for this topic are given by the work of Lewis et al.[25].

2.3 Stabilization of aero dispersions

Aero dispersion can exists over a long time, the forces within cause an inhibition of the sedimentation and stabilize the dispersion. These forces are typically aerodynamic forces, the most important force of this type is the drag force. Like in almost all aero dispersions, the carrier medium, the gas, is in motion. In the atmosphere, thermal flows create drag forces against the gravity by inducing vertical gas motion. In case these drag forces are higher than gravity, the aero dispersion exists for a long time. In addition to drag forces, there are also turbulent, molecular and electric diffusions. Turbulent, molecular or electric diffusion create particle motion, which can support or impair the dust separation.

2.3.1 Turbulent diffusion

Turbulent flows are characterized by fluid particles which are moving transversely and directly to flow. This motion is a mutual exchange of eddies and a simultaneous exchange of momentum. Exchange processes occur through turbulent flows. Turbulent diffusion is negligible at low gas velocities (< 5 [m/s]) and for large particles (>100 [μm])[15]. The prediction of the rate of turbulent diffusion typically requires a complex numerical model, and often a computational fluid dynamics (CFD) approach has to be adopted. This because turbulent diffusion rates are local quantities, depend (to a first approximation) on the local shear rate, and are often anisotropic, i.e., vary with the spatial direction. Detailed information about turbulent diffusion in gas-solid suspensions is provided the work of Senior and Grace[26]. The application of turbulent diffusion in a numerical model is shown in the work of Wang et al.[27].

2.3.2 Molecular diffusion

Brownian motion causes a diffusion of molecules and suspended particles. Particles change from positions with high concentrations to positions with a lower concentration. The diffusion transport rate can be described by the first law of Fick (2-19). (constant pressure and temperature is assumed)

$$\frac{dM_d}{dt} = -D_M \cdot S \cdot \frac{dc_d}{dx} \tag{2-19}$$

The time dependency of the particle concentration can by described by the second law of Fick (2-20):

$$\frac{dc_d}{dx} = D_M \frac{d^2 c_d}{dx^2} \tag{2-20}$$

The rate of diffusion depends on pressure, temperature, concentration gradient and the coefficient of diffusion. Gas type and particle size influence the coefficient of diffusion. The diffusion coefficient can be described by the particle motion from Stokes' law, the Cunningham correction (2-11), and equation (2-20).

$$D_M = \frac{k_B \cdot T \cdot \left(1 + \frac{2 \cdot A_{Cu} \cdot l_{gm}}{d_p}\right)}{3\pi \cdot \mu \cdot d_p} \tag{2-21}$$

Table 5: Coefficient of diffusion for several particle diameters (20 [°C]; 1.013·10⁵ [Pa])[28]

Particle size	[µm]	10	1	0.1	0.01	0.001
D_M	[cm²/s]	$2.4\cdot10^{-8}$	$2.7\cdot10^{-7}$	$6.1\cdot10^{-6}$	$4.0\cdot10^{-4}$	$3.8\cdot10^{-2}$

Table 5 shows the coefficient of diffusion, depending on the particle size. Thus, diffusion is only important for dust separation technologies for particles with a size < 1 [µm]. Diffusion affects the following areas of dedusting: the stability of aero dispersions, the concentration balance and the dust separation itself. Particles flow to separation surfaces, stick to these surfaces, and are separated. Often, molecular diffusion is used in CFD-modelling, because a manual calculation is tedious or a numerical calculation of this effect is required anyhow.

2.3.3 Electro diffusion

Electrostatic forces are able to stabilize aero dispersions in case particles are charged. An inhomogeneous spatial distribution is caused due to an electric field. The behaviour of unipolar, charged dispersed particles is described in the work of Townsend[29], Wilson[30], Foster[31], Fuchs[32], Pich[33] and Whitby[34]. The approach resulting from these authors is present in formula (2-22).

$$\nabla \cdot E = 4\pi \cdot n_V \cdot q \tag{2-22}$$

$$B = \frac{w_p}{q \cdot E} \tag{2-23}$$

$$\nabla \cdot w_p = -\frac{1}{n_V} \cdot \frac{dn_V}{dt} \tag{2-24}$$

$$-\frac{1}{n_V} \cdot \frac{dn_V}{dt} = 4\pi \cdot q^2 \cdot n_V \cdot B \tag{2-25}$$

The solution of the above differential equation with $n_{V(t=0)} = n_{V_0}$ as initial conditions gives formula (2-26).

$$\frac{n_V}{n_{V_0}} = \frac{1}{\left(4\pi \cdot n_{V_0} \cdot q^2 \cdot B \cdot t\right) + 1} \tag{2-26}$$

Equation (2-26) describes the decrease of the particle number concentration with increasing time, i.e., $n_V \rightarrow 0$ for $t \rightarrow \infty$. The decrease can be quantified by the half-life period of an unipolar charged particle. Table 6 and Table 7 show results for the half-life period from the work of Pich[33].

Table 6: Half-life period of unipolar charged aerosols[33]

$$\left(n_{V_0} = 10^5 \left[\frac{1}{cm^3} \right], e = 1,6 \cdot 10^{-19}[C] \right)$$

d [μm]	t [s] q=1·e	t [s] q=2·e	t [s] q=5·e	t [s] q=50·e
0.02	$9.7 \cdot 10^2$	$2.42 \cdot 10^2$	$3.88 \cdot 10^1$	0.39
0.1	$1.95 \cdot 10^4$	$4.88 \cdot 10^3$	$7.81 \cdot 10^2$	7.81
0.2	$6.33 \cdot 10^4$	$1.58 \cdot 10^4$	$2.53 \cdot 10^3$	$2.53 \cdot 10^1$
1.0	$5.04 \cdot 10^5$	$1.26 \cdot 10^5$	$2.02 \cdot 10^4$	$2.02 \cdot 10^2$
2.0	$1.18 \cdot 10^6$	$2.94 \cdot 10^5$	$4.71 \cdot 10^4$	$4.71 \cdot 10^2$
10.0	$5.90 \cdot 10^6$	$1.47 \cdot 10^6$	$2.36 \cdot 10^5$	$2.36 \cdot 10^3$

The relations for bipolar charged aerosols are complex, and therefore the calculation of bipolar particles would go beyond the scope of this thesis. A short excerpt of the work from Pich[33] is shown in Table 7.

Table 7: Half-life period of bipolar charged aerosols[33]

$$\left(n_{V_0} = 10^5 \left[\frac{1}{cm^3} \right], e = 1,6 \cdot 10^{-19}[C], \frac{n_{V_{0-}}}{n_{V_{0+}}} = 16 \right)$$

d [μm]	t [s] q=1·e	t [s] q=2·e	t [s] q=5·e	t [s] q=50·e
0.02	$2.54 \cdot 10^3$	$6.35 \cdot 10^2$	$1.02 \cdot 10^2$	1.02
0.1	$5.11 \cdot 10^4$	$1.28 \cdot 10^4$	$2.05 \cdot 10^3$	$2.05 \cdot 10^1$
0.2	$1.66 \cdot 10^5$	$4.14 \cdot 10^4$	$6.64 \cdot 10^3$	$6.64 \cdot 10^1$
1.0	$1.32 \cdot 10^6$	$3.30 \cdot 10^5$	$5.30 \cdot 10^4$	$5.30 \cdot 10^2$
2.0	$3.09 \cdot 10^6$	$7.71 \cdot 10^5$	$1.23 \cdot 10^5$	$1.23 \cdot 10^3$
10.0	$1.55 \cdot 10^7$	$3.85 \cdot 10^6$	$6.19 \cdot 10^5$	$6.19 \cdot 10^3$

Table 6 and Table 7 show the half-life period of charged aerosols by the influence of particle diameter, loading and time.

2.4 Adhesive forces

Adhesive forces are important for dust separation. They exist between dust particles and between dust particles and walls. In case adhesive forces exists, agglomeration between particles can arise and improve the separation. In electrostatic precipitators and filters, adhesive forces have a significant influence on separation performance. The forces that separate the dust on the electrodes or filter materials are adhesive forces. Figure 8 provides a comparison of important adhesive forces of dust separation.

Adhesive forces can be classified in to three groups:

- Van der Waals forces

- Capillary forces

- Coulomb forces
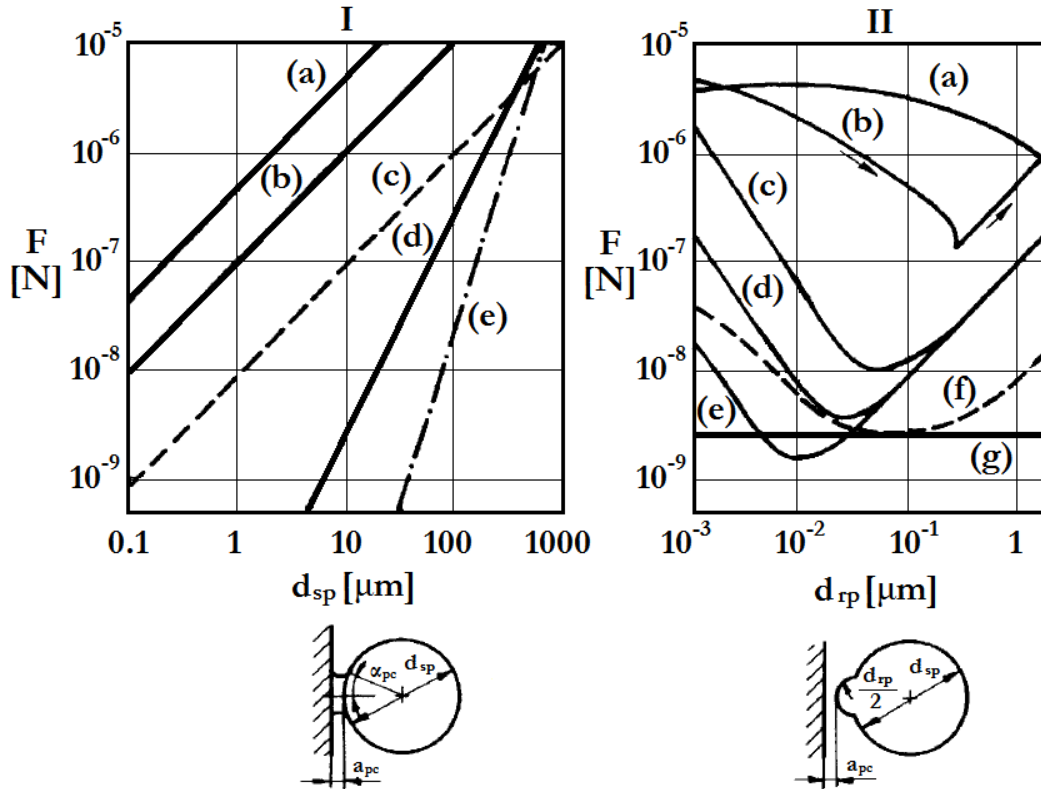
Figure 8: Interactions between particles [35];
(separation distance a_{pc}= 0.4 [nm], surface tension σ_{pg}= 0.72·10^{-3} [N/cm²], particle density =3000 [kg/m³])

I: smooth sphere and plate; (a) liquid bridges α_{pc}= 20 [°], (b) Van der Waals $h\bar{\omega}$ = 8·10^{-19} [J], (c) Electrostatic (conductive) U = 0.5 [V], (d) Electrostatic (non-conductive) σ = 10^{2} [e/μm²], (e) gravity

II: rough sphere and plate; (a) liquid bridges d_{sp} = 10 [μm] α_{pc}= 20 [°], (b) liquid bridges d_{sp} = 10 [μm] α_{pc}= 2.5 [°], (c) Van der Waals d_{sp} = 100 [μm]$h\bar{\omega}$ = 8·10^{-19} [J], (d) Van der Waals d_{sp} = 10 [μm]$h\bar{\omega}$ = 8·10^{-19} [J], (e) Van der Waals d_{sp} = 1 [μm]$h\bar{\omega}$ = 8·10^{-19} [J], (f) Electrostatic (conductive) d_{sp} = 10 [μm] U = 0.5 [V], (g) Electrostatic (non-conductive) d_{sp} = 10 [μm]σ = 10^{2} [e/μm²]

2.4.1 Van der Waals forces

Krupp[36] described the Van der Waals forces as all forces between molecules or atoms without chemical binding forces. Van der Waals forces between two plates are:

$$F_{VdW} = S \cdot \frac{h\overline{\omega}}{8\pi^2 \cdot s_0{}^3}$$

(2-27)

Here $h\overline{\omega}$ is the Lifshitz-van der Waals-constant, and s_0 is the distance between adhesive bodies. For particles having the diameter d_p, formula (2-28) is valid:

$$F_{VdW} = S \cdot \frac{h\overline{\omega}}{16\pi \cdot s_0{}^2} \cdot d_p$$

(2-28)

The Lifshitz-van der Waals-constant is approximately 0.6 [eV] for synthetic material and between 2 and 11 [eV] for metals and semiconductors. Formula (2-29) is valid for adhesive bodies with different materials.

$$h\overline{\omega}_{12} \approx \sqrt{h\overline{\omega}_{11} \cdot h\overline{\omega}_{22}}$$

(2-29)

In case of multiple contact points, the force can be added up. When it comes to a deformation at the contact point, adhesive forces increase since the contacting area increases. Layers consisting of water molecules exist in aero dispersions. The extend of these layers depends on pressure, temperature and relative humidity, and the layers influence the adhesive force. In the case of a decreasing particle distance, the contact surface increases and adhesive forces increase. The van der Waals forces drop quickly with an increasing distance, thus the roughness of the particles is of key importance. In case the distance is $>1 \cdot 10^{-8}$[m], van der Walls forces can be neglected.

2.4.2 Capillary forces

Capillary forces are typically the dominating adhesive force, depending on particle roughness and relative humidity of the carrier gas[37]. Dust particles can be simplified to spherical particles with a surface roughness. This approach is part in the work of Halsey and Levine [37] and shown in Figure. Halsey and Levine described three different regimes for the capillary force caused by a wetting fluid and the total amount of fluid present per particle contact (Figure 10). These regimes are the asperity, roughness and the spherical regime. The calculation of the capillary forces varies from regime to regime and is summarized in equation (2-30), (2-31) and (2-32).

Figure 9: The contact zone between two rough particles of radius r_p[37]. The scale of height deviations from the mean is l_{Cap} and the height fluctuations are correlated over a distance d_{Cap}. The lateral size of the contact zone in which the macroscopic curvature of the particles is not apparent is $\approx \sqrt{l_{Cap} \cdot r_p}$
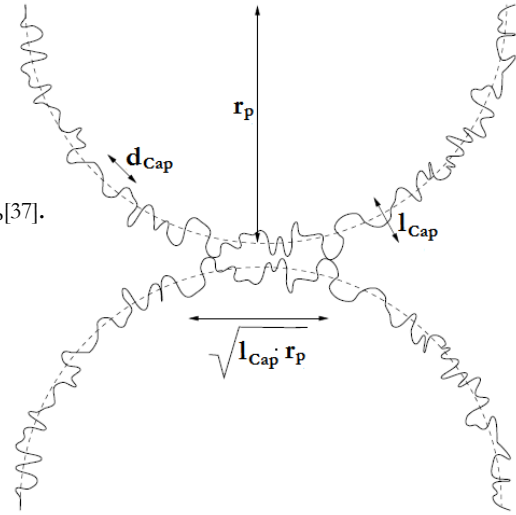
Asperity Regime

$$F_A \approx \frac{\Gamma \cdot V_{cap,1}}{l_R^2} \cdot \left(\frac{V_{cap}}{V_{cap,1}}\right)^{\frac{2-\chi}{2+\chi}}, \text{for } V_{cap} < V_{cap,1} \tag{2-30}$$

Roughness Regime

$$F_A \approx \frac{\Gamma \cdot V_{cap,1}}{l_R^2}, \text{for } V_{cap,1} < V_{cap} < V_{cap,2} \tag{2-31}$$

Spherical Regime

$$F_A = 2\pi \cdot \Gamma \cdot r_p, \text{for } V_{cap} > V_{cap,2} \tag{2-32}$$
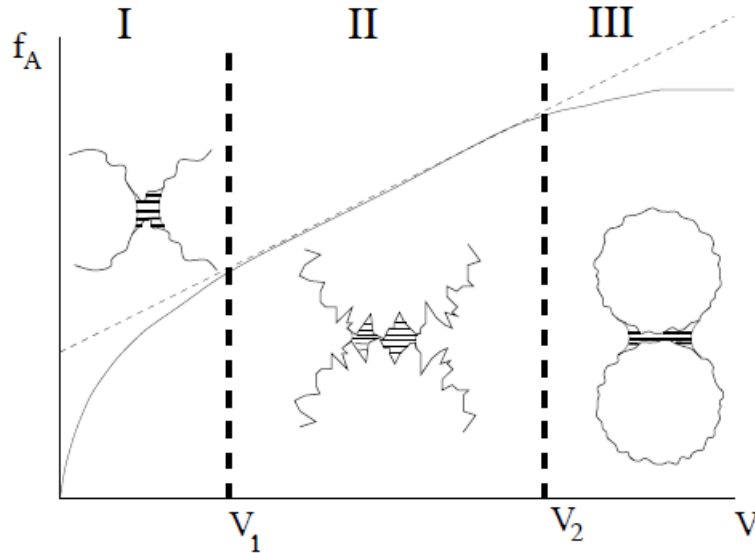
Figure 10: The behaviour of capillary adhesive force between two rough, approximately spherical particles [37]. The three regimes of the force vs. volume of the wetting layer are: I - Asperity Regime, II - Roughness Regime, and III - Spherical Regime. The insets show the extent of the wetting region typical for each regime.

2.4.3 Coulomb forces

If charged dust particles exist, a description with the law of Coloumb is possible. For two charged points (q_1, q_2) and the distance s_0 formula (2-33) is valid.

$$F_{Co} = \frac{q_1 \cdot q_2}{4 \cdot \pi \cdot \varepsilon_0 \cdot \varepsilon_r \cdot s_0^2}$$

(2-33)

Here ε_0 is the constant of induction, and ε_r is the dielectric constant. Dust particles with the same charge repel each other, while particles with unequal charges attract each other. Formula (2-33) changes to formula (2-34) for charged dust particles in the same layer[38].

$$F_{Co} = \frac{q^2}{8\pi \cdot \varepsilon_0 \cdot d_p \cdot \delta_{dc}} \cdot \frac{\ln\left(1 + \frac{\delta_{dc}}{s_0}\right)}{\left(\gamma + \frac{1}{2} \cdot \ln\frac{d_p}{s_0}\right) \cdot \left(\gamma + \frac{1}{2} \cdot \ln\frac{d_p}{s_0 + \delta_{dc}}\right)}$$

(2-34)

Here δ_{dc} is the penetration depth of the charge, and γ is the Euler constant = 0.5772. The resulting Coulomb forces are between $5 \cdot 10^{-10}$ and $6 \cdot 10^{-10}$ [kg·m/s^2] with an elementary charge of 10^3 for each particle, a penetration depth of $5 \cdot 10^{-10}$-$10 \cdot 10^{-10}$ [m] and a particle diameter of d=1 [μm]. The Coulomb forces are typically lower than the van der Waals forces. An exception is the high particle charge in electrostatic precipitators.

In the case of dust particle/plate system in an electric field, like in an electrostatic precipitator, more forces exists. Lowe and Lucas[39] provide a good approximation for this case (2-35).

$$F_{Cel} \approx d_p^2 \cdot \left(C \cdot E \cdot i \cdot \varrho_e - \frac{E^2}{32}\right)$$

(2-35)

Here i is the spray current (charges per time unit), ϱ_e is the specific electrical resistance, and C is a constant.

2.4.4 Agglomeration[40]

For agglomeration to occur a contact between particles and adhesive forces are required. The probability of collisions depends on dust concentration and particle relative motion. Reasons for particle collisions are:

- forces due to the carrier medium (molecular diffusion, turbulent diffusion, flow forces)
- forces between the dust particles (van der Waals forces, Coulomb forces)
- external forces (magnetic, electric, gravity, centrifugal and sound forces)

Turbulent diffusion, flow forces and external forces produce collisions of particles with a particle diameter > 1 [μm]. Molecular diffusion and external forces build particle collisions with a particle diameter < 1 [μm]. Van der Waals forces and Coulomb forces only make a small contribution due to their low range.

3 Dust separators

The following subsections deals with basics, types, characteristics and design principles of dust separators. In every chapter with the title "basic" a general description is given and the mode of action of dust separators is explained. The different types with specific details are detailed in the types section. Advantages and disadvantages with characteristic properties are listed in the chapter with the heading "characteristics". In the design principles section the detailed design methods are specified. The following separators are described:

- Gravity dust separator

- Centrifugal dust separator

  - Cyclones

  - Rotary flow dust removal system

  - Dedusting centrifuge

- Combinations of gravity and centrifugal dust separators

- Electrostatic dust separator

- Special design dust separator

  - Rotational particle separator
  - Electrocyclone

3.1 Gravity dust separator

The description of the gravity dust separators is based on the work of Batel[15].This chapter provides a detailed view of dust separation effects in flues gas pipe components, gutters and dust chambers. Dust separators which use flow redirection and inertia for separation are described in chapter 3.3.

3.1.1 Basics and mode of action of a gravity dust separator

An aero dispersion flows through gravity dust separators horizontally. Particles move with the settling velocity of equation (2-16) to the separation surface (Figure 11) and separate perfectly (in theory) at this surface to the dust bunker. The settling velocity is almost identical to the separation velocity, because turbulent diffusion is low. Large dimensions, low gas velocities (1.5-2 [m/s]) and big particle diameters (>100 [μm]) are the reasons for the low turbulent diffusion.
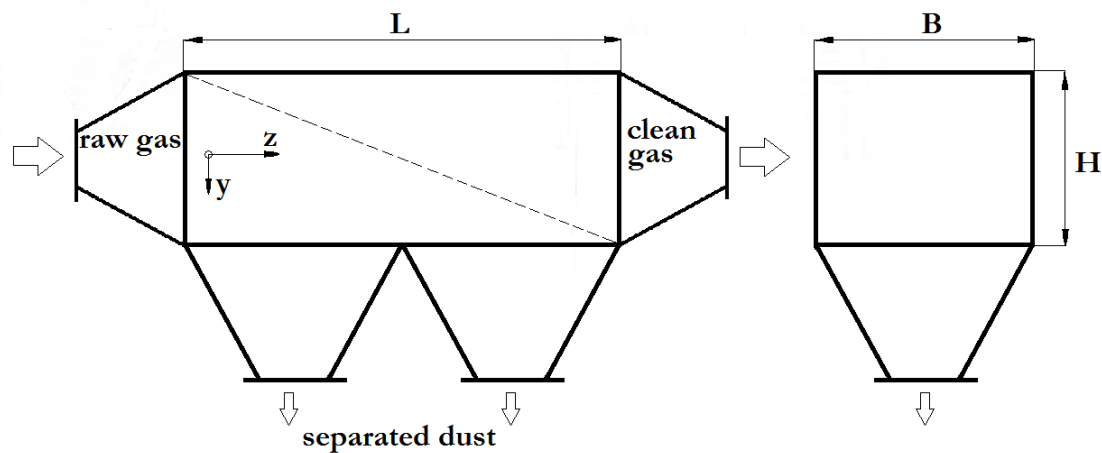
Figure 11: Scheme of a gravity dust separator

The advantages of a gravity dust separators are:

- low construction costs
- a simple construction
- a low pressure drop
- no temperature limitation
- no problems with abrasion

The disadvantages are:

- a big space requirement
- the separator is only able to separate big particles ($d_p > 100$ [μm])

3.1.2 Types and Characteristics of gravity dust separators

Gravity dust separators are basically chambers with a design like shown in Figure 11. Important for the separation efficiency is the separator's total (horizontally projected) separation area. A disadvantage is the possibility that already separated dust can be re-entrained by the flow. Thus, the gravity dust separator is unsuitable for fine dust particles, but useful as a pre-separator for combustion plants or blast furnaces.

3.1.3 Design principles of a gravity dust separator

a) Separation of particles with the same diameter

This calculation works with following assumptions:

- constant gas velocity

- homogeneously distributed dust in the gas flow

- the horizontal particle velocity is equal to the gas velocity $\left(w_h = v_g\right)$

A dustless room is formed under the influence of the settling velocity. The height can be calculated by formula (3-1).

$$y \approx l_s \frac{w_p}{v_g} \tag{3-1}$$

The local dust loading of the displacement chamber $c^*_{(l_s)}$ is calculated with equation (3-2).

$$c^*_{(l_s)} = c_{raw} \frac{H_s - y}{H_s} = c_{raw} \left(1 - \frac{y}{H_s}\right) = c_{raw} \left(1 - \frac{l_s \cdot w_p}{v_g \cdot H_s}\right) \tag{3-2}$$

With equation (2-2) and $\left(l_s = L_s\right)$ follow formula (3-3).

$$\eta_t = \frac{c_{raw} - c_{raw} \left(1 - \frac{L_s \cdot w_p}{v_g \cdot H_s}\right)}{c_{raw}} = \frac{L_s \cdot w_p}{v_g \cdot H_s} \tag{3-3}$$

In the case of the result of formula (3-3) being higher than 1, the particle is separated before the length L_s of the separator is reached. Since the gas velocity is the volumetric gas flow rate divided by B·H, the height of the separator is irrelevant for the separation efficiency. The height only influences the gas velocity, and hence the tendency for re-entrainment of particles.

b) Separation of particles with different diameters

The separation of particles with different diameters by gravity could be seen as a huge number of separators with one particle size per separator. For each separator formula (3-3) is valid. In case the particle size distribution is described by the amount of residue R, then the percentage of every particle size is $dR(d)$.

$$\eta_t = \int\limits_{R=0}^{R=1} \frac{w_p(d_p) \cdot L_s}{v_g \cdot H_s} \, dR(d) \qquad \text{(3-4)}$$

With equation (3-4) and (2-15) follow equation (3-5).

$$\eta_t = \frac{\left(\varrho_s - \varrho_g\right)}{18\eta \cdot v_g \cdot H_s} g \int\limits_{R=0}^{R=1} d_p^{\,2} \, dR \qquad \text{(3-5)}$$

Applied to a model of different layers with one particle size the fractional separation efficiency can be calculated by formula (3-6).

$$\eta_f(d_p) = \frac{w_p(d_p) \cdot L_s}{v_g \cdot H_s} \qquad \text{(3-6)}$$

These separation efficiency will not change with the size distribution of the dust but with the dimensions and the process parameters of the separator.

3.2 Centrifugal dust separator

Chapter 3.2 is based on the work of Robel et al.[16], Batel[15], Hoffman and Stein[41]. They provide a detailed description of the basics and design principles of centrifugal dust separators. The following separators are described:

- Cyclones
-

- Rotary flow dust removal system

- Dedusting centrifuge

3.2.1 Cyclones

Cyclones are the most common centrifugal dust separators in industry. This chapter deals with the basics, the mode of action, types and characteristics of cyclones.

3.2.1.1 Basics and mode of action of a cyclone dust separator

Centrifugal dust separators use the centrifugal motion of dust particles in case of flow redirection. This principle allows the separation of the particles from the gas. The flow redirection arises from a gas flow through a cylindrical body[16].

Advantages of centrifugal dust separators

- simple structure without moving parts

- high availability

- wide temperature range

- low temperature decrease

Disadvantages of centrifugal dust separators

- medium to low separation performance

- separation efficiency strongly dependents on flow rate

- bad separation of fine particles

Typical applications of centrifugal dust separators are the pre-separation before other dust collecting systems, or the distinctive separation of dust with the particle size over 10 [μm] median.
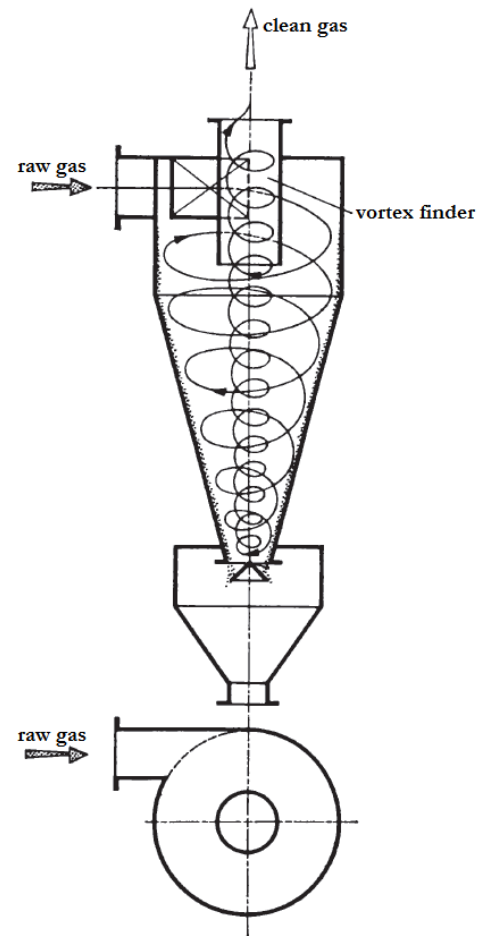
Figure 12: Flow lines in a cyclone [15]

Components of a centrifugal dust separator

- cylinder upper body with a tangential gas-inlet (slot or pipe)

- cone

- vortex finder

- dust container

- dust removal system

- gas-outlet

- swirl vane (only in axial-cyclones)

3.2.1.2   Types of cyclone dust separators

Various flow rates, dust concentrations and applications require different types of centrifugal dust separators. There are three different types of centrifugal dust separators:

- Tangential cyclone

- Axial cyclone

- Multicyclone
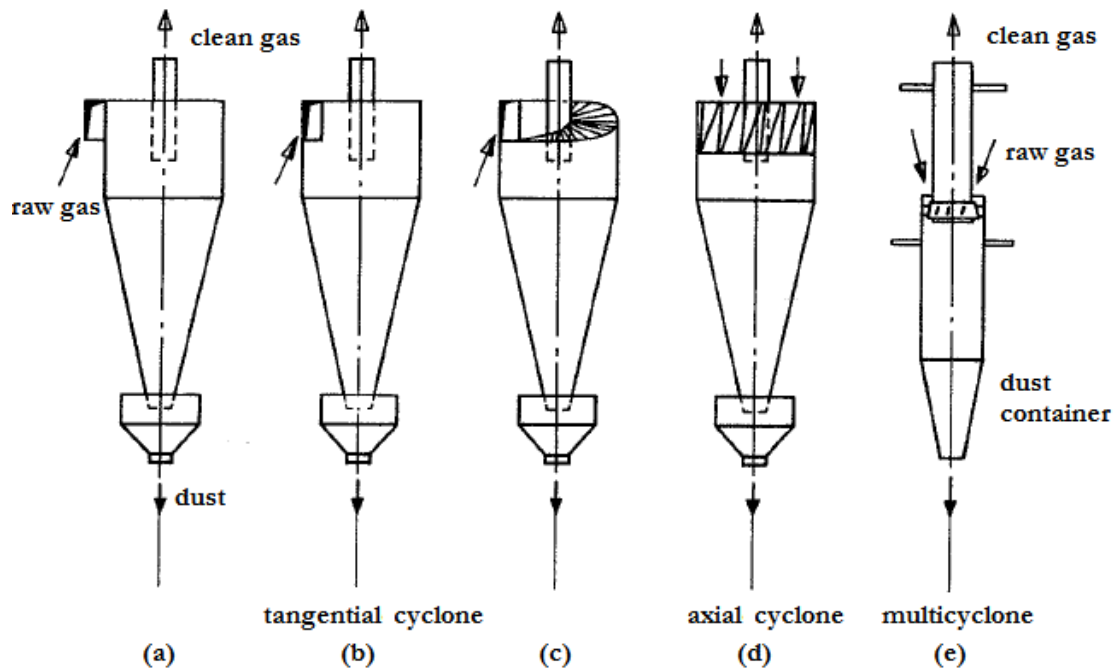
Figure 13: Types of centrifugal dust separators ((a) tangential cyclone with a spiral inlet, (b) tangential cyclone with a tangential inlet, (c) tangential cyclone with an axial inlet, (d) axial cyclone with swirl vanes, (e) single multicyclone tube[16]**.**

In the axial cyclone, the parallel flowing raw gas at the inlet is converted into a rotating flow through the cylindrical body. Centrifugal forces produce a radially-outward particle transport. All three types of tangential cyclones are shown in Figure 13 (a-c). Axial cyclones have an axial gas inlet, so the rotational flow is generated by a swirl vane with guide vanes. The dust transport of the axial cyclone is similar to the tangential cyclone. In both systems, the clean gas leaves the cyclone through the vortex finder located at the centre of the cyclone. Multicyclones consist of several axial cyclones, and have the same dust container. The gas flows parallel through all multicyclone tubes. According to the requirements and operating conditions of centrifugal dust separators, they can be divided into five groups:

- Centrifugal dust separators with a high separation performance - "high-performance cyclones"

- Centrifugal dust separators with a low separation performance - "cyclone pre-separator"

- Centrifugal dust separators for fibrous and coarse materials - "chippings cyclone"

- Multicyclones

- Centrifugal dust separators for special applications (Cyclones are made of concrete or other special materials)

3.2.1.3 Characteristics of cyclone dust separators

High-performance cyclones are normally used as single stage cyclones (Figure 14) or as an interconnection of cyclones in series. In case of high volumetric flow rates, a parallel operation of cyclones is needed (Figure 15).The maximum number of cyclones in a parallel operation is ten. In the case of a higher number of cyclones, the distribution of the particle loaded raw gas could cause problems.

The aim of the cyclone design is to find a simple separator with a low pressure drop and a high separation efficiency in a double-stage application. This separator, used as a single-stage operating cyclone, is also an economical solution for applications with lower dust emissions.

Typical dimensions are shown in Table 14 for high-performance cyclones and in Table 15 for cyclone pre-separators. These tables are located in the Appendix A - centrifugal dust separator. Figure 14 provides an overview of the cyclone design.
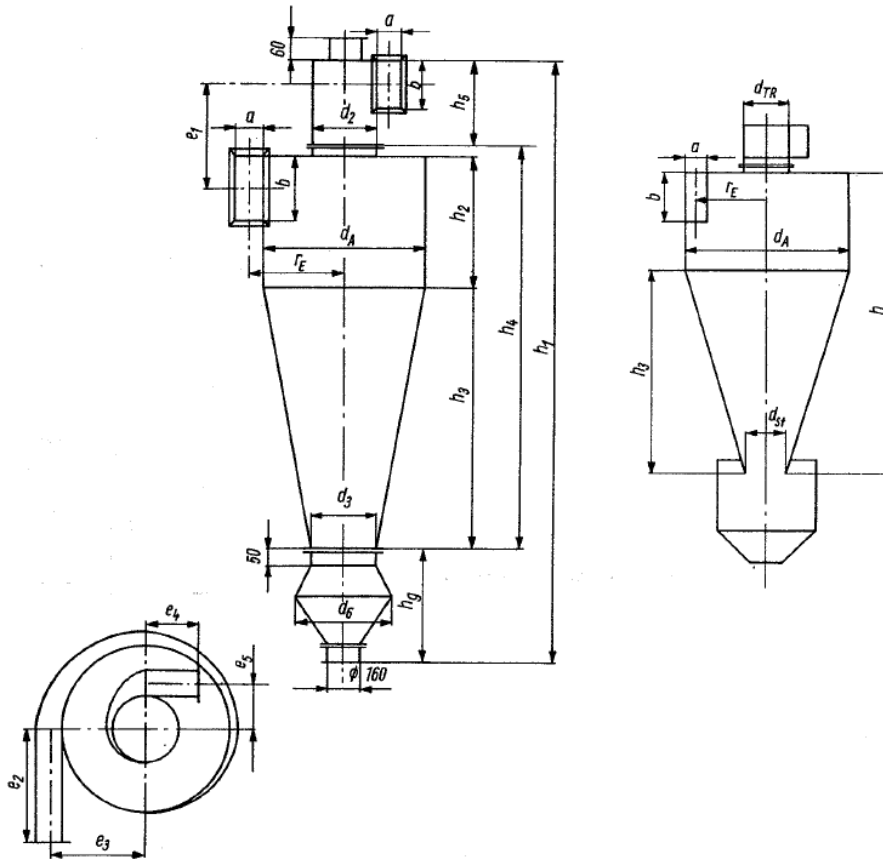
Figure 14: Defined dimensions of a centrifugal dust separator[16]
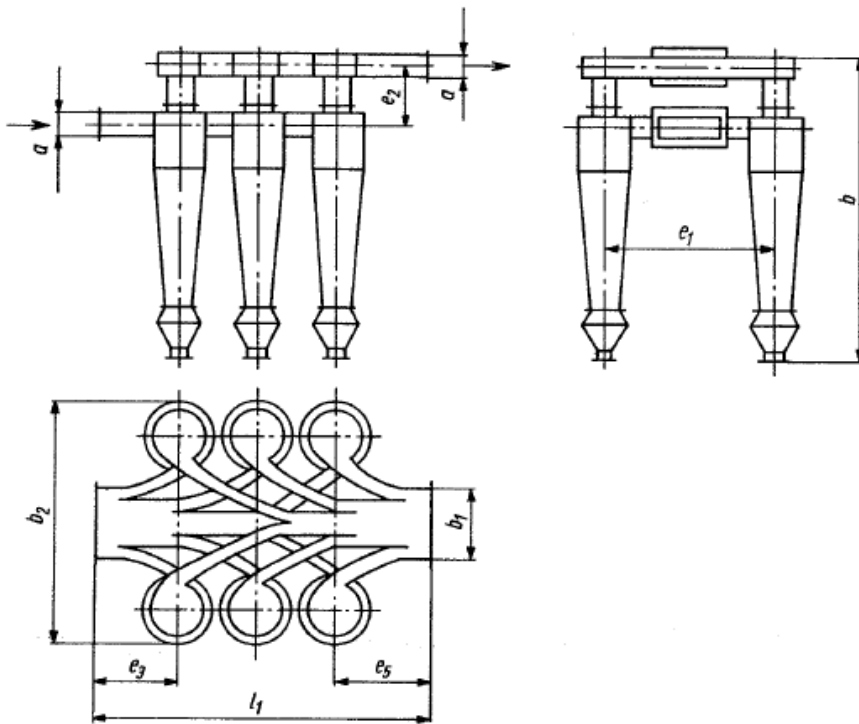
Figure 15: Typical dimensions of a centrifugal dust separator (multi-unit parallel arrangement)[16]

Robel et al.[16] describe the typical parameters of cyclones. For the basic design of a cyclone it is important to know these parameters. Furthermore, a validation of design tools is necessary. The inlet velocity of high performance cyclones is approximately 13 [m/s] for all sizes. Parameters like the pressure drop for the cyclone gas site range between 550 and 650 [Pa]. The pressure drop varies for different types of dust (i.e., an increasing dust concentration of 5 [g/m³] can increase the pressure drop by 30 [Pa])[16].

A multicyclone contains a specific number of tangential or axial cyclones with a parallel flow arrangement. The number of cyclones depends on the volumetric flow rate. All cyclones are linked with the same raw and clean gas chamber. Multicyclones have a high attrition at the swirl vanes in each axial cyclone. This disadvantage is typical for axial cyclones.

The inlet should be flow-optimized for all cyclone applications because the inlet flow has a huge effect on the separation efficiency. Guide blades are often used for flow control. At the dust-outlet a sealed cell is required to prevent the leakage of separated dust.

Single cyclones or multicyclones can be operated with low pressure or overpressure without any effects to the separation efficiency.

3.2.1.4 Design principles of cyclones

Despite the extensive research in the field of centrifugal separation, it is not possible to determine the phase separation in a mathematically exact way. Empirical studies with specific applications are part of the cyclone design methods. The mathematical consideration allows the splitting into the cylindrical and the conical part of the separation. Muschelknautz[42] describes in the chapter "Zyklone zum Abscheiden fester Partikel aus Gasen" of the VDI Wärmeatlas one of the commonly used design methods for cyclones in industry. This method was developed by Professor Edgar Muschelknautz and called "The Muschelknautz method (MM)". The VDI guidelines for gas-particle cyclones describe the flow field in a cyclone, the pressure drop and the separation efficiency of a cyclone. The separation efficiency and the pressure drop are significant for all dust separators. Important equations and figures from the VDI guidelines are subsequently listed and provide an overview of the VDI design method.

Muschelknautz defined a constriction coefficient for different inlet types of a cyclone.

Tangential inlet

The constriction coefficient for a tangential inlet is described by formula (3-7).

$$\alpha_{cc} = \frac{1 - \sqrt{1 + 4\left[\left(\frac{\beta}{2}\right)^2 - \left(\frac{\beta}{2}\right)\right]\sqrt{1 - \frac{1-\beta^2}{1+c_{raw}}\left(2\beta - \beta^2\right)}}}{\beta} \tag{3-7}$$

The wall velocity for a slot-type can be calculated by formula (3-8).

$$u_a = \frac{v_g \frac{r_e}{r_a}}{\alpha_{cc}} \tag{3-8}$$

Spiral inlet

The wall velocity for a spiral inlet requires two additional parameters. These parameters are the friction surface $A_{R,sp}$ (formula (3-10)) and the wall friction coefficient λ_s (formula (3-11)). The wall velocity is described by formula (3-9).

$$u_a = \frac{v_g \frac{r_e}{r_a}}{1 + \frac{\lambda_s}{2} \cdot \frac{S_{R,sp}}{V} v_g \sqrt{\frac{r_e}{r_a}}} \tag{3-9}$$

$$A_{R,sp} = \varepsilon_{wa} \left[\frac{b_{ci} + 2r_a}{2}\left(b_{ci} + h_e\right)\right] \tag{3-10}$$

$$\lambda_s = \lambda_0 \left(1 + 2\sqrt{c_{raw}}\right) \tag{3-11}$$

Axial inlet with swirl vanes

Typical for axial inlets are the application in multicyclones. The wall velocity is described by formula (3-12). A typical value for the blade angle is between 15 and 30 [°].

$$u_a = \frac{v_g \cdot \cos \delta_b \cdot \frac{r_e}{r_a}}{\alpha_{cc}} \tag{3-12}$$

The gas velocity at the wall of the vortex finder can be calculated by equation (3-13). The velocity depends on the wall friction coefficient λ_s (equation (3-14)) and the total internal wall surface S_R.

$$u_i = \frac{u_a \frac{r_a}{r_i}}{1 + \frac{\lambda_s}{2} \cdot \frac{S_R}{V} u_a \sqrt{\frac{r_a}{r_i}}} \qquad (3\text{-}13)$$

$$\lambda_s = \lambda_0 + 0.25 \sqrt{\eta_t \cdot c_{raw} \cdot Fr_i \frac{\varrho_g}{\varrho_s \cdot (1 - \varepsilon_{Str})} \cdot \left(\frac{r_a}{r_i}\right)^{-\frac{5}{8}}} \qquad (3\text{-}14)$$

The Froude number is provided by (3-15).

$$Fr_i = \frac{v_{vf}}{\sqrt{2g \cdot r_i}} \qquad (3\text{-}15)$$

The Reynolds number of the cyclone flow is described by formula (3-16).

$$Re_R = \frac{2r_e \frac{v_{ax}}{v_g}}{2\frac{h_c}{r_m}\left(1 + \left(\frac{v_{ax}}{u_m}\right)^2\right)} \qquad (3\text{-}16)$$

The wall friction coefficient λ_0 can be extracted from Figure 16. The relative roughness $\frac{k_s}{r_a}$ is an estimate of the absolute roughness of the inner surface of the cyclone walls, divided by the inner radius of the cyclone [41].
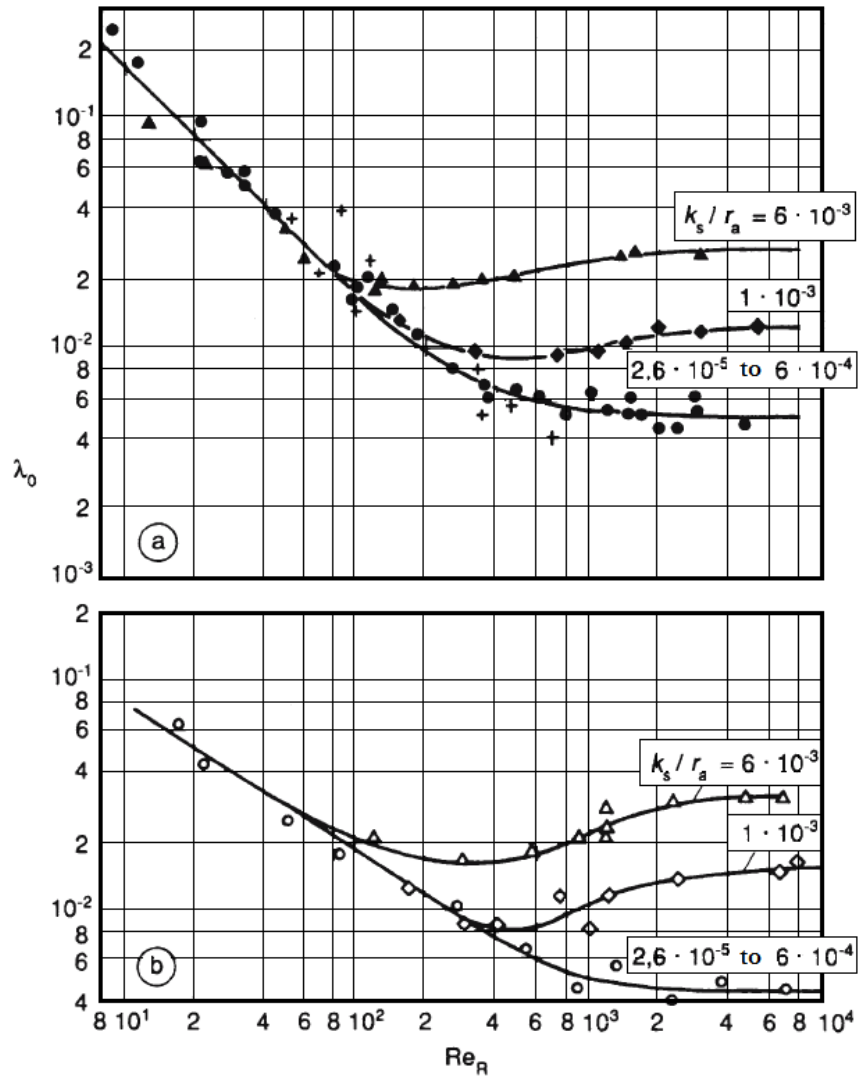
Figure 16: Wall friction coefficient; (a) for a cylindrical cyclone, (b) for a conical cyclone[42]

The pressure drop of cyclones

The total pressure drop is calculated with formula (3-17) and consists of the pressure drop of the inlet, the separation chamber and the vortex finder.

$$\Delta p_{ct} = \Delta p_{ci} + \Delta p_{csc} + \Delta p_{cvf} \tag{3-17}$$

The pressure drop of the inlet depends on the inlet design and is shown in Table 8.

Δp_{ci}	inlet design
0	tangential inlet
$-\dfrac{\pi \cdot r_i{}^2}{b_{ci} \cdot h_e}\left(1 + \dfrac{\pi}{4}\left(\dfrac{r_i}{r_a}\right)^2\left(1 - \dfrac{1}{\alpha_{cc}{}^2}\right)\right)\dfrac{\varrho_g}{2}v_{vf}{}^2$	spiral inlet
$-(0.2 \ldots 0.5)\dfrac{\varrho_g}{2}v_{vf}{}^2$	axial inlet with swirl vanes

The pressure drop of the separation chamber (3-18) depends on the wall velocity of the cyclone, the surface S_R and the wall friction coefficient λ_s.

$$\Delta p_{csc} = -\lambda_s \frac{S_R}{0.9 \cdot V}\frac{\varrho_g}{2}(u_a \cdot u_i)^{\frac{3}{2}} \tag{3-18}$$

Muschelknautz makes the assumption that 90 [%] of the incoming flow participates in the flow along the walls and in the formation of the inner vortex[41]. This is the source of the factor 0.9 in formula (3-18). The pressure drop in the vortex finder is described with formula (3-19) and depends on the ratio of the velocity of the inner vortex and the mean axial velocity in the vortex finder.

$$\Delta p_{cvf} = -\left[2 + 3\left(\frac{u_i}{v_{vf}}\right)^{\frac{4}{3}} + \left(\frac{u_i}{v_{vf}}\right)^2\frac{\varrho_g}{2}v_{vf}{}^2\right] \tag{3-19}$$

The separation efficiency of cyclones

The particle separation in cyclones works with two mechanisms. The first separation mechanism occurs at the inlet. The fraction of the incoming solids that exceed the limit loading concentration is separated. Particles with a higher diameter than the cut size diameter d_e^* (equation (3-20)) were separated at the cyclone wall while particles with a lower diameter move inside the cyclone. This principle is shown in Figure 17.

$$d_e^* = \sqrt{w_p \frac{18\mu}{\Delta\varrho \cdot a_c}} \tag{3-20}$$
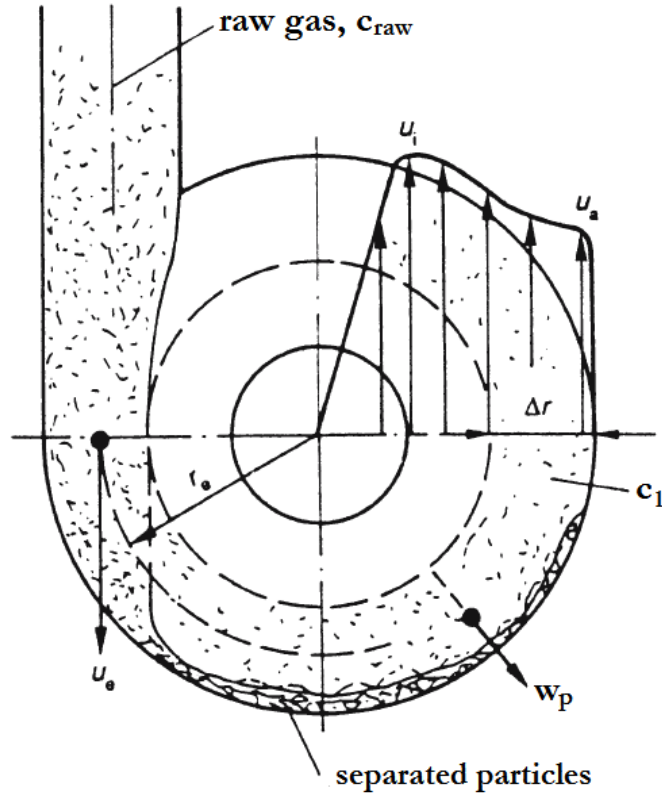
Figure 17: Separation of incoming solids that exceed the limit loading in a cyclone[42]

The separation at the inlet is described by the separation efficiency η_i (equation (3-21)).

$$\eta_i = 1 - \frac{c_l}{c_{raw}} \qquad \text{(3-21)}$$

The second separation mechanism occurs in the inner vortex. This separation is characterized by the critical particle diameter (equation (3-22))of the mean flow.

$$d^* = \sqrt{\frac{18\mu \cdot 0.9 \cdot V}{\Delta\varrho \cdot a_c \cdot u_i{}^2 \cdot 2\pi \cdot h_i}} \qquad \text{(3-22)}$$

The critical particle diameter defines the fractional separation efficiency curve for a specific cyclone geometry. These geometries are described in Table 9 and the corresponding curves are shown in Figure 18.

Table 9: Typical cyclone geometries (VDI Wärmeatlas [42]**)**

curve	a	b	C
design			
inlet type	axial	tangential	Tangential
$\dfrac{h}{r_i}$	15	13	10
$\dfrac{h_i}{r_i}$	10	10	7.5
$\dfrac{r_a}{r_i}$	2	3	4
$\dfrac{S_i}{S_{vf}}$	2.7	0.9	0.44
$\dfrac{b_{ci}}{r_a}$	0.4	0.27	0.19
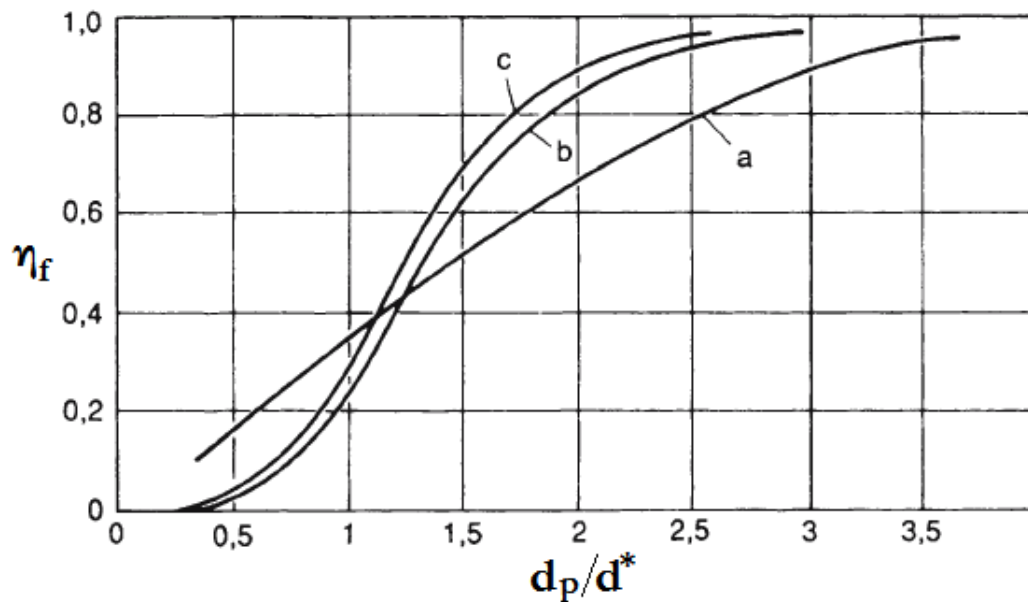
Figure 18: Fractional separation efficiency curves of cyclones (VDI Wärmeatlas [42]**)**

The separation efficiency of the inner vortex is calculated via the cyclone's fractional separation efficiency, the mean particle diameter and the mass fraction of each particle fraction (j) (formula (3-23)).

$$\eta_{iv} = \sum_{j=1}^{m} \eta_F(\bar{d}_j) \cdot \Delta R(\bar{d}_j) \tag{3-23}$$

The total separation efficiency is described with equation (3-24) and consists of the separation efficiency at the inlet and in the inner vortex.

$$\eta_t = 1 - \frac{c_l}{c_{raw}} + \frac{c_l}{c_{raw}} \cdot \eta_i \tag{3-24}$$
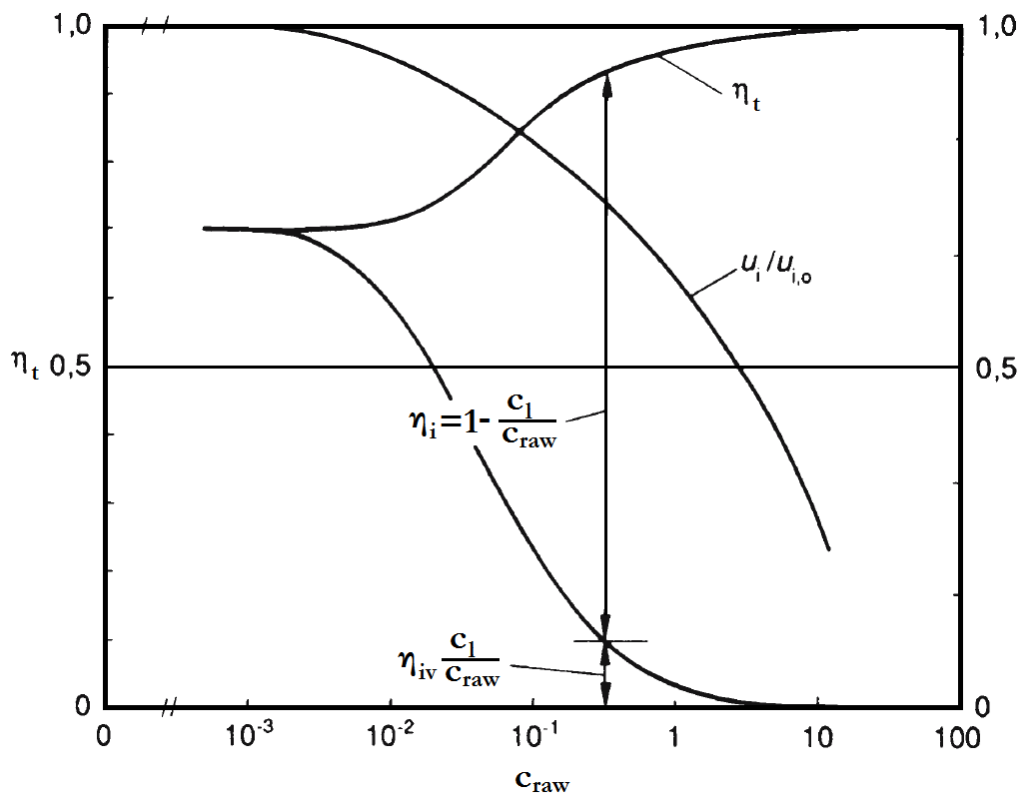
Figure 19: Separation efficiencies with increasing mass loading[42]

Figure 19 shows the separation efficiency at the inlet and the separation efficiency at the inner vortex by an increasing mass loading of the gas. The total separation efficiency with its dependency on the other separation efficiencies is also described in Figure 19.

Trefz[43] described an optimized method for the calculation of the total separation efficiency (equation (3-25)). This method considers a secondary flow with 10 [%] of the main flow[42].

$$\eta_t = \left(1 - \frac{V_{sec}}{V}\right)\left[1 - \frac{c_l}{c_{raw}} + \frac{c_l}{c_{raw}}\,\eta_{iv}\right] + \frac{V_{sec}}{V}\left[1 - \frac{\mu_D}{c_{raw}} + \frac{\mu_D}{c_{raw}}\,\eta_{vf}\right] \tag{3-25}$$

$$\frac{V_{sec}}{V} = 0.0497 + 0.0684\,\frac{\ln u_i/u_a}{\ln r_a/r_i} + 0.0949\left(\frac{\ln u_i/u_a}{\ln r_a/r_i}\right)^2 \tag{3-26}$$

The secondary flow is able to carry a higher amount of particles, because its lower wall velocity produces a lower absorption of turbulence. The limit loading of the secondary flow is many times higher than the limit loading of the main flow[43].

The separation efficiency of the vortex finder increases with an increased length of the vortex finder and an increased velocity in the vortex finder. In case that the vortex finder is too short, the secondary flow transports a high amount of particles into the clean gas flow. At a low particle loading in the raw gas, the secondary flow takes 15 [%] of the main flow[43].

Separation efficiency and the pressure drop depend in general on the following parameters:

- cyclone dimensions
- production quality (welding seams, surfaces)
- gas flow-rate per cyclone (inlet and outlet velocity at the vortex finder)
- gas properties (temperature, density, viscosity)
- dust concentration in the raw gas
- dust properties (particle size distribution, density, bulk density)

3.2.1.5 Operating behaviour

This chapter discusses some influencing variables of the operating behaviour of centrifugal dust separators. The following paragraphs are excerpts of the work of Robel et al.[16].

Dust concentration

A higher dust concentration results in an increased separation efficiency. This is valid for typical concentrations (c_{raw}< 300 [g/m³]) and standard cyclones. For small or special cyclones this may be different.

Inlet flow situation

The inlet design influences the separation efficiency. Hejma[44] describes the different inlet designs for cyclones in his work. In Figure 20 the different inlet conditions with their influence (k_{icg}) on the clean gas are shown. The factor k_{icg} describe the influence of the inlet design on the separation efficiency. The separation efficiency increases with a lower influence factor. The ideal inlet has a inflow angle of -15[°] and a length between $2 \cdot d_{icg}$ and $5 \cdot d_{icg}$[16].
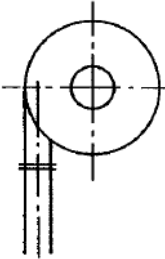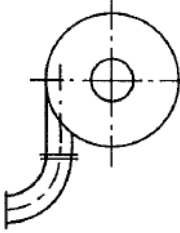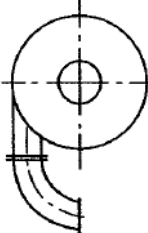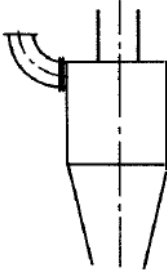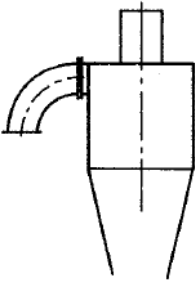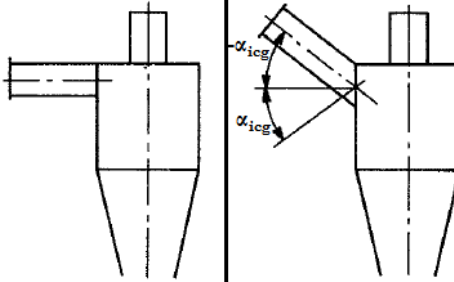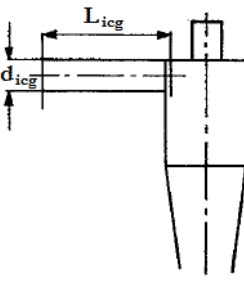
direct inlet	external bend	internal bend	top bend
$k_{icg} \approx 100$ [%]	$k_{icg} \approx 200$ [%]	$k_{icg} \approx 100$ [%]	$k_{icg} \approx 170...250$[%]
$\Delta p \approx 100$ [%]	$\Delta p \approx 91$ [%]	$\Delta p \approx 104$ [%]	$\Delta p \approx 95$ [%]

bottom bend	inflow angle				a pipe between the bend and the cyclone		
$k_{icg} \approx 100$ [%]	$\alpha_{icg} = 0$[°]	$\alpha_{icg} = +15$ [°]	$\alpha_{icg} = +30$[°]	$\alpha_{icg} = -30$[°]	$L_{icg}= 0$	$L_{icg}=3d_{icg}$	$L_{icg}=10d_{icg}$
$\Delta p \approx 104$ [%]	$k_{icg} \approx 100$[%]	$k_{icg} \approx 60$ [%]	$k_{icg} \approx 70$ [%]	$k_{icg} \approx 200$[%]	$k_{icg} \approx 100$ [%]	$k_{icg} \approx 80$ [%]	$k_{icg} \approx 70$ [%]

Figure 20: Inlet flow situations at cyclones[44]

The ideal inlet design is provided by:

- a flow direction with an angle of 15° from below

- a rotational flow, supported by a manifold

- an inflow length of 2 to 5·d by an angle of 0°

Dust discharge

The vortex-core of cyclones ends at the surface of separated dust, at discharge organs, or at internals at the bottom area of the cone. In the case of a long dust outlet, the vortex ends at the separated dust and rips this dust from the bunker in the flow. Furthermore, the separation efficiency declines. In this case a high cone diameter is important. A diameter $d_3 > 1.2\text{-}1.4 \cdot d_{TA}$ is needed. The same effect is achieved by a vortex limiter at the inlet of the dust outlet. Typical designs are pictured in Figure 21 and Figure 22. The factor k_{ocg} describe the influence of the outlet design on the separation efficiency. The separation efficiency increases with a lower influence factor.
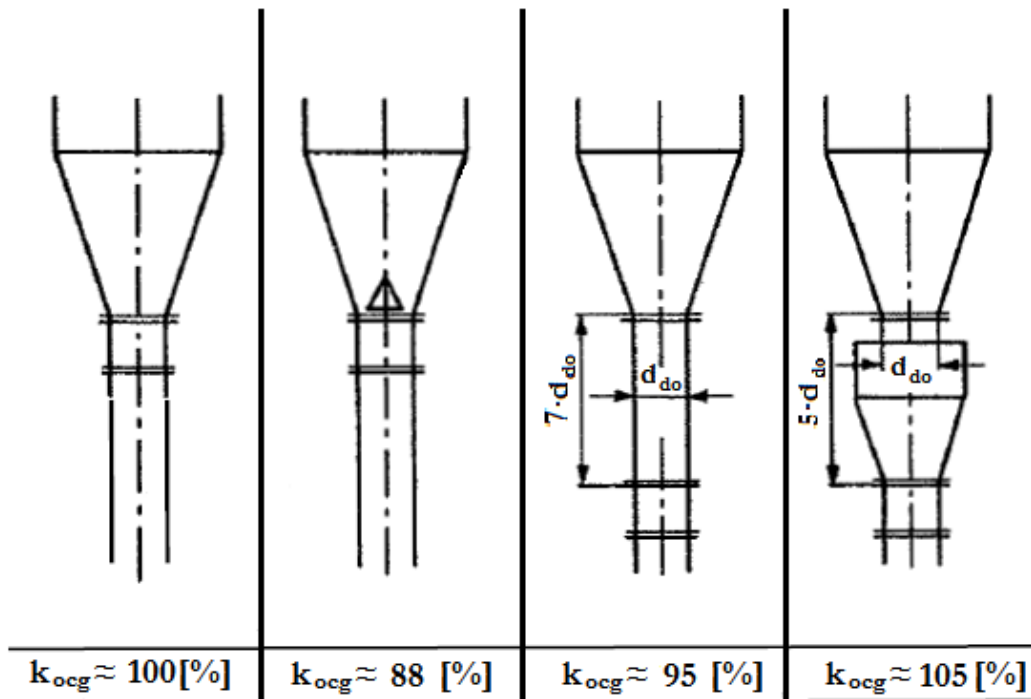
Figure 21: Influence of the dust outlet[16]
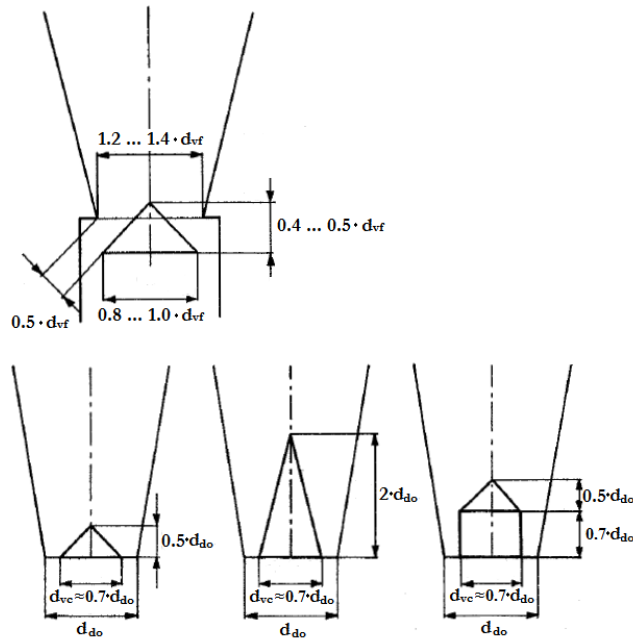
Figure 22: Design of vortex limiter[16]

Dust outlets have different influences on separation efficiency and pressure drop. Figure 23 shows the influence of typical dust outlet types. This figure was extracted from the work of Obermair and Staudinger[45]. They found that a fall tube is beneficial at high r_a/r ratios and that every dust outlet modification at axial cyclones is disadvantageous. The results from the separation tests of Obermair and Staudinger[45] are summarized in Figure 24. The geometries in Figure 23 and Figure 24 are equal.
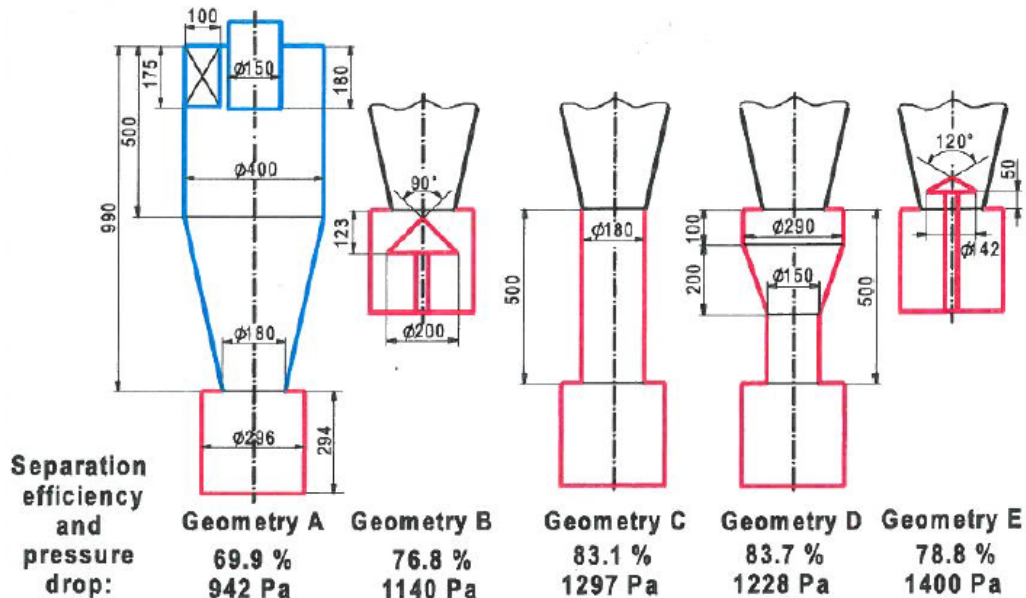
Figure 23: Dust outlets and their influence of pressure drop and separation efficiency[45]
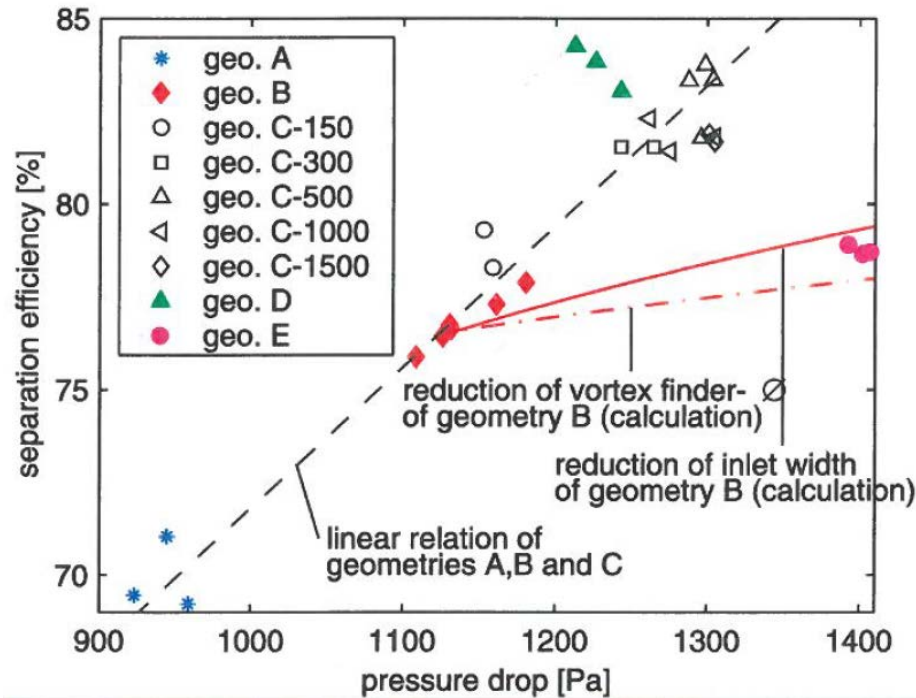
Figure 24: Separation test results of different dust outlet geometries[45]

Parallel or serial operation

Parallel and serial assemblies of cyclones have different operational behaviours. Robel et al.[16] describe that separation problems with a high gas flow rate can be solved with one big cyclone or with several small cyclones in a parallel operation. The separation efficiency increases with more cyclones because the separation velocity at the same pressure drop is lower. Requirements are homogenous dust loadings and flow conditions. For parallel operating cyclones a low number of cyclones with the same dust bunker is important, because a short circuit flow is possible in case of further production tolerances. As a result of different pressure drops between the cyclones the flow is distributed inhomogeneously. In this case, the separation efficiency is lower than the separation efficiency of a single cyclone. The cyclones should be split from the dust bunker (rotary valve, double flap valve).

In case an agglomeration of the dust is possible, the cyclones could work in a serial operation. Without agglomeration of the dust, the serial operation cannot be successful.

Abrasion

A high abrasion in the cylindrical part of the cyclone caused by sharp-edged dust particles. In the conical part the dust streaks are decisively. Abrasion can be reduced if the gas velocity is reduced to a minimum and uneven surfaces are smoothed. (Robel et al.[16])

3.2.2 Rotary flow dust removal system

The rotary flow dust removal system is a special construction of a centrifugal dust separator. Details and information in this chapter are reproduced from the work of Batel[15].

3.2.2.1   Basics and mode of action of a rotary flow dust removal system

The rotary flow dust separator is a centrifugal dust separator with two autonomous adjustable gas flows. Figure 25 shows the scheme of a rotary flow dust removal system. Schmidt[46] and Klein[47,48] describe the basics and the experimental behaviour of this separator. The raw gas is introduced into the cylindrical dust separation room by a distributor. Clean air is added through a second distributor to increase the vortex flow. A potential-vortex-flow structure in the outer ring and a rotational flow in the inner ring are produced. Both flows get mixed in a mixing area of the separator. This separator has similar flow conditions as the cyclone. However, there is one important difference. The dust is fed by the rotational flow and the separation area exists in the mixing area of the flows (at the transition from the potential-vortex flow and the rotational flow).
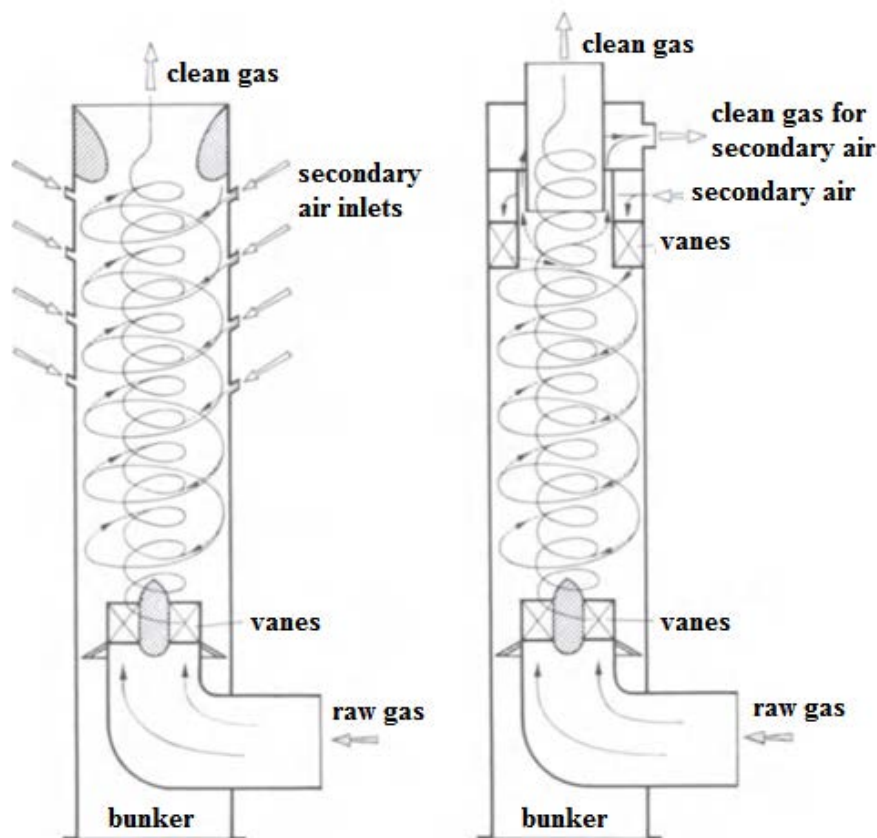
Figure 25: Scheme of a rotary flow dust removal system[46]

3.2.2.2   Design principles of a rotary flow dust removal system

The separator could be designed with the axial cyclone model from chapter 3.2.1.4. Main parameters like the separation efficiency depend on the residence time, dimensions, particle size and the velocity of circulation. The motion velocity increase by the radius r_i and a constant angular velocity. Simultaneously the separation length is growing. This mathematical theory excludes turbulent diffusion.

3.2.2.3   Characteristics of a rotary flow dust removal system

The dust loading will not affect the separation efficiency, because there is no separation of the dust particles in the flow mixing area against a sink-flow necessary. The separation size is one order of magnitude smaller than the separation size of a comparable tangential cyclone ($d_t \approx 0.4$ [μm], critical particle size 5 [μm], separator size $d_a = 200$ [mm]). The pressure drop is significantly higher than in a cyclone.

3.2.3 Dedusting centrifuge

Centrifuges are rare in the field of dedusting, as they require a high construction effort. The dedusting centrifuge is also a special construction of a centrifugal dust separator like the rotary dust removal system. Details and information in this chapter are reproduced from the work of Batel[15].

3.2.3.1   Basics and mode of action of a dedusting centrifuge

The scheme of a dedusting centrifuge is shown in Figure 26. The dust is separated in two concentrically arranged cylinders. The cleaning happens at low speed without a raw gas feed.
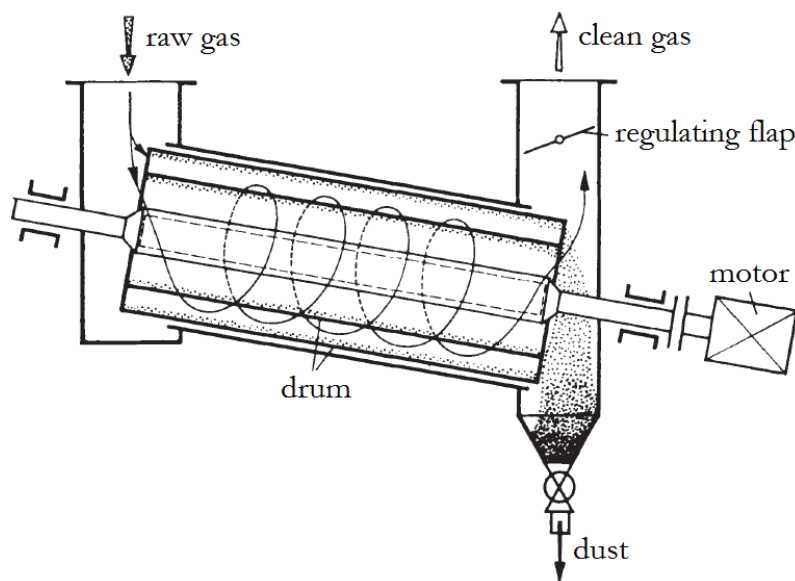
Figure 26: Scheme of a dedusting centrifuge[15]

3.2.3.2 Design principles of a dedusting centrifuge

In these design equations molecular, turbulent and electrical diffusion were not considered. They were based on chapter 3.2.1.4 and the following assumptions:

- A plug flow exists in the separation chamber $\left(w_z = v_g\right)$.

- The gas rotates like a rigid body

- The gas is in solid body rotation.

- The dust concentration in the separation chamber is a function of the axial and radial position $(c^* = f(z, r))$.

- Cylindrical coordinates are used for the calculation.

The equation of continuity is shown with equation (3-27) or (3-28).

$$\frac{\partial}{\partial t} \int_{V_{sc}} c^* dV_{sc} = -\int_{V_{sc}} \nabla \cdot (c^* \cdot w_p) dV_{sc} \tag{3-27}$$

$$\frac{\partial c^*}{\partial t} = \nabla \cdot (c^* \cdot w_p) \tag{3-28}$$

At stationary state formula (3-28) is simplified to formula (3-29).

$$w_z \frac{\partial c^*}{\partial z} + \frac{1}{r} \cdot \frac{\partial}{\partial r} (r \cdot w_r \cdot c^*) = 0 \tag{3-29}$$

The fluid-particle relative velocity is shown in formula (3-30).

$$w_r = \frac{1}{18\mu} \Delta\varrho \cdot d_p{}^2 \cdot \omega^2 \cdot r = k_{rv} \cdot r \tag{3-30}$$

Equation (3-29) changes with $w_r = k_{rv} \cdot r$ to equation (3-31).

$$w_z \frac{\partial c^*}{\partial z} + \frac{k_{rv}}{r} \cdot \frac{\partial}{\partial r} (r^2 \cdot c^*) = 0 \tag{3-31}$$

$$\frac{k_{rv}}{r} \cdot \frac{\partial}{\partial r} (r^2 \cdot c^*) = \frac{k_{rv}}{r} \left(2r \cdot c^* + r^2 \cdot \frac{\partial c^*}{\partial r}\right) = 2k_{rv} \cdot c^* + k_{rv} \cdot r \cdot \frac{\partial c^*}{\partial r} \tag{3-32}$$

Formula (3-31) changes to equation (3-33).

$$w_z \frac{\partial c^*}{\partial z} + 2k_{rv} \cdot c^* + k_{rv} \cdot r \cdot \frac{\partial c^*}{\partial r} = 0 \tag{3-33}$$
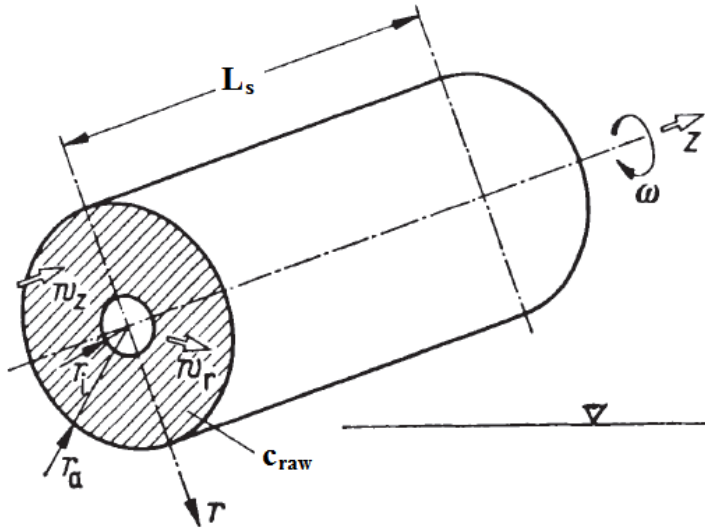
Figure 27: Calculation of rotational flows [15]

The solution of the partial differential equation is found by the method of characteristics. The characteristic equation is described with formula (3-34).

$$\frac{dr}{k_{rv} \cdot r} = \frac{dz}{w_z} = -\frac{dc^*}{2k_{rv} \cdot c^*} \tag{3-34}$$

This system of equation has two solutions. The first solution is described by equation (3-35) and (3-36).

$$\frac{dr}{r} = \frac{k_{rv}}{w_z} dz \tag{3-35}$$

$$\ln r \mid_{r_0}^{r} = \frac{k_{rv}}{w_z} dz \mid_{z_0}^{z} \tag{3-36}$$

The second solution is described by equation (3-37) and (3-38).

$$\frac{dc^*}{c^*} = -\frac{2 \cdot k_{rv}}{w_z} dz \tag{3-37}$$

$$\ln c^* \mid_{c_{raw}}^{c^*} = -\frac{2k_{rv}}{w_z} z \mid_{z_0}^{z} \tag{3-38}$$

Two areas have to be distinguished:

1. Characteristics from z=0

$$c_{raw} = const$$

$$r_0 \leq r \text{ and } r_i \leq r_0 \leq r_a$$

2. Characteristics from $r_0 = r_i$

$$c_{raw} = 0$$

$$0 \leq z_0 \leq l_s \text{ mit } z_0 \leq z$$

Area 1:

$$\ln \frac{r}{r_0} = \frac{k_{rv}}{w_z} z \tag{3-39}$$

$$r = r_0 \cdot e^{\frac{k_{rv}}{w_z} z} \tag{3-40}$$

With $r_i \leq r_0 \leq r_a$ for z=0 the following borders ((3-41), (3-42)) are valid.

$$r_1 = r_i \cdot e^{\frac{k_{rv}}{w_z} z} \tag{3-41}$$

$$r_2 = r_a \cdot e^{\frac{k_{rv}}{w_z} z} \tag{3-42}$$

This area is shown in Figure 28.
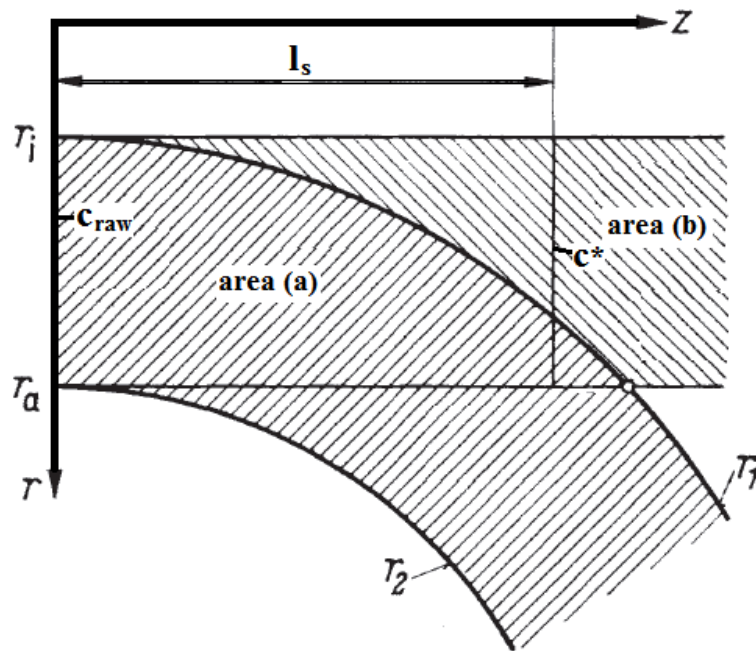
Figure 28: Areas of concentration in a rotational flow[15]

The concentration in this area is calculated with formula (3-43) and formula (3-44).

$$\ln \frac{c^*}{c_{raw}} = -\frac{2k_{rv}}{w_z} z \tag{3-43}$$

$$c^* = c_{raw} \cdot e^{-\frac{2k_{rv}}{w_z}z} \tag{3-44}$$

The concentration is constant regardless of the radius, because the displacement velocity increases simultaneously to the volume with the radius. The dust loading c^* varies only in the flow direction. In the second area the concentration is $c^*=0$, because no dust is fed in the core (i.e., $r < r_i$).

The intersection of these areas are calculated from equation (3-41).

$$r_a = r_i \cdot e^{\frac{k_{rv}}{w_z}z} \tag{3-45}$$

$$z_s = \frac{w_z}{k_{rv}} \cdot \ln \frac{r_a}{r_i} \tag{3-46}$$

In the case that the length L_s of the separation chamber is longer than the parameter z_s the dust is completely separated ($\eta_t = 1$). For $l_s< z_s$ the separation efficiency can calculated by formula (3-47).

$$\eta_t = \frac{c_{raw} - c_{clean}}{c_{raw}} \tag{3-47}$$

The dust load at the end of the separation room is calculated by formula (3-48).

$$c_{clean} = \frac{r_a^2 - r_1^2}{r_a^2 - r_i^2} c^* \tag{3-48}$$

With equation (3-41) and (3-44) formula (3-49) is valid for $l_s< z_s$.

$$\eta_t = 1 - \left(e^{-\frac{2k_{rv}}{w_z}l_s}\right) \cdot \frac{r_a^2 - r_i^2 \cdot e^{\frac{2k_{rv}}{w_z}l_s}}{r_a^2 - r_i^2} \tag{3-49}$$

If the particles do not have the same diameter, the last equations could by calculate with the parameters of chapter 2.2.

3.2.3.3 Characteristics of a dedusting centrifuge

The main advantage of a dedusting centrifuge is the small critical particle size that can be separated. In comparison to the rotary flow dust separator, the separation efficiency is not limited by turbulent diffusion[15]. Higher peripheral velocities are possible. The lower border of the critical particle size is determined by molecular diffusion.

3.3 Combinations of gravity and centrifugal dust separators

A combination of gravity and centrifugal dust separators may prove effective indeed because flue gas direction changes are often required and a combined dust separator has a low space requirement[15]. This chapter provides a general overview of combined gravity and centrifugal dust separators and is based on the work of Batel[15]. Detailed design principles are described in chapter 3.1 for gravity and in chapter 3.2 for centrifugal dust separators.

3.3.1 Basics of gravity and centrifugal combined dust separators

Gravity forces for particle motion are relatively low in relation to centrifugal forces. With this argument the idea is born to support gravity forces with centrifugal forces. The results are separators with single or multiple flow redirections. The separation forces are significantly higher than gravity.

3.3.2 Design principles of gravity and centrifugal combined dust separators

To calculate the separation efficiency of a combined gravity and centrifugal dust separator a simplified model is necessary. This model describes a curved gravity dust separator with no revolution and is shown in Figure 29.
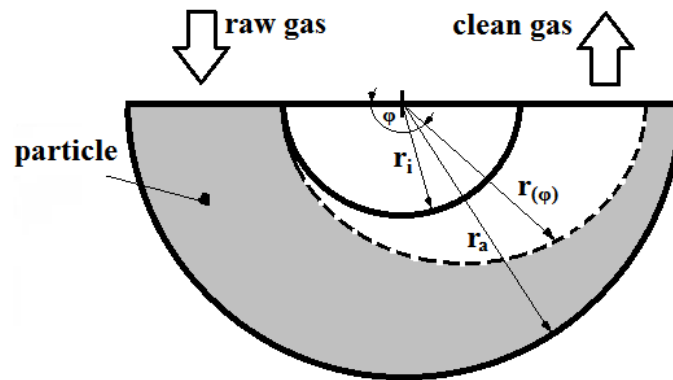
Figure 29: Principle of a combined gravity and centrifugal dust separation

Equation (3-50) describes a curve that determines a dust free room in the separator. This curve is shown in Figure 29.

$$c^*(\varphi) = c_{raw} \frac{r_a - r(\varphi)}{r_a - r_i} \qquad \textbf{(3-50)}$$

The parameters c_{raw} and c^* at the position $(\varphi = \pi)$ were available with equation (3-50) and the calculation of η_t is possible. The following equations are valid for homogeneous dust and a constant gas velocity. Dust particles would leave the separator at the radius r with the tangential

component $w_t = v_g$ of velocity, if no gravity or centrifugal forces exist. The centrifugal forces produce the component w_r. The solution without centrifugal forces for the dotted line in Figure 29 is shown with equation (3-51).

$$r(\varphi) = r_i \frac{v_g + w_g}{v_g + w_g \cdot \cos\varphi} \tag{3-51}$$

The dedusting is applied at the volume of the separation chamber by the form of the model. This approach is not suitable for a plane construction. The dotted line in Figure 29 with centrifugal forces is described by equation (3-52).

$$r(\varphi) = r_i + \frac{1}{18\mu}\left(\varrho_s - \varrho_g\right) \cdot d_p^{\,2} \cdot v_g \cdot \varphi \tag{3-52}$$

The described curve is an Archimedean spiral. The total separation efficiency depends on the radial displacement. This displacement is a function of gas velocity, the angle φ, but not of the curvature.

3.3.3 Types and characteristics of gravity and centrifugal combined dust separators

Combined gravity and centrifugal dust separators can be categorized into two groups:

- flow redirections without flow distribution

- flow redirections with flow distribution

Some examples are shown in Figure 30 and Figure 31.
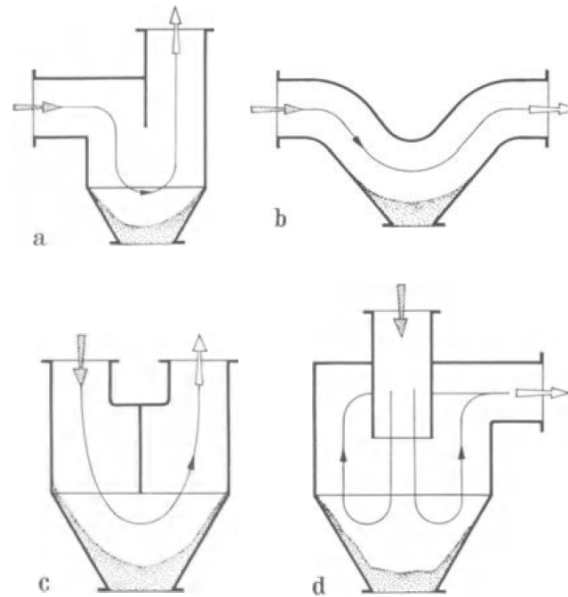
Figure 30: Redirection separator without flow distribution[15]
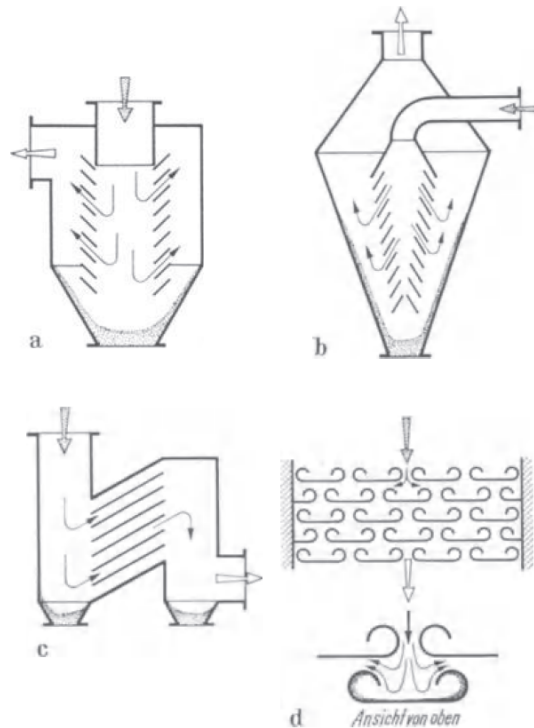
Figure 31: Redirection separator with flow distribution[15]

3.4 Electrostatic dust separator

In chapter 3.1, 3.2 and 3.3 the particles are separated by a displacement of gravity and centrifugal forces. Another separation principle is the separation by electrical forces. An electric dust separator is an apparatus, that separates solid or liquid particles from a carrier gas by producing an artificial electric field. Electrostatic precipitators are described well in the work of Parker[49], Batel[15] and Robel et al.[16]. These authors provide the information for this chapter.

3.4.1 Basics of electrostatic precipitators

In case a charge is introduced in an electrical field, then a force, the Coulomb force, acts on the charged object. This electrostatic force is described by formula (3-53).

$$F_{Co} = q \cdot E \qquad \text{(3-53)}$$

$$q = n_v \cdot e \qquad \text{(3-54)}$$

Equation (3-53) and (3-54) describe the required environment in the separation room. A unipolar charging of the particles and a strong electrical field with the right direction is necessary. Dust particles have a mixed charge or no electric charge at the inlet of the separator. A separation is only possible with a same-polarity charge. This charging takes place at separate chamber or in the same chamber by an overlapped operation. The overlapped operation is typical for an electrostatic precipitator. Figure 32 shows a scheme of an electric dust separator.
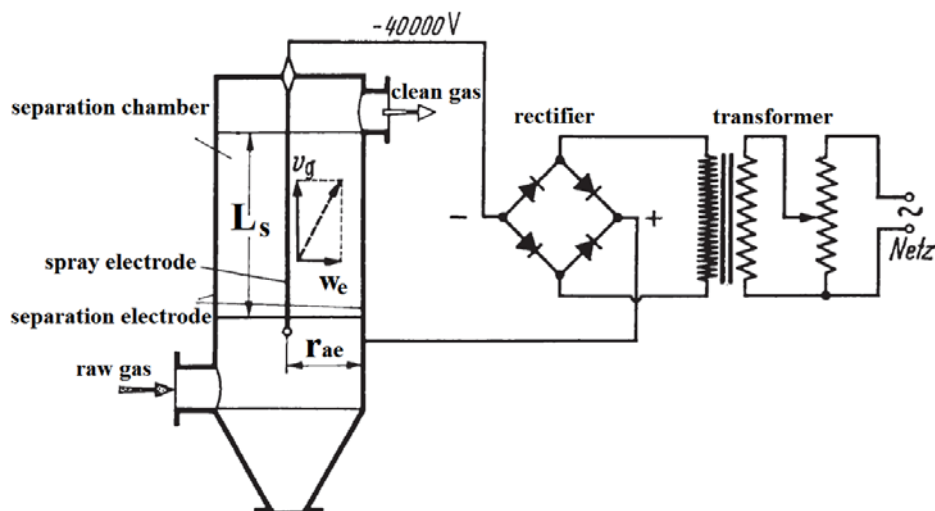
Figure 32: Scheme of a electrostatic precipitator (r_{ie} radius spray electrode, r_{ae} radius dust separation room)[15]

The separation chamber consists of a grounded tube. In the middle of this tube is a thin wire positioned which is isolated to the housing. At this wire a negative voltage (e. g., -40 000 [V]) is applied and a potential gradient between the wall and the wire exists. The particles move to the

wall of the tube because they get a negative charging close to the wire. This wall is called the separation electrode and the wire is called spray electrode. The current between the electrodes is called spray or ion current. Transformer and rectifier are required to produce the high voltage direct current. The principle of electrostatic dedusting is work through five different processes:

- Generation of electric charges

- Charging of particles

- Displacement of particles

- Separation of the particles by the separation electrode

- Cleaning of the separation surface

3.4.1.1   Generation of electric charges

The current depends on the number and velocity of charges. Formula (3-55) describes the field strength between two concentrically cylinders (Figure 33).

$$E = \frac{U}{r \cdot \ln\frac{r_a}{r_i}} \qquad\qquad \text{(3-55)}$$
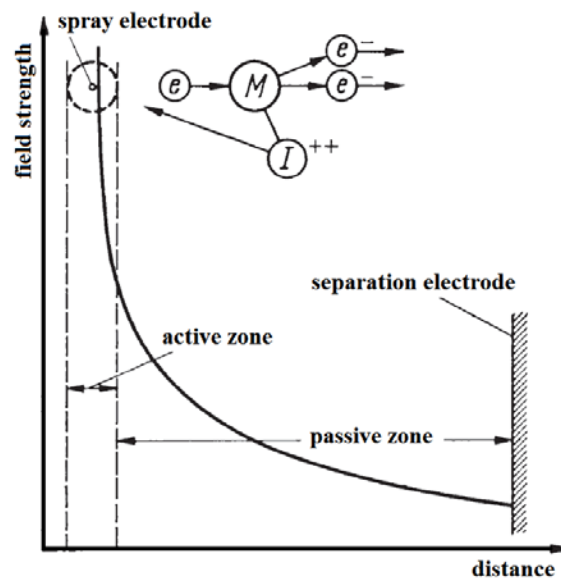
Figure 33: Charge generation in the spray field (e...electron, I...ion, M...molecule)[15]

Formula (3-56) describes a strong potential gradient in the vicinity of the thin wire with the radius r_{ie}. Free electrons are getting accelerated by the potential gradient and impact at gas atoms or gas molecules. New free electrons and positive gas ions arise. In the case of adsorbed free electrons, negative gas ions exist. This process is increasing like an avalanche in the area of the potential gradient. The area is known as "active zone". The produced electrons enter the spray electrode. Negative charges leave the active zone and move to the separation electrode. This displacement is

based on the electrical field. The separation chamber is completely filled with charges. A measurement for these charges is the spray current. A minimum voltage, a potential gradient in the active zone and a good space utilization in the separation room is required for a stabile corona and a good dust separation. In the case of an incompletely space utilization, a spark discharge and a breakdown of the electric field are possible.
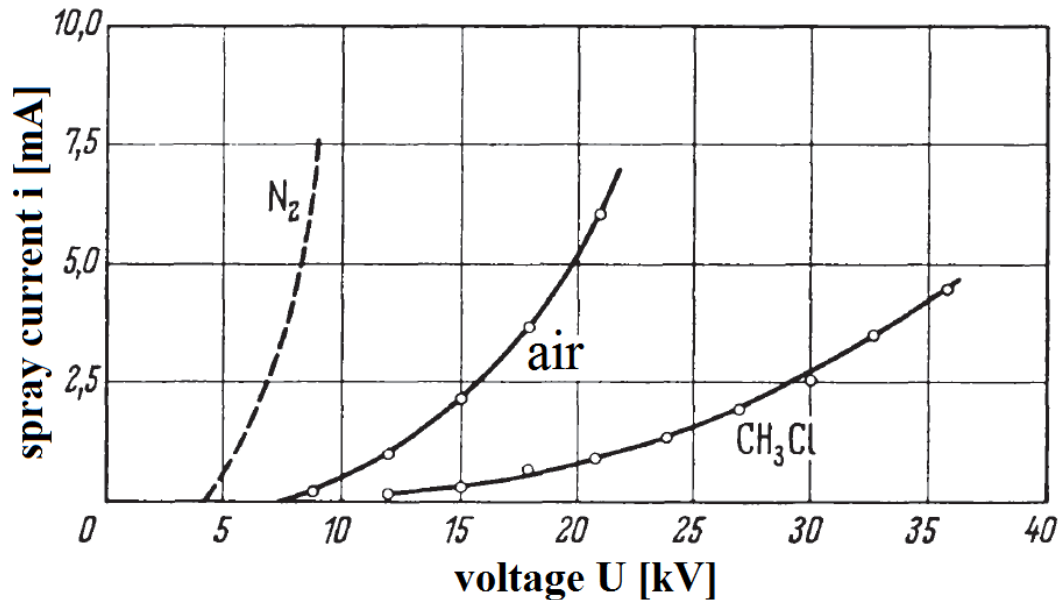
Figure 34: Spray current, depending on voltage at different gases and equal geometrical dimensions[15]

Figure 34 shows the dependence of the spray current on the gas. Electrons are up to 1000 times faster than gas ions at atmospheric conditions. Molecules of nitrogen, hydrogen, helium, neon and argon hardly adsorb any electrons. The charges in these gases consist of electrons and cause a higher spray current. Oxygen, water vapour, chlorine, carbon dioxide and sulphur dioxide have a strong electron affinity. The negative charges consist of gas ions and cause a lower spray current. These gases are called electronegative gases.

Pressure and temperature also influence the ion mobility. The ion mobility decreases with higher pressure or density. The temperature has a minor influence on the ion mobility. In the case of a gas with a high amount of electronegative gas components, a stable negative corona is possible.
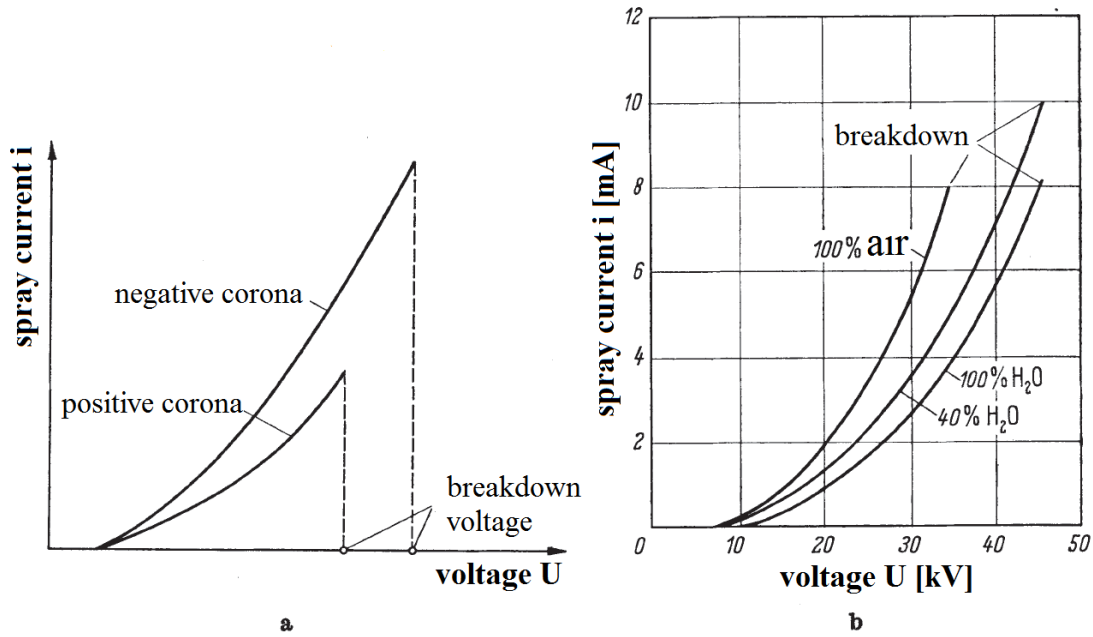
Figure 35: Current-voltage-curves in electric dedusting[15]
a) positive and negative Corona, b) negative Corona in air and water vapour air mixture

Figure 35 shows important curves for electrostatic dust separation. These curves display the spray current and the breakdown voltage. The breakdown voltage depends on the gas, temperature, pressure, type of corona and the processes at the separation electrode. A positive corona generates the required space charges, but this type of corona is unsuitable for dedusting because the breakdown field strength is too low (Figure 35).

Electric dedusting does not require current-voltage curves that are too steep. Nitrogen (Figure 34) is not suitable for a stable corona. The range between corona initial voltage and breakdown voltage is too small. Air has good characteristics for dedusting and an improvement is possible through the addition of water vapour, SO_2 or SO_3. The corona initial voltage must be determined through experiments. A critical field strength is needed and can be calculated by formula (3-56)[50].

$$E_{crit} = 31m \cdot \left(1 + \frac{0.308}{\sqrt{r_{ie}}}\right) \qquad \text{(3-56)}$$

r_{ie} [cm] radius of the spray wire, m coefficient of the wire surface (m=1 for polished surfaces). The required initial voltage is calculated by formula (3-57) and the spray current by formula (3-58).

$$U_i = 31m \cdot \left(1 + \frac{0.308}{\sqrt{r_{ie}}}\right) \cdot r_{ie} \cdot \ln\frac{r_{ae}}{r_{ie}} \qquad \text{(3-57)}$$

$$i = n^* \cdot e \cdot S \cdot U_i \cdot E \qquad \text{(3-58)}$$

The ion mobility in air has a value of 1.8 [cm²/Vs]. This parameter must be determined through experiments. Dust particles in the separation room can reduce the spray current and thereby the field strength and the ionization process[51].

3.4.1.2 Charge uptake by particles

Particles are getting charged during their way from the inlet to the separation electrode. Charged gas molecules adsorb to dust particles and charge them. The charging rate depends on the charge density and the charge motion. Typical for an evacuated room are charging motions along the field lines, but more motions is generated by gas molecule impacts in the gas filled chamber. These motions are called Brownian motion. The charging with the electric field is based on field charges while the charging via Brownian motions is based on diffusion charges. Particles with a diameter larger than 1 [µm] are primarily charged by the forces of the electrical field. In the case of diameters lower than 1 [µm], particles are charged by diffusion.

Charging by the electrical field

The field charging deals with the impacts by motion of charges in the electric field. Diffusion is excluded. Figure 36 shows the direction of the field lines. The field lines distort in the vicinity of a dust particle because particles have a higher dielectric constant than air. As a consequence, particles obtain more charges that correspond with their cross sectional area.
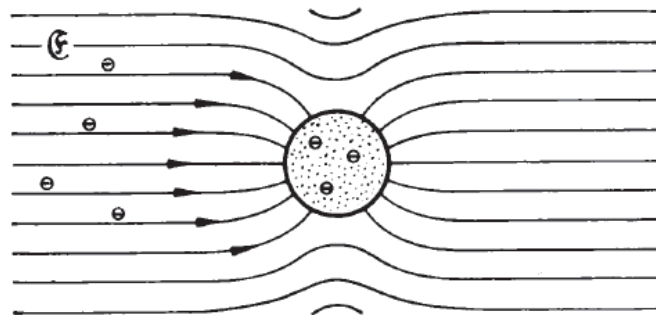
Figure 36: Direction of electric field lines near a dust particle[15]

The number of inflowing ions increases with the amount of ions at the particle. It can be recognized that the charge depends on the density of ions, electric field, particle size, time and the electrical properties of the dust. This charging process was investigated by Pauthenier and Moreau-Hanot[52], Rohmann[53], White[54] and Böhm[55].

Pauthenier[52] define equation (3-56) with the following simplifications:

- spherical particles

- the particle distance is big in relation to the particle diameter

- the ion concentration and the electric field are homogenous

- charged particles have no influence on uncharged particles

$$q = n \cdot e = \frac{3 \cdot \varepsilon_r}{\varepsilon_r + 2} \cdot \frac{d_p{}^2}{4} \cdot \frac{t}{t + t_c} \cdot E \qquad \text{(3-59)}$$

Lowe and Lucas[39] discovered that the maximum charge with an ion concentration of 10^8 to 10^9 elementary charges per cm³ is reached in less than one tenth of a second. Consequently, it may be sufficient to calculate with the limited charge at $t \to \infty$.

$$q = \frac{3 \cdot \varepsilon_r}{\varepsilon_r + 2} \cdot \frac{d_p{}^2}{4} \cdot E \qquad \text{(3-60)}$$

Charging by molecular diffusion

The influence of the field charge disappears for small particles (d < 1 [μm]) and Brownian motion creates the impacts between charged species and dust particles. Arendt and Kallmann[56] investigated the charging process by diffusion (valid for a tube electrostatic dust separator).

$$e \cdot \frac{dn^*}{dt} \left(1 + \frac{d_p{}^2}{16} \cdot \frac{c_{iv}}{n^* * U_i * e} \right) = \pi \frac{d_p{}^2}{4} \cdot f \cdot c_{iv} \cdot e^{-\frac{2n^* \cdot e^2}{d \cdot k_B \cdot T}} \qquad \text{(3-61)}$$

The number of particles in the borderline case can be approximated by the result of Ladenburg[57] (Equation (3-62), with d_p [cm]).

$$n^* \approx 10^6 \cdot d_p \qquad \text{(3-62)}$$

White[54] described the charging by diffusion with an alternative approach and developed formula (3-63) with similar results.

$$q = n_v \cdot e = \frac{d_p \cdot k_B \cdot T}{2e} \cdot \ln \left(1 + \frac{\pi \cdot d_p \cdot c_{iv} \cdot n^* \cdot e^2}{2 \cdot k_B \cdot T} \cdot t \right) \qquad \text{(3-63)}$$

Lowe and Lucas[39] compared both mechanisms and discovered that the number of added charge of particles with a size of 1 [μm] are equivalent.

3.4.1.3 Discharge of particles

Discharge forces are calculated by formula (3-53) and (3-55). Charges are created by the corona discharge and influence the field strength. The field distribution is described by Poisson's differential equation (3-64).

$$\frac{1}{r} \cdot \frac{d}{dr}(E \cdot r) - 4\pi \cdot n^* \cdot e = 0 \tag{3-64}$$

If the spray current is related to 1 [cm] spray wire length, then the charge density could be modified to formula (3-65) and formula (3-64) to (3-66).

$$n^* \cdot e = \frac{i_1}{2} \cdot \pi \cdot r \cdot U_i \tag{3-65}$$

$$\frac{dE}{dr} + \frac{E}{r} - \frac{2i_1}{r \cdot U_i \cdot E} = 0 \tag{3-66}$$

Formula (3-67) is the result of the integration with $r = r_{ie}$ and $E = E_{crit}$.

$$E = \left\{ \left(\frac{r_{ie}}{r} \cdot E_{crit} \right)^2 + \frac{2i_1}{U_i} \cdot \left[1 - \left(\frac{r_{ie}}{r} \right)^2 \right] \right\}^{\frac{1}{2}} \tag{3-67}$$

At high spray currents and $r_{ae} \ll r_{ie}$ formula (3-67) can by simplified to (3-68).

$$E = \left(\frac{2i_1}{U_i} \right)^{1/2} \tag{3-68}$$

Troost[58] developed a simplification for plate electrostatic precipitators (formula (3-69)).

$$E = \left(\frac{8i_1 \cdot s_p}{U_i \cdot h_{se}} \right)^{1/2} \tag{3-69}$$

The discharge velocity of dust particles in an electric field is now calculated by the equation (3-53), the simplification $F_R = F_{Cel}$ (Figure 37) and Stokes law with the correction of Cunningham[22] and Davies[23].
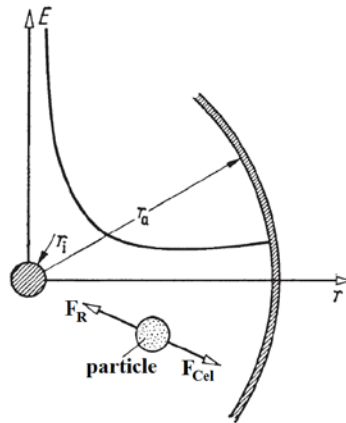
Figure 37: Forces at a dust particle in an electrostatic precipitator (not true to scale)[15]

The summarized equation is described in formula (3-70).

$$n_V \cdot e \cdot E = 3\pi \cdot \mu \cdot d_p \cdot w_s / \left(1 + \frac{2A_{Cu} \cdot l_{gm}}{d_p} \right) \tag{3-70}$$

$$w_s = \frac{n \cdot e \cdot E \cdot \left(1 + \frac{2A_{Cu} \cdot l_{gm}}{d_p}\right)}{3\pi \cdot \mu \cdot d_p} \tag{3-71}$$

For d > 1 [μm], and the assumption that the field strength of the charge and the discharge is equal, formula (3-72) is valid.

$$w_s = \frac{\varepsilon_r}{(\varepsilon_r + 2) \cdot \pi \cdot \mu} \cdot \frac{d_p}{4} \cdot E^2 \tag{3-72}$$

For d < 1 [μm] and particle charging via the diffusion mechanism, formula (3-73) is valid.

$$w_s = \frac{10^6 \cdot e \cdot E \cdot \left(1 + \frac{2A_{Cu} \cdot l_{gm}}{d_p}\right)}{3\pi \cdot \mu} \tag{3-73}$$

The discharge velocity of particles with d > 1 [μm] increases proportionally with an increasing d or field strength. For particles with d < 1[μm] the velocity is independent of the particle size (without Cunningham correction). A high field strength effects a good separation. The upper limit of the field strength is provided by the breakthrough resistance of the gas.

3.4.1.4   Separation of the particles at the separation electrode

The unipolar charged particles move due to the electric field to the separation electrode and stick to it. If the drag forces of the gas flow are lower than the adhesive forces then the particle is separated.

The influence of the separated dust depends on the specific dust resistance. This parameter describes the electric resistance of an area with 1 [cm²] and a dust thickness of 1 [cm]. It could be classified into three areas:

a) low specific resistance ($< 10^4$ [Ω cm])

Dust particles with this specific resistance have a high conductivity and change their charging instantly into the polarity of the separation electrode. The particles that get rejected back into the gas flow by this charge cycle generate a bounding behaviour. The separation of this particle size range is difficult. Typical examples are pure carbon ($3 \cdot 10^3$ [Ω cm]) and some pure metal oxides.

b) medium specific resistance (10^4 - $2 \cdot 10^{10}$ [Ω cm])

Particles in this range are ideally for separation with electrostatic precipitators.

c) high specific resistance ($2 \cdot 10^{10}$ [Ω cm])

Particles with a higher resistance than $2 \cdot 10^{10}$ [Ω cm] retain their charges and build an insulating coating. A high amount of the spray electrode current does not permeate this insulating layer. Positive charges gather under the dust layer and negative charges at the gas side. A potential gradient exists and produces a discharge by an electric impulse.

If the electrostatic dust separation is difficult in the case of a high specific resistance, the dust resistance could be modified by an injection of water, SO_3 or ammonia[59,60].

The characteristic behaviour of the specific dust resistance depending on the temperature is shown in Figure 38. The resistance is increasing with the temperature to a maximum. Before this maximum is reached, the surface resistance is predominant. Particles adsorb a liquid film, thereby the conductivity improves. The liquid film decreases with an increasing temperature and the resistance grows.
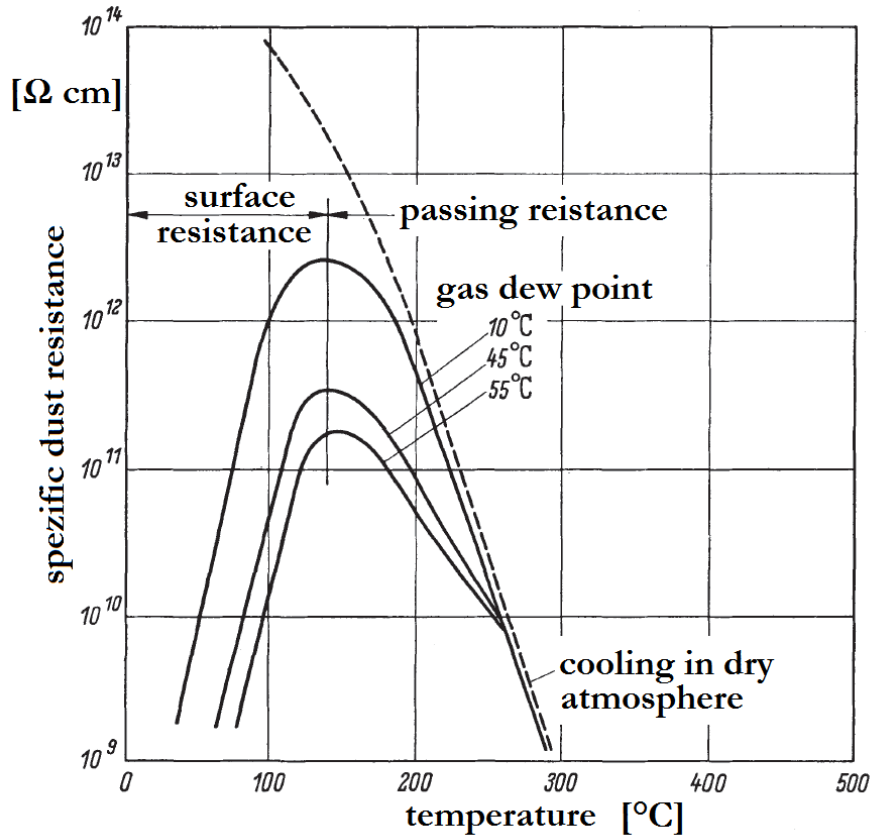
Figure 38: Dependency of the specific resistance on the temperature[61]

The effect of the specific resistance is growing at higher temperatures. This resistance is described by equation (3-74).

$$\varrho_e = A_{sr} \cdot e^{\alpha_{sr}/T}$$

<div align="right">(3-74)</div>

The effect of moisture and temperature on the electrical resistivity is shown in Figure 39 by an example of coal fly ash. The influence of moisture decreases at higher temperatures.
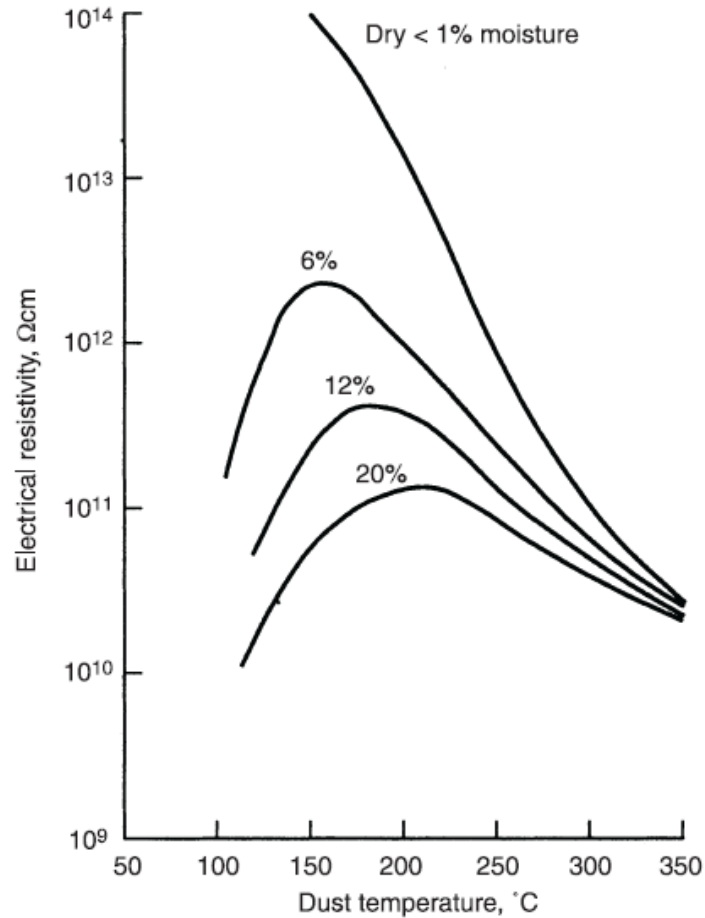
Figure 39: The effect of moisture on electrical resistivity[49]

3.4.1.5 Cleaning of the separation surface

An effective cleaning process is required for a continuous operation of the separator. During the cleaning it is important that the dust is kept away from the gas flow. Cleaning methods are electrode washing, shaking or vibrating of the electrodes. In all cases a good transport of the separated dust into the dust bunker is possible by constructive design elements like bypass tubes or flow dead spaces.

3.4.1.6 Separation performance of electrostatic precipitators

In an early work of Deutsch[62] the separation performance of electrostatic precipitators is explained. He makes the following assumptions: a homogenous dust distribution in the gas flow, all particles at the separation electrode are separated, and the discharge velocity is independent of the particle size.

$$dM_d = -2r_{ae} \cdot \pi \cdot c^* \cdot w_E \cdot dt \tag{3-75}$$

The total separation efficiency can calculated by equation (3-76).

$$\eta_t = 1 - \frac{c_{clean}}{c_{raw}} = 1 - e^{-\frac{2w_E \cdot L_s}{r_{ae} \cdot v_g}} \tag{3-76}$$

For a rectangular separation chamber equation (3-77) is valid (Deutsch relationship[62]).

$$\eta_t = 1 - e^{-\frac{w_E \cdot L_s}{s_p \cdot v_g}} \tag{3-77}$$

Formula (3-77) is sufficiently exact for the assumptions stated above. Deutsch[62] verified his equation with many measurements. Heinrich calculates migration velocities from measured total separation efficiency rates. His work is shown in Figure 40.
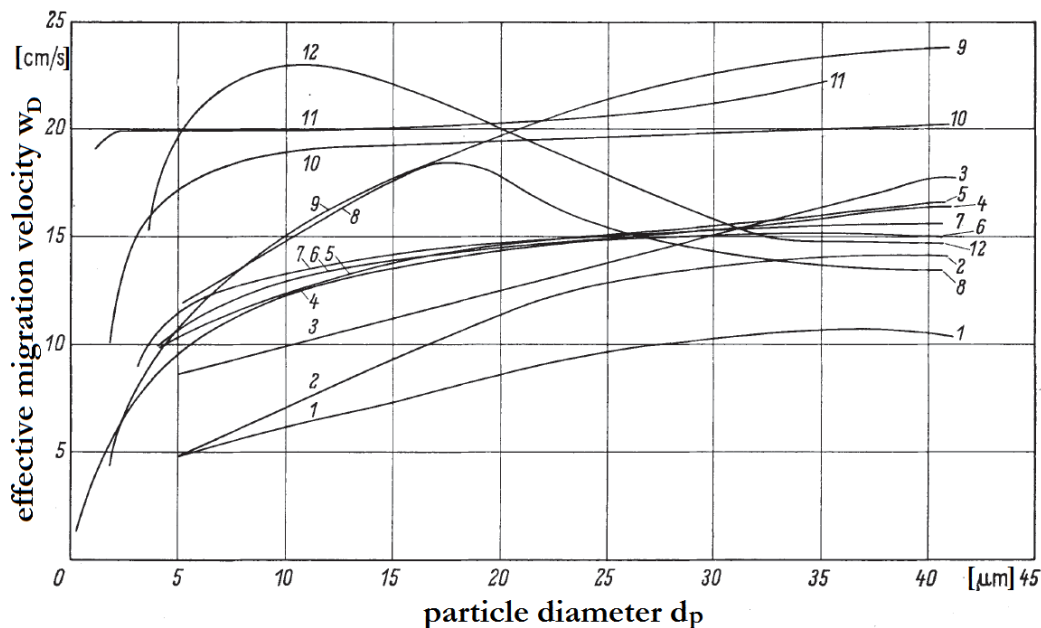
Figure 40: Dependency of the effective migration velocities w_D on the particle size[63]
1 flue dust, horizontal electrostatic precipitator v_g=0,84 [m/s]; 2 flue dust, horizontal electrostatic precipitator v_g=1,07 [m/s]; 3 flue dust, horizontal electrostatic precipitator v_g=1,83 [m/s]; 6 flue dust, horizontal electrostatic precipitator v_g=1,9 [m/s]; 7 flue dust, horizontal electrostatic precipitator v_g=2,72 [m/s]; 9 flue dust, horizontal electrostatic precipitator v_g=1,9 [m/s]; 10 flue dust, horizontal electrostatic precipitator v_g=1,6 [m/s]; 8 flue dust, vertical electrostatic precipitator v_g=2,5 [m/s]; 12 flue dust, vertical electrostatic precipitator v_g=1,9 [m/s]; 4 catalyst dust, horizontal electrostatic precipitator v_g=1,7 [m/s]; 11 carbon dust, vertical electrostatic precipitator v_g=1,17 [m/s]

A comparison of the Deutsch relationship and the Matts-Ohnfeldt relationship with an increasing gas flow is shown in Figure 41. Both equations provide good results and they are commonly used. The Matts-Ohnfeldt[49] relationship of the separation efficiency is shown in equation (3-78).

$$\eta_t = 1 - e^{-\frac{L_s}{s_p}\sqrt{\frac{w_E}{v_g}}} \tag{3-78}$$
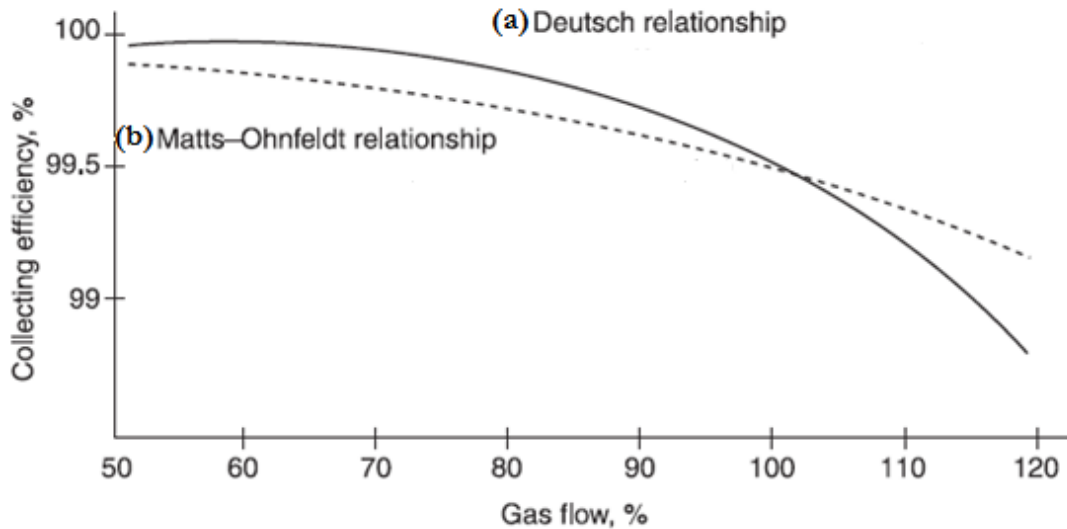
Figure 41: Effect of gas velocity upon separation efficiency; (a) equation (3-77), (b) equation(3-78)[49]

3.4.2 Mode of action of electrostatic precipitators

Robel et al.[16] provides an overview of the operation of electrostatic precipitator. The raw gas flows through a separation chamber with two kinds of electrodes. These two electrodes are sharp-edged spray electrodes (charging bars) and plane collecting electrodes (separation electrodes). The particles (liquid or solid) are loaded unipolar by a Corona discharge and therefore they are moved by an electric field to the separation electrode. The Corona discharge and the electric field is produced by a voltage of 30 to 80 [kV] at the sharp-edged spray electrodes. At the opposite site are the collecting electrodes as the grounded positive pole.

3.4.3 Types of electrostatic precipitators

An electrical dust separation system consists of the electrostatic precipitator and the high-voltage generator. The components of the electrostatic precipitator are:

- The housing of the gas in- and outlet
- The dust bunker
- A system of collecting electrodes
- A system of separation electrodes
- The cleaning unit for the electrodes
- The high voltage bushing

There are many types of electric dust separators. They can be classified according to the type of the collecting electrode or flow direction. Electrostatic precipitator can work in a dry or wet operation. Wet electrostatic precipitators are not part of this thesis.

The type of the collecting electrode

Typical are plate-, tube shaped or honeycombed separators. (Figure 42)
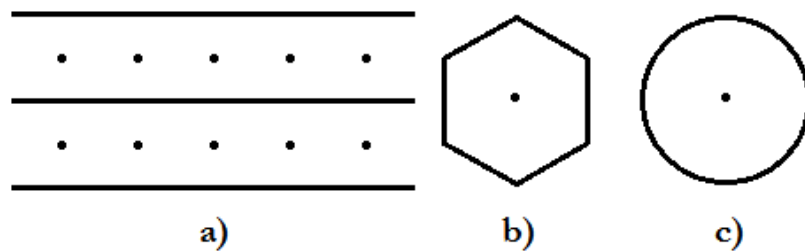
Figure 42: Shapes of collection electrodes
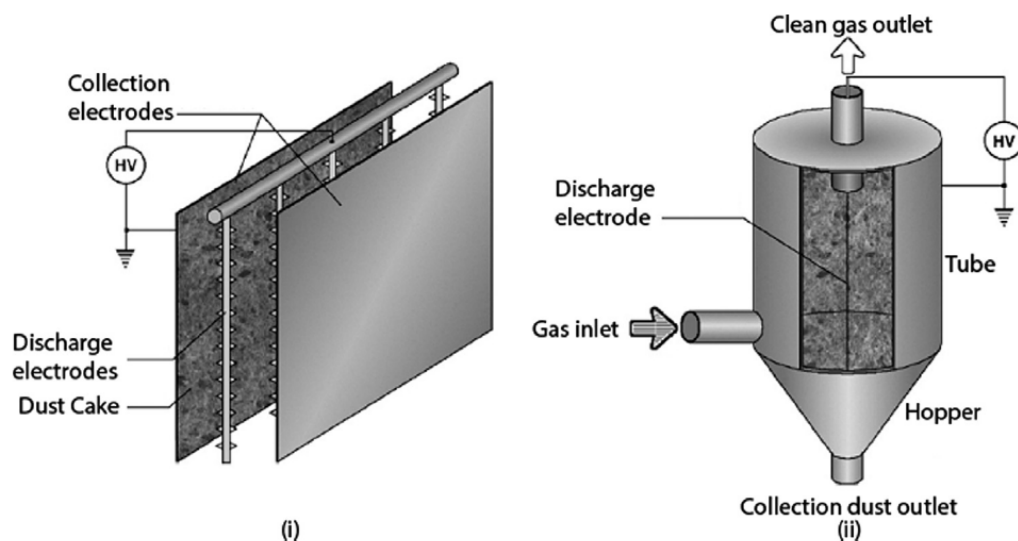
Figure 43: Two types of electrostatic precipitators: (i) parallel-plate and (ii) tubular[64]

The most common types of electrostatic precipitators are the parallel-plate and the tubular electrostatic precipitator (Figure 43). Electrodes can be realized in many different forms and profiles. Some typical electrode forms are illustrated in Figure 44.
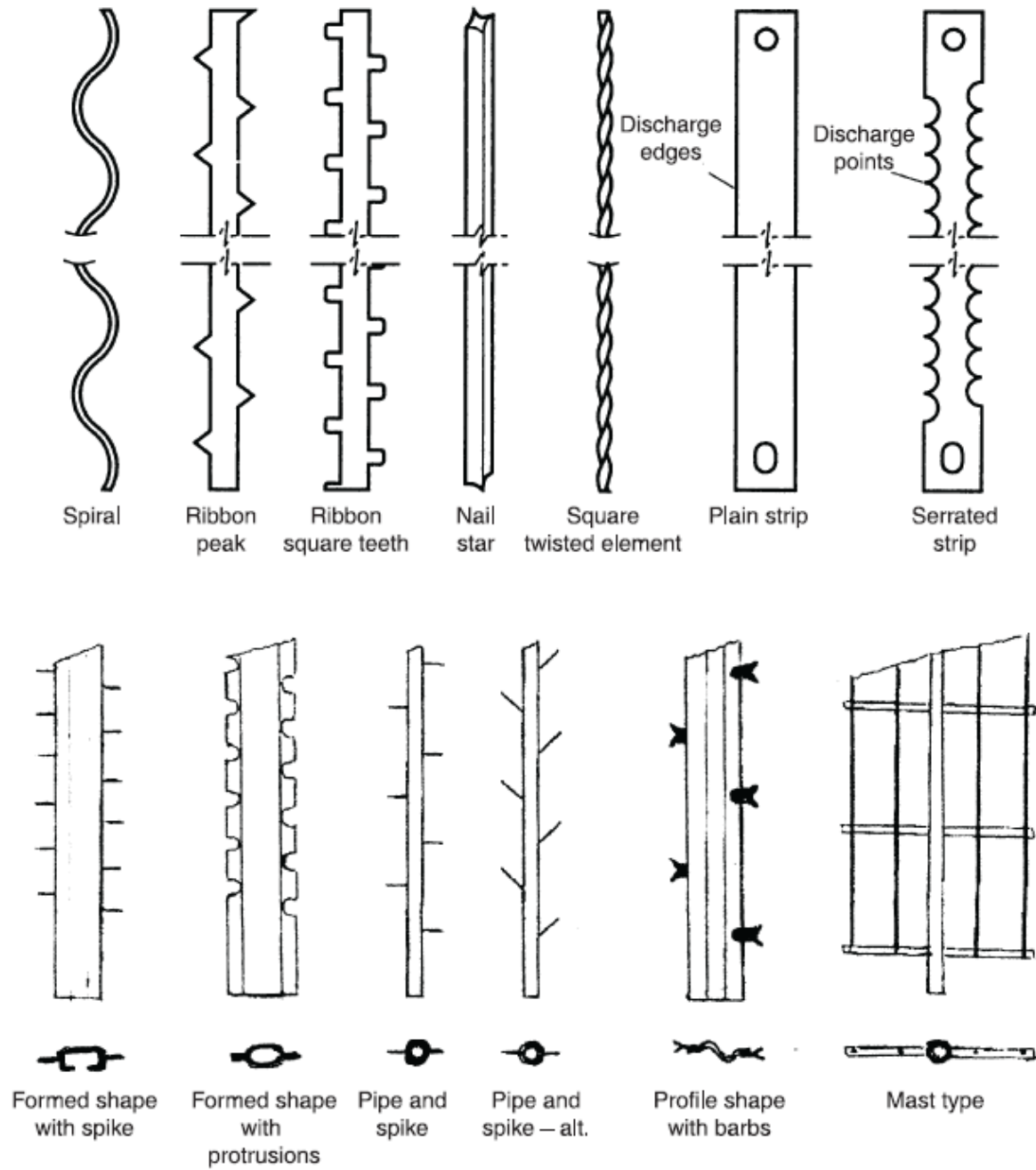
Figure 44: Typical electrode forms[49]

The type of flow direction

Electrostatic precipitators operate with a vertical or a horizontally flow direction. Both types are shown in Figure 45.
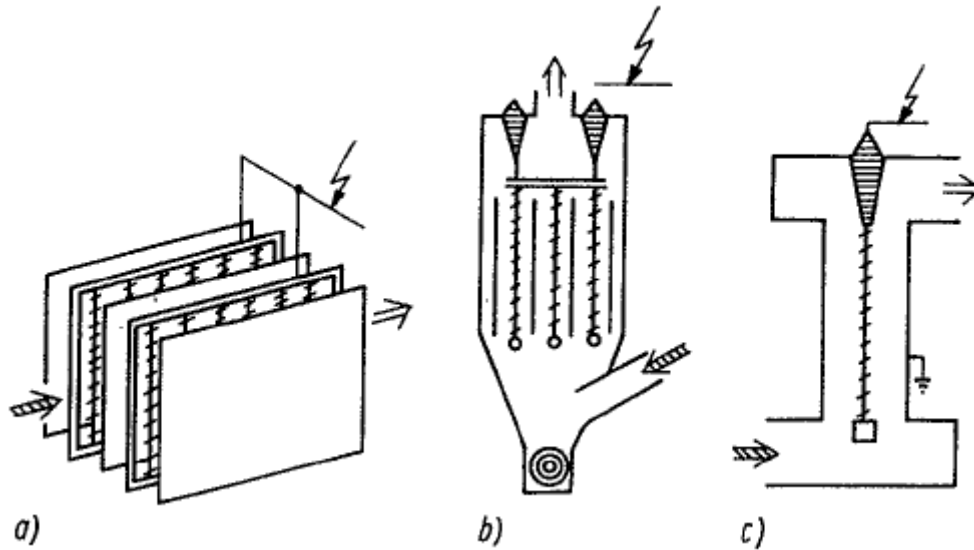
Figure 45: a) horizontal electrostatic precipitator; b) and c): vertical electrostatic precipitator[16]

The structure of a typical horizontal electrostatic precipitator is shown in Figure 47. Separators of this type consist of a gas inlet, gas outlet, gas distribution wall, spray electrodes, separation electrodes, the plate head rods, the separation electrode beating equipment, the spray electrode beating equipment, the insulator, the dust hopper and the dust discharge.

The type of arrangement

Electrostatic precipitators operate in a single-stage or in a two-stage arrangement. The single-stage type is the most common industrial precipitator. The same electrodes produce the charging and migration in one stage. The second type is the two-stage precipitator with a charging and a collecting stage. This precipitator is typical for air cleaning applications. Both types are shown in Figure 46. A horizontal dry electrostatic precipitator with its equipment is illustrated in Figure 48.
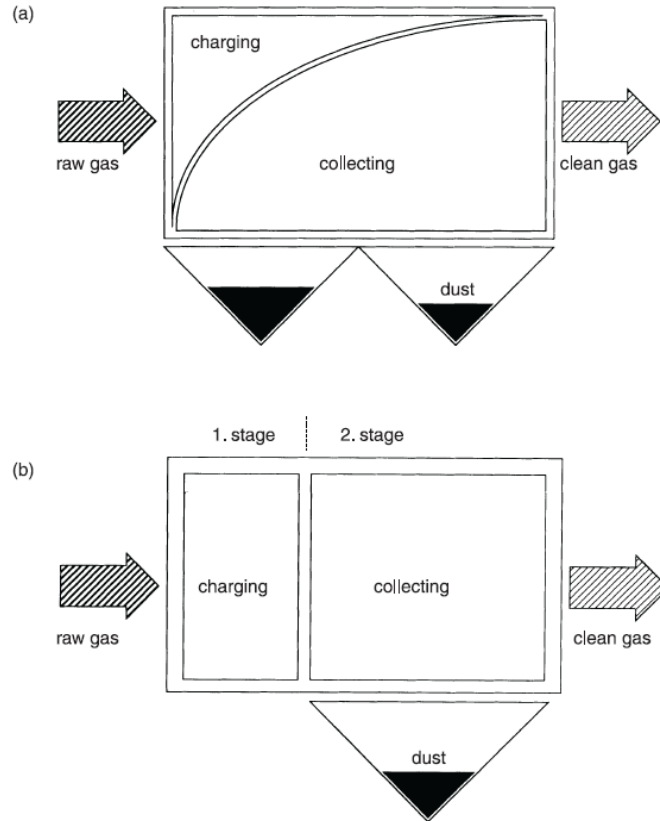
Figure 46: Basic precipitator arrangements; (a) single-stage type, (b) two-stage type[49]
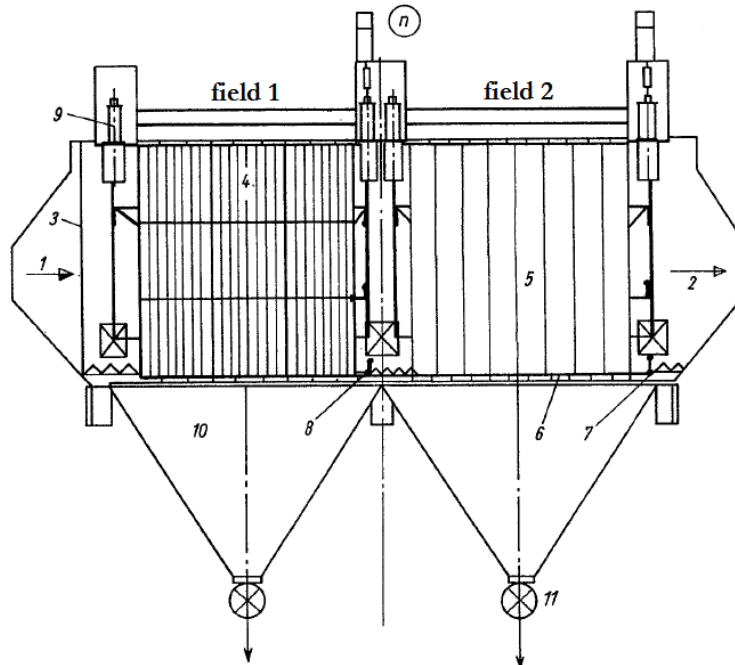
Figure 47: Horizontal dry electrostatic precipitator with two fields[16]

(1) gas inlet (diffusor), (2) gas outlet, (3) gas distribution wall, (4) spray electrode, (5) separation electrode, (6) plate head rods, (7) separation electrode beating equipment, (8) spray electrode beating equipment, (9) insulator, (10) dust hopper, (11) dust discharge, n spray electrode beating equipment drive
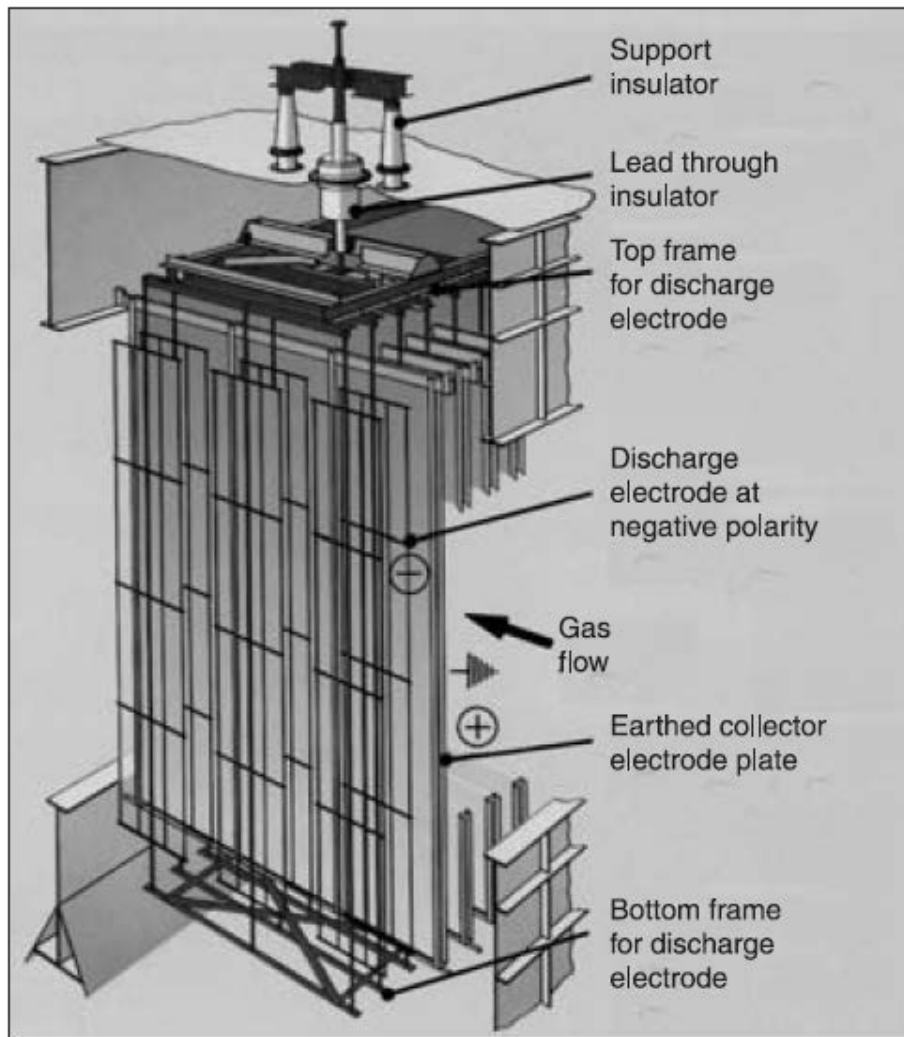
Figure 48: Typical mechanical arrangement of a dry precipitator (courtesy Lodge Sturtevant Ltd)[49]

3.4.4 Characteristics of electrostatic precipitators

Electrostatic precipitators have the following advantages:

- a separation of small solid or liquid particles is possible

- electric separators work in a temperature range to 750 [K] (in special cases to 1300 [K])

- the temperature and pressure drop through the separator is low

- a low operation and maintenance effort

- a good partial load behaviour

Disadvantages of electrostatic precipitators:

- high investment costs

- high space requirement

- gas-dust conditions affect the operation and separation efficiency

- electrical energy is a potential source of ignition

High-voltage generator

The high-voltage generator equipment consists of:

- the direct voltage generator

- the control cabinet

- the electrical connection system

- the damping resistance for the protection of the high-voltage rectifier and the high-voltage cable

The selection of the high-voltage generator requires the parameters of the maximum connected load, the nominal direct current, the nominal voltage and the peak value of the voltage.

Influence of the electric field strength

The electric field strength affects the separation efficiency. Especially the particle separation of particles with a diameter between 10^{-1} and 10^{0} [µm] is sensitive to the electric field strength. Results to this effect from Nussbaumer and Lauber[65] are shown in Figure 49.
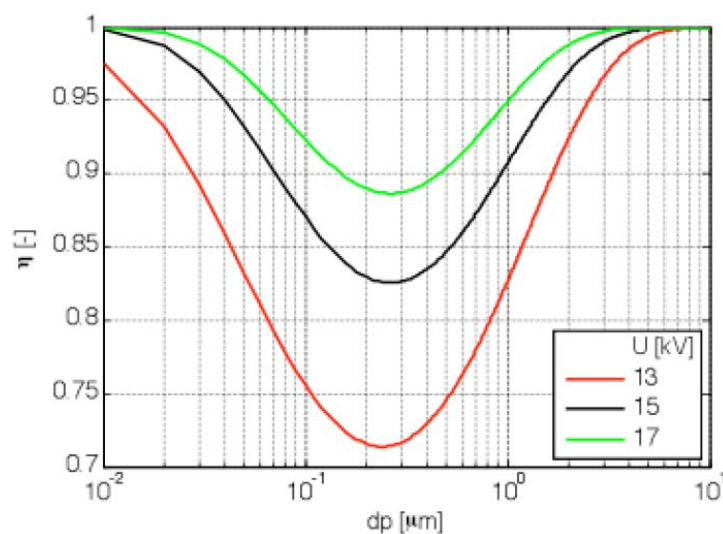
Figure 49: Influence of the electric field strength on the separation efficiency[65]

3.4.5 Design principles of electrostatic precipitators

The separation of the particles from the gas works in a three way process. At first, the particles move in the direction of the separation electrode, then they stick to the separation electrode. Finally, the particles get separated into a dead flow zone. The details of these processes are described in chapter 3.4.1.

A high total separation efficiency can be achieved with two different strategies. These strategies are described in the work of Beer[66].

A high voltage level

A high voltage level (70-80 [kV]) allows a high migration velocity and reduces filter surface and filter volume. This is a good strategy to save costs in big plants.

A low voltage level

A low voltage level (20-25 [kV]) reduces the migration velocity and requires more filter surface. This method is advantageous in small plants.

The importance of gas distribution in electrostatic precipitators

The gas distribution has a significant influence on pressure loss, erosion, particle deposition and thermal losses. Typical gas velocities range from 12 to 20 [m/s] and change to approximately 1.5 [m/s] in the precipitator. Diffusers are required to change these velocities. Inlet splitters are a good method to achieve a good gas distribution. (e.g. in Figure 50)
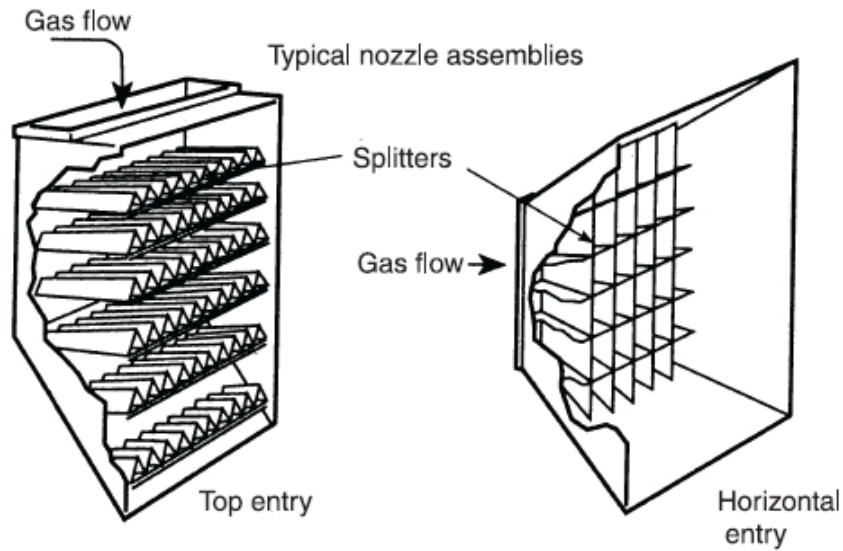
Figure 50: Inlet splitters[49]

The gas distribution in the electrostatic precipitator is shown in Figure 51. This figure shows a quantitative sketch of the gas flow distribution in an electrostatic precipitator.
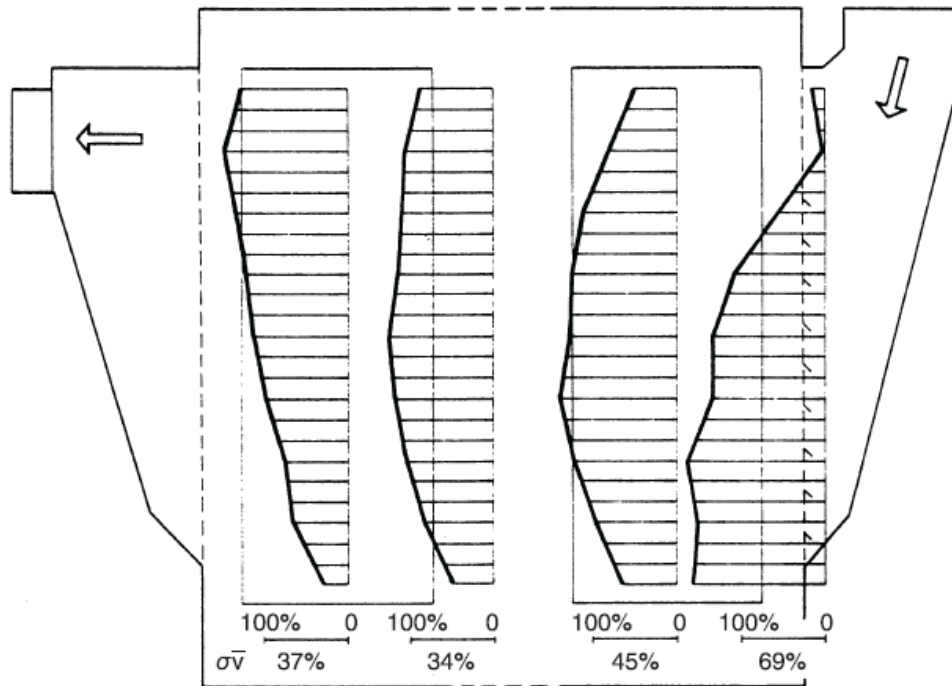
Figure 51: Gas flow distribution in a electrostatic precipitator[49]

3.5 Filter

Batel[15] described filters as separators with a solid and porous filter material. The separation works with a barrier and screening effect. Particles are moved by inertia, electric forces and molecular diffusion. Particles leave the gas flow by adhesion on the filter material. Hoffman and Stein[41] described the filtration as the most common method for removing fine particles from gases.

3.5.1 Basics and mode of action of filters

The dust is separated by a mesh of natural or synthetic fibres while the gas is passing this material. A typical filter system is described in Figure 52.
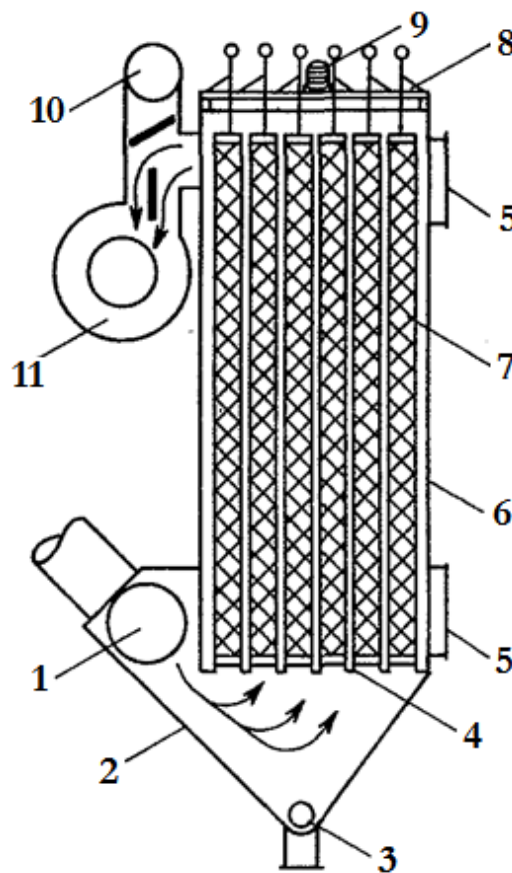
Figure 52: Vibration hose separator[16]

1 raw gas channel, 2 dust chamber, 3 screw conveyor, 4 chamber bottom with tube sockets, 5 entrance, 6 separation housing, 7 filter tubes, 8 vibration frame with tube mounting, 9 vibration equipment, 10 flushing gas pipe, 11 clean gas pipe

The filter material has a pore size which is larger than the separated particle because particles build a layer (the filter cake) on the filter material when the filtration starts. This layer affects the separation efficiency and the pressure drop of the filter.

3.5.2 Types of filter

There are several designs of filtration separators. There is a distinction made between vacuum and pressure operation, tube and surface filter, filter with or without cleaning system.
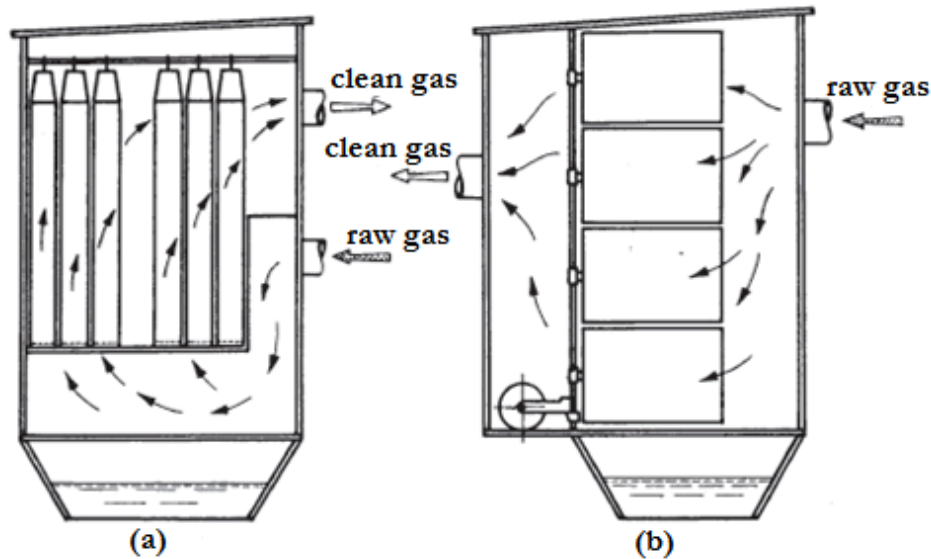
Figure 53: Fabric filter; left: tube filter, right: surface filter[15]

3.5.2.1 Tube separator

Tube separators have a cylindrical filter material. This construction allows a regeneration during the operation. The cleaning of the filter tubes works with an air pressure cleaning system or vibration. Tube filter consist of a rectangular housing, many vertical oriented filter hoses with a diameter of more than 100 [mm] and a length of more than 2 [m]. In the case of a high raw gas volume flow, the separator is split in more separation chambers with adjusted gas flow channels. A gas flow volume of 2000 to 120000 [m³/h] in a suction and pressure operation is possible. Figure 52 shows a fabric hose separator.

3.5.2.2 Bag filter

Bag filter have a similar construction to fabric hose separators. The difference is the type of filter material used. The filter material of bag filter has a simple design and a bag shape. Figure 54 shows a typical bag filter.
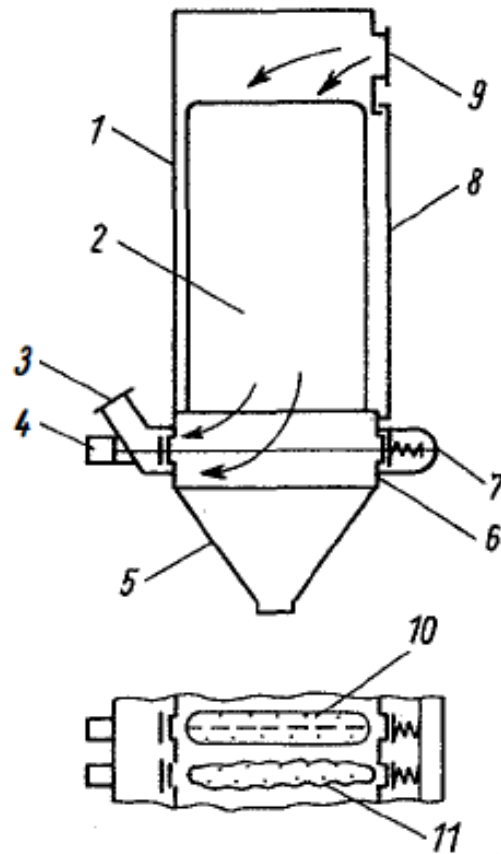
Figure 54: Bag filter[15]

1 housing, 2 filter bag, 3 clean gas outlet, 4 control magnet for the valve operation, 5 dust chamber, 6 valve bag, 7 flushing gas pipe, 8 chamber door, 9 raw gas inlet, 10 filter bag (bloated by flushing gas), 11 filter bag (in operation)

3.5.2.3   Hot gas tube separator

Hot gas tube separators work with a filter material made from glass. They are able to separate dust from gases with a maximum temperature of 280 to 350 [°C].

3.5.2.4   Filter material

Filter materials are porous media with a defined construction to separate particles from a carrier gas. Important properties are:

- dust separation efficiency
- pressure drop
- life time
- costs

The dust separation efficiency and the pressure drop are stated by the manufacturer, and this information together with empirical data builds the basis for all design processes. The following parameters are important to describe filter materials[16].

The Permeability can be calculated by formula (3-79).

$$K_D = \frac{V_{raw}}{S_f \cdot \Delta p_{ft} \cdot t} = \frac{v_g}{\Delta p_{ft}} \qquad \textbf{(3-79)}$$

(A constant pressure drop is assumed)

The Hagen number is a typical indicator for the fabric structure. B_G is a parameter for the fabric permeability.

$$H_a = \frac{R_{eff}}{B_G} \qquad \textbf{(3-80)}$$

Table 10: Typical filter materials[67]

filter material	abb.	brand name (e.g.)	temp. [°C] nom	max	chemical resistance	relative costs
polypropylene	PP	Meraklon, Hostalen	90	100	good	1
polyacrylnitrile	PAN	Dralon, Orlon	125	140	good	1
polyester	PE	Diolen, Trevira	150	160	moderate	1
polyphenylene sulphide	PPS	Ryton, Tedur	180	200	good (NO_x limited)	2
glass			250	250	satisfactory (no HF)	4
polyimide	PI	P84	280	280	good	4
polytetrafluoroethylene	PTFE	Teflon, Rastex, Gore	260	280	good	6

3.5.2.5 Filter cleaning

The cleaning system of the filter material works mechanically or pneumatically and allows a continuous filter operation. Figure 55 shows typical cleaning methods of filter tubes. The cleaning process causes shear stresses and strain the filter material. The lifetime of the filter material depends on the cleaning process and the number of cleaning cycles.
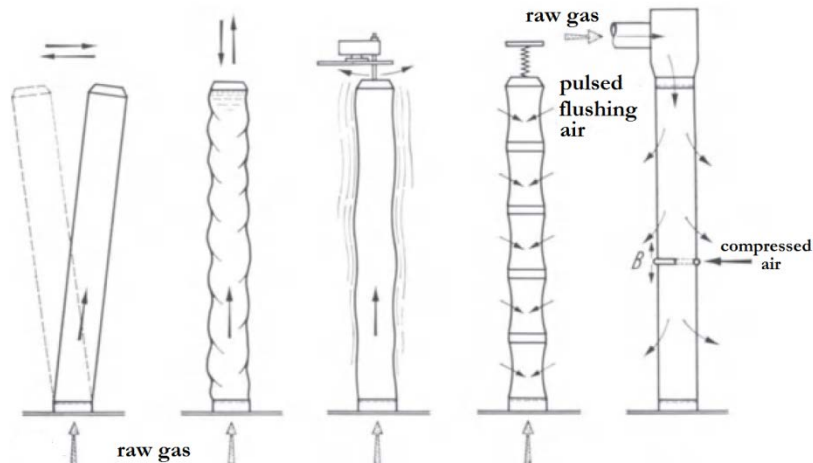
Figure 55: Cleaning methods of filter tubes[15]

A cross section of a filter tube is shown in Figure 56. The air is pressed into the tube and the filter material moves outwards the centre to drop the filter cake in the dust bunker.
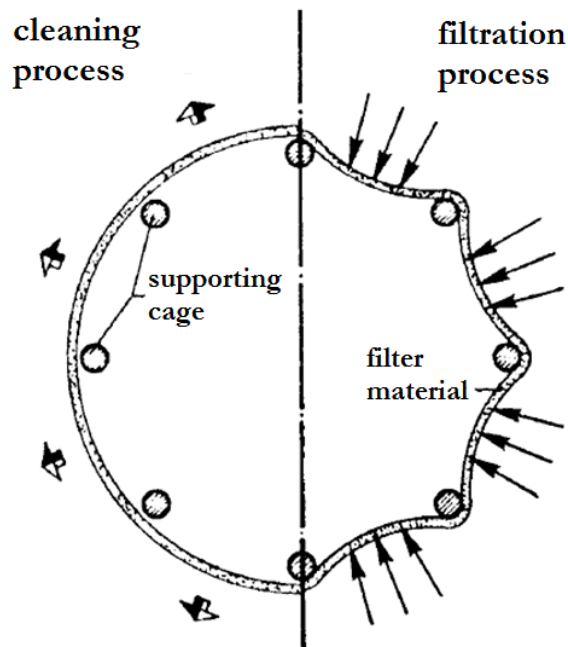
Figure 56: Operation and cleaning of a filter tube - cross sectional view[68]

3.5.3 Characteristics of filters

Filters are characterized by following parameters:

- separation or passage efficiency

- pressure drop

- required filter area for a defined separation

- clean gas properties

- energy and space demand

- investment and operation costs

- maintenance costs

Advantages of filter

- a simple construction

- a high separation efficiency

- a good separation of fine dust

- a good resistance against corrosion

- a low influence of gas property changes

- a simple maintenance

Disadvantages of filter

- sensitivity to wet and aggressive gases

- high abrasion depending on the cleaning process

- a upper limit of the gas temperature

- high energy costs (pressure drop)

- no internal gas cleaning with oil fog

- at high dust concentrations (>100 [g/m³]) in the raw gas a pre-separator (a cyclone e.g.) is required

Dust, filter fabric and the apparatus form a single unit. Performance parameters can only be described by considering all three parts.

Fabric filter are sensitive to moist gases, so they are ideal for the use in combustions with dry fuels[69].

3.5.4 Design principles of filters

Important design items are:

- the correct choice of the filter material

- an optimal filter area load

- a well working filter cleaning system

- an adapted maintenance policy

Different dust properties produce different separation effects. These are settling, sieve, barrier, inertia, hard, diffusion or electrostatic effects. The barrier effects are geometrically based. Robel et al.[16] published the following general context of separation effects.

settling effect $\quad\quad\quad\quad\quad\quad\quad\quad \eta_{0_a} \sim d_p{}^2 / v_g$

sieve effect $\quad\quad\quad\quad\quad\quad\quad\quad\quad \eta_{0_s} \sim d_p$

barrier effect $\quad\quad\quad\quad\quad\quad\quad\quad \eta_{0_i} \sim d_p{}^n \quad\quad\quad\quad\quad\quad 1 < n < 2$

inertial effect $\quad\quad\quad\quad\quad\quad\quad\quad \eta_{0_p} \sim v_g \cdot d_p{}^2 \quad\quad\quad\quad\quad$ as first approximation

diffusion effect $\quad\quad\quad\quad\quad\quad\quad \eta_{0_d} \sim (v_g \cdot d_p)^{-2/3} \quad\quad\quad$ as first approximation

electrostatic effect $\quad\quad\quad\quad\quad\quad \eta_{0_e} \sim (v_g \cdot d_p)^{-1}$

Pressure drop

The pressure drop increases with the dust load at the filter material. Figure 57 shows the pressure drop behaviour with an increasing dust load. The pressure drop occurs in the cake phase.
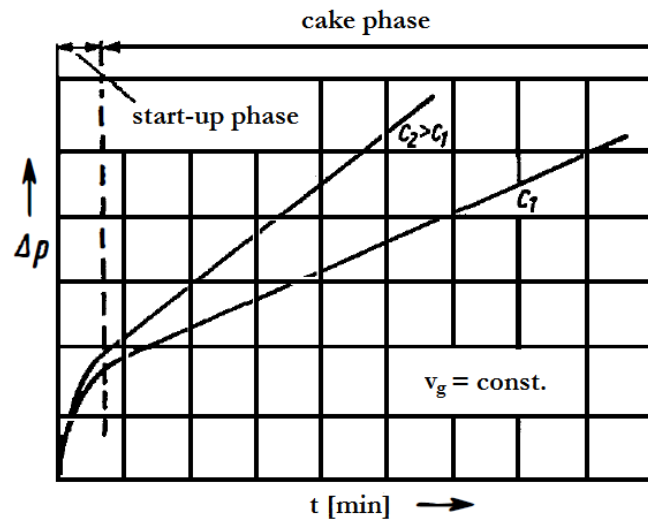
Figure 57: Pressure drop during the dust load[15]
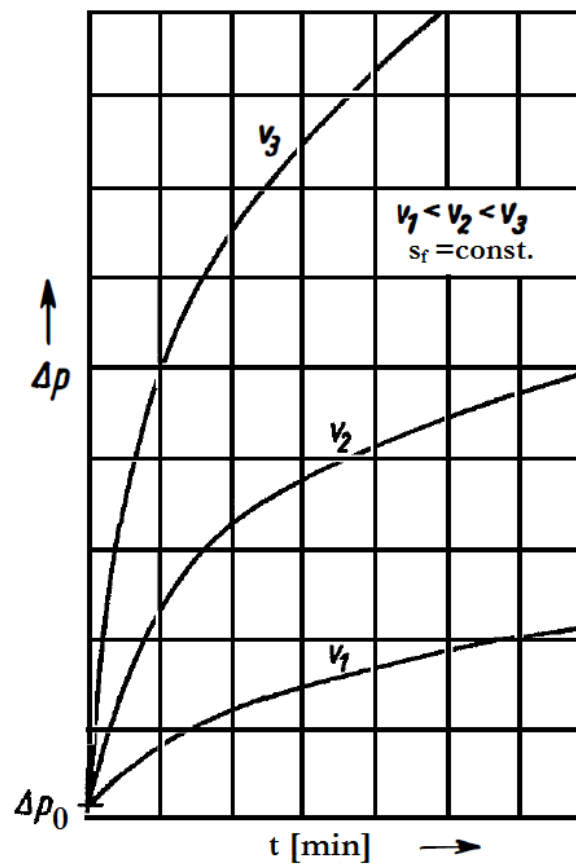
Figure 58: Influence of velocity on the pressure drop[15]

Figure 58 describes the influence velocity on the pressure drop. The pressure drop is an important parameter for the filter design process. There are three good approaches to calculate the pressure drop. The first equation was developed by D'Arcy and described in equation (3-81).

$$v_g = K_D \frac{\Delta p}{s_f \cdot \mu} \tag{3-81}$$

The value K_D depends on the pore size of the filter material. This parameter is also time dependent because the sedimentation at the filter material is increasing with time.

Hagen and Poisseuille published the second method with a substitute of the pore to a capillary system.

$$v_g = N_c \frac{\pi d_c^3}{4} v_c \tag{3-82}$$

$$N_c = \varepsilon \frac{4}{\pi d_c^2} \tag{3-83}$$

$$v_c = \frac{d_c^2 \cdot \Delta p}{32 L_c \cdot \mu} \tag{3-84}$$

With equation (3-82), (3-83) and (3-84) is equation (3-85) formed.

$$\dot{V} = S_{flow} \cdot v = S_{flow} \cdot \varepsilon \cdot \frac{d_c^2 \cdot \Delta p}{32 L_c \cdot \mu} \tag{3-85}$$

If the diameter d_c in formula (3-85) is unknown then a good approximation from Kozeny[70,71] (3-86) is helpful.

$$d_c = \frac{\frac{\varepsilon}{(1-\varepsilon) \cdot \rho_s}}{S_c} \tag{3-86}$$

Equation (3-85) changes with equation (3-86) to (3-87).

$$v_g = \frac{1}{k_{ps}} \cdot \varepsilon \cdot \frac{\Delta p}{32 L_c \cdot \mu} \cdot \frac{\varepsilon^2}{(1-\varepsilon)^2 \cdot \rho_s^2 \cdot S_c^2} \tag{3-87}$$

The calculation of the pressure drop is with this equation easy. Only the parameter k_{ps} is a constant and depends on the pore structure[72].

The separation efficiency is calculated by equation

$$\eta_t = e^{-\frac{1-\varepsilon}{\varepsilon} \cdot \frac{4}{\pi} \cdot \frac{L_c}{d_c} \cdot \eta_f} \tag{3-88}$$

3.6 Special design dust separator

This chapter provides an insight in some special dust separators for biomass combustion plants. Details can be found in the literature which is listed in the reference list.

3.6.1 Rotary particle separator (RPS)[10]

The rotary particle separator is a special centrifugal dust separator with the aim to achieve a better separation efficiency of fine particles. It was developed by T. Brunner and I. Obernberger (BIOS Bioenergy Systems, Sandgasse 47, A-8010 Graz, Austria), J. J. H. Brouwers (University of Twente, P.O. Box 217, 7500 AE Enschede, Netherlands) and Z. Preveden (Kohlbach Ges. m. b. H. & CoKG, Wolfsberg, Austria).This separator consists of the following components:

- a static cyclone body

- a rotating filter element

- a cleaning system

- an internal fan or impeller fixed at the top of the filter element

Figure 59 shows the structure of a rotational particle separator.
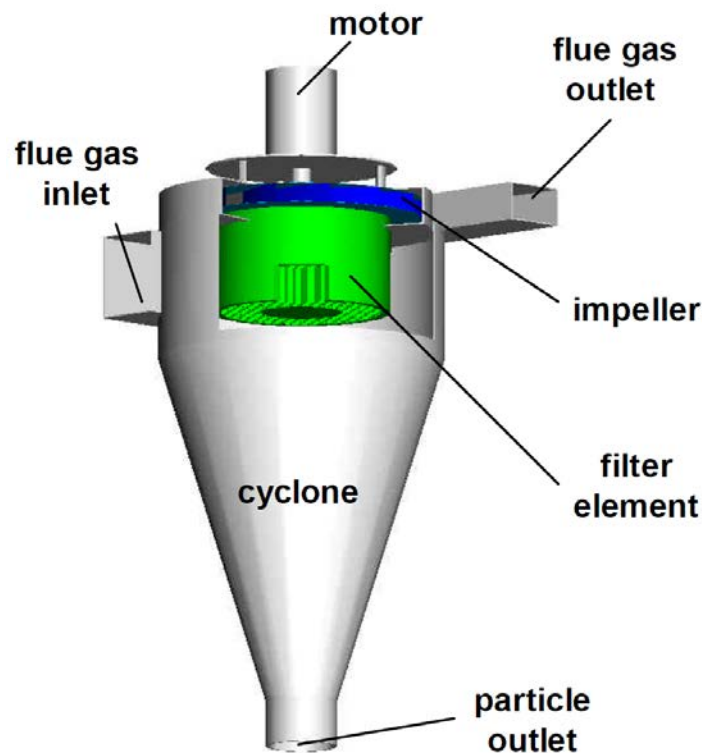
Figure 59: Structure of the RPS (type with integrated fan)[10]

3.6.1.1 The cyclone

Particles with a diameter of 8 [μm] and higher can be separated by the cyclone body. This component works like a cyclone separator with a tangential inlet.

3.6.1.2 The rotating filter element

The rotating filter element (Figure 60) consists of a multitude of small parallel channels with a diameter of about 1.5 [mm]. It is positioned in the centre of the cyclone and rotates around the vertical axis. The pre-cleaned flue gas flows through the filter element like through a vortex finder of a cyclone. Dust particles are separated to the filter walls by centrifugal forces in the filter element. A periodically cleaning operation removes the particles without disturbance of the operation. Figure 61 shows the particle motion in the filter element.
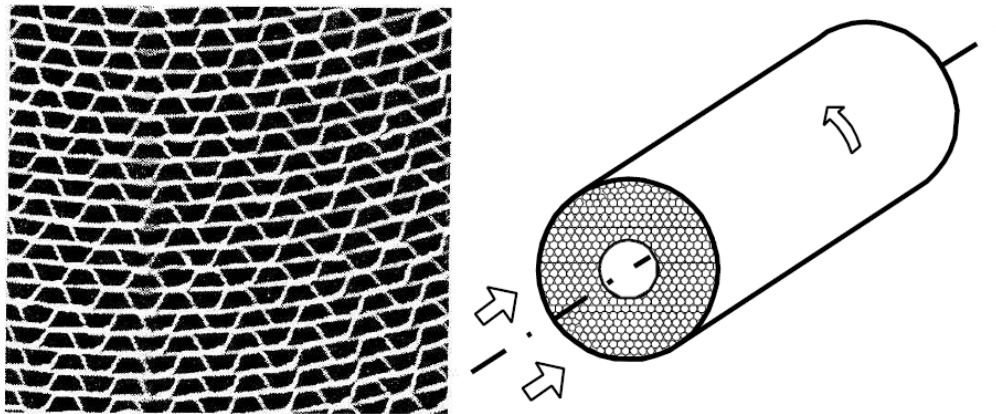
Figure 60: Scheme and cross section of the filter element[10]
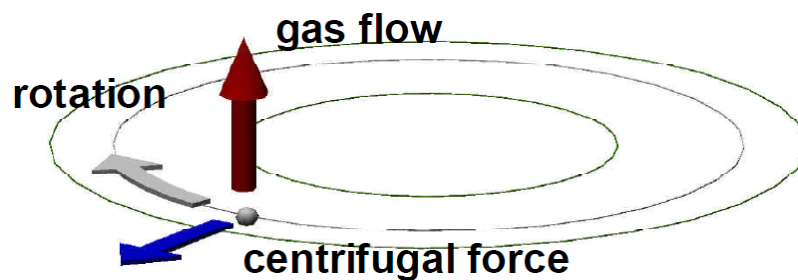
Figure 61: Particle motion in the filter element[10]

3.6.1.3 Advantages of the RPS

The advantages of a rotational particle separator are the low investment costs (50-70% of conventional technologies), the similar pressure drop to a multicyclone, the operating costs that are similar to an electrostatic precipitator, a small space requirement and the higher separation efficiency compared to multicyclones.

3.6.1.4 Disadvantages of the RPS

The disadvantages of a rotational particle separator are the less effective cleaning system of the filter element and the incompletely developed separator design. Small channels in the filter element hinder the cleaning process and detached particles get into the clean gas flow. This is the reason for higher clean gas concentrations than raw gas concentrations in some experimental results (Appendix C – Rotational particle separator). Centrifugal forces increase with an increasing radius, so the centrifugal separation principle works less effective in the filter element channels with a lower radius than in the channels with a higher radius. Particles are able to pass the filter element without separation.

3.6.1.5 Experimental results of the RPS

Obernberger and Brunner[73] described in their interim report for the KOHLBACH GmbH & Co. an achieved dust concentration of the clean gas after the RPS of between 15.0 and 37.0 [mg/Nm³] (13%O_2) for softwood and between 52.0 and 101.0 [mg/Nm³] (13%O_2) for hardwood. The higher concentration for hardwood is an effect of the smaller particle size. Detailed results are shown in Appendix C – Rotational particle separator.

3.6.2 Electrocyclone[8]

Typical cyclones are limited by a defined particle size. A method to separate lower particle sizes is to combine a centrifugal dust separator with an electrostatic precipitator. The electrocyclone has an electrode to produce an electric field in its main axis. The separation efficiency of an electrocyclone is better than the separation efficiency of a typical cyclone. The big disadvantage is that the separation efficiency reduces significantly at higher flow rates. The structure of an electrocyclone is shown in Figure 62.
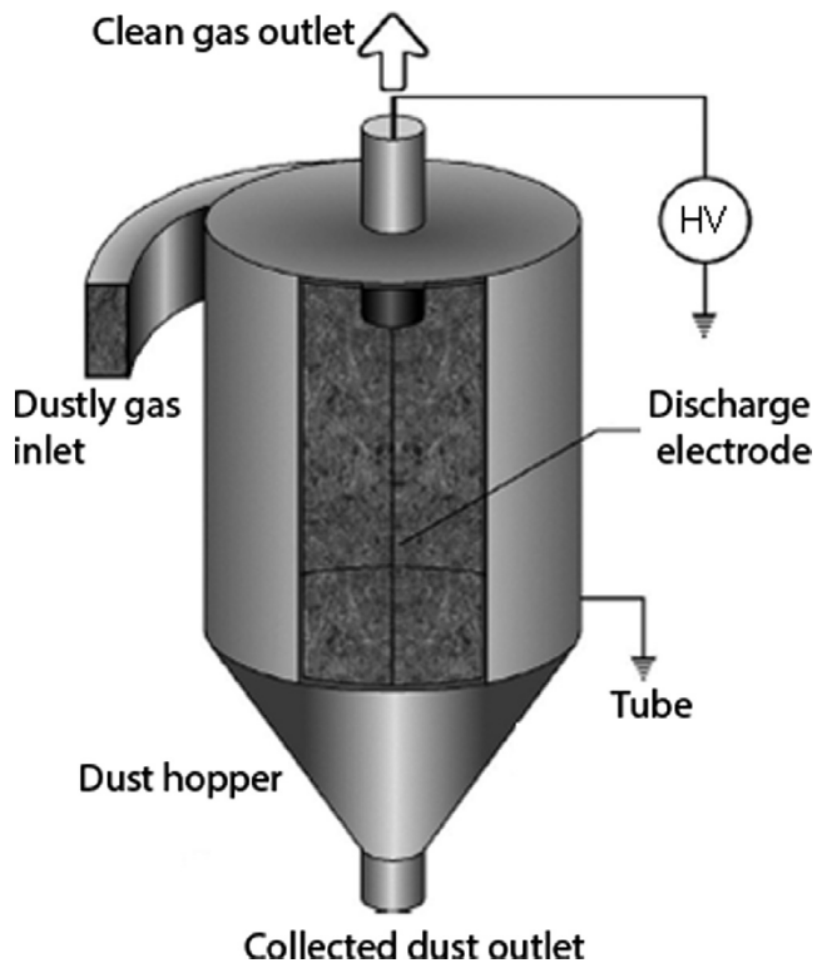
Figure 62: Structure of an electrocyclone[64]

3.7 Overview

This chapter provides an overview of influencing factors, selection procedures, performance and quality of design principles in the field of dust separation.

3.7.1 Influencing factors of dust separation

Batel[15] defined 13 influence factors of dust separation. These factors are described in detail in this chapter.

Gas flow rate

The gas flow rate affects on the type and the size of the separator, the design of the gas pipe system, the size of the ventilator and the size of the gas pre-treatment. If a deviation above the dimensioned gas flow rate exists then a reduction of the separation efficiency of electrostatic separators and filter occurs. An increase of the pressure drop, the energy expenditure and the abrasion is possible. A higher abrasion reduces the lifetime of a separator and its components. A less effective separation and dust sediments are also results of a gas flow rate under the calculated value.

Gas temperature

The gas temperature affects the separation type, the ventilator type, the design of the gas pipe system and the used materials. If the temperature is higher than the desired temperature then a higher gas flow rate exists, material erosion and a less effective separation are possible. A temperature that is too causes a lower gas flow rate and a possible dew point shortfall.

Static gas pressure

The separation type and the component design depend on the static gas pressure. A deviation of the calculated static pressure could result in less effective gas convection.

Water and acid dew point

The water and acid dew point affects the separator and insulation design, corrosion protection, used materials, separation type and the usage of a flue gas conditioning. An attainment of the dew point increases corrosion and dust deposits.

Gas composition

A deviation from the calculated gas composition could produce defective explosion prevention, an incorrect separator design and a wrong choice of the separator type. The use of false materials also increases the corrosion.

Raw gas dust concentration

The raw gas dust concentration affects the separator size and separator type, the design of the ventilator, the usage of a pre-separator and the design of the dust discharge system. If a deviation

above the calculated raw gas dust concentration exists, then a higher clean gas dust concentration, cleaning problems and an overfilling of the dust discharge system can occur. A raw gas dust concentration below the calculated value causes a less effective separation and makes the design of the separator unsuitable.

Particle size distribution of the dust

The particle size distribution has an effect on the separation process, the design of flue gas pipes and the size of the separator. If the dust is finer then the assumed distribution, the separation efficiency goes down, cleaning problems and dust deposits increase. A coarser dust increases the abrasion and the dust deposits.

Electrical dust resistance

Another influence parameter is the electrical dust resistance. It influences the type of the separation process, the separator size and the flue gas conditioning. A higher electrical dust resistance reduces the separation efficiency of an electrostatic precipitator through the inhibition of coronas or back coronas and cleaning problems that are caused by adhesive forces. A lower electrical dust resistance also reduces the separation efficiency. Details of the electrical dust resistance are described in chapter 3.4.1.4.

Wear performance of the dust

The wear performance of the dust affects the detail design of critical components and the choice of the gas velocities. A higher abrasion tendency makes a failure of the ventilator, or leakages of important components possible.

Adherence, adhesive properties

Adherence and adhesive properties effect separation types, design of cleaning and dust discharge systems. Dust deposits, problems with the cleaning, a reduction of the separation efficiency and malfunctions are possible.

Space requirement

The space requirement of the separator affects the size of the whole plant (free space should be used).

Continuous or discontinuous operation

The operation behaviour affects the separator design, the insulation, the heating and the operation of the dust separator. At frequently changing operations a shortfall of the dew point is possible.

Dedusting costs

The dedusting type and process defines the dedusting costs. Investment costs are important for electrostatic separators and filters. Operation costs are important for centrifugal dust separators.

3.7.2 Selection procedure of dust separation plants

Batel[15] listed 7 criteria to find an ideal dust separation plant. These criteria are:

1. actual clean gas dust concentration ≤ required clean gas dust concentration

2. costs → MIN

3. maintenance costs → MIN

4. reliability, availability → MAX

5. delivery time → MIN

6. space requirement → MIN

7. mass → MIN

No dust separation plant is able to comply with all criteria. Usually one defines one of the criteria and two or three suitable constraints.

3.7.3 Technical overview of dust separators

A technical overview to all separators (excluding gravity dust separators) described in this thesis is provided in Table 11.

Table 11: Technical overview of dust separators

	centrifugal dust separator[74]	electrostatic precipitator[74]	filter[74]	RPS[10]
energy consumption[75] [kWh/1000m³/h]	0.3-0.65	0.26-1.96	0.75-1.9	-
pressure drop[75] [Pa]	600-1500	150-300	500-2000	-
gas velocity[75] [m/s]	15-25	1.5-3.0	5-20	-
influence of temp.	low	low	high	low
sensitivity to sparks	low	low	high	low
influence of gas properties	high (especially: gas velocity)	medium	medium	low
separation efficiency	0.5-0.9	0.95-0.99	>0.99	<0.64
achievable clean gas concentration[mg/Nm³] (at 13 Vol. % O_2)	150	-	-	34-38
minimal particle size	3-20 [µm]	< 1 [µm]	< 1 [µm]	< 1 [µm]
space requirement	low	high	high	low
risk of fire	no	yes (due to unburned material)	yes	no
addition of additives	yes	no	yes	yes

Batel[15] described different working areas for dust separators. Reasons for this definition are different discharge forces, resistances and separator geometries. The working areas and their definition are shown in Figure 63 and Table 12.
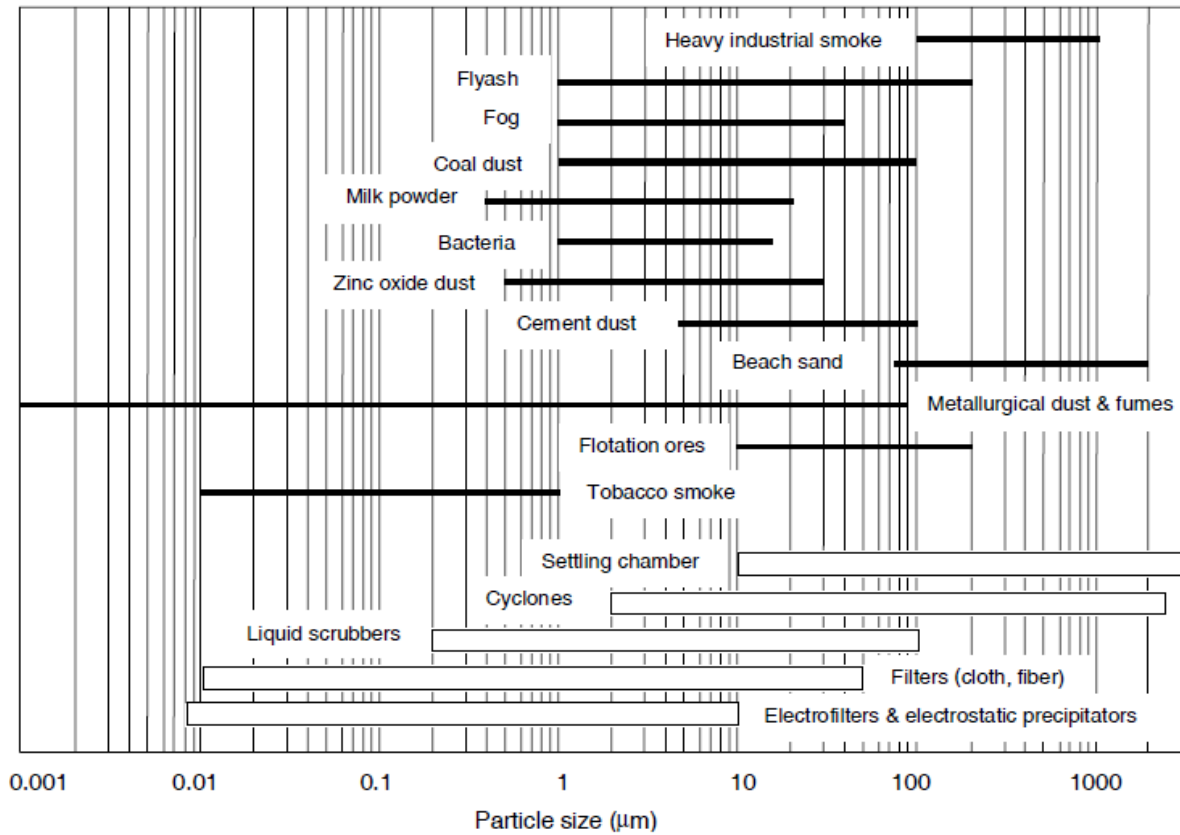
Figure 63: Particle sizes and working areas of dust separators[41]

Table 12: Working areas of dust separators[41]

separator	separation forces	working area	investment costs	operation costs
gravity dust sep.	gravity forces	$d_p > 10$ [µm]	medium	low
centrifugal dust separator	centrifugal forces	$d_p > 2$ [µm]	low	medium to high
electrostatic precipitator	electrostatic forces	$d_p > 0.01$ to 50 [µm]	high	high
filter	screening effects, inertial effects, diffusion, electrostatic forces	$d_p > 0.01$ to 60 [µm]	high	high

The most interesting parameter is the minimum particle size. This particle size has a high influence on many variables like dust properties, separator design and operation behaviour. The values in Figure 63 and Table 12 are achievable but not guaranteed. The smallest forces acting on the (relevant, i.e., small) particles to be separated occur in the gravity dust separator, because the forces depend on the particle volume. Discharge forces go down with a decreasing particle size cubed. This behaviour results in a comparably large particle size of ca. 10 [μm] that can be separated. Centrifugal dust separators are able to separate dust with a lower particle size because centrifugal forces have a major impact on the separation. Unfortunately, also centrifugal forces are proportional to the particle volume, and hence rapidly decrease with decreasing particle diameter. The lower particle limit of centrifugal dust separators is approximately at 2 [μm]. This limit is achievable by conditions related to centrifuges. For electrostatic precipitators no typical lower limit exists, since the physics of particle charging allow particles to migrate with a speed almost independently of their size. Turbulent diffusion, molecular diffusion, electro hydrodynamic secondary flow[76] and problems with the cleaning process produce a practical lower limit of 0.01 [μm]. Similarly, the separation border of filters is very low and approximately 0.01 [μm]. A definition of the lower limit is difficult, because a mean value between a physical and a technical-economic optimum is searched.

3.7.4 Assessment of dust separation design principles

A pure theoretical design of a dust separator is not possible. Success can only be achieved with a good combination of theoretical groundwork, empirical information, experiments and simulation. In recent years, it has become standard practice in the biomass combustion community to use CFD to model individual components of biomass combustion plants. A detail description of simulation in the field of biomass combustion and its dust separation is too comprehensive for this thesis but it has to be mentioned due to its sheer importance for every design process. This chapter provides a short comparison of traditional design methods like the VDI guidelines and modern methods like CFD. Experiments are not part of this thesis.

The following effects are not considered in typical design methods for dust separators[16]:

- coagulation of the dust before and inside the separator

- adhesive dust properties

- engineering solutions of the separator assembly
    - internals for wear reduction
    - internals for reduction of the vortex core
    - design of the dust discharge

- installation conditions
    - flue gas pipes before and after the separator

- conditions of operation
    - temperatures below the dew point
    - excess air

Traditional design methods[77]

Traditional design methods are quick to do, because they are based on guidelines (e.g., VDI Wärmeatlas, Section Lcd "Zyklone zum Abscheiden fester Partikel aus Gasen"[42]) and need no additional design tools or high performance computers. A design with paper and pencil is possible. The guidelines typically assume an extremely simplified flow situation (e.g., assumed velocity profiles, no description of turbulence, no particle collisions and poor account of particle-gas interactions) and are valid only for certain cyclone configurations and process parameters (e.g., only for gas-particle systems and spherical particles). The big advantage of this method is the low costs with a sufficient high design quality for standard cyclones.

The disadvantages of this method are the limited validity for non standardized geometries and the less effective options for optimization, because traditional design methods are based on empirical data of standardized separators. Traditional design methods do not provide any information on (i) critical regions for particle depositions, (ii) tendency for abrasion, or (iii) inhomogeneous flow situations (e.g., short circuiting near the vortex finder of a cyclone).

Modern design methods - CFD [77]

CFD is described as a typical modern design method. It works with the solutions of Newton's equation of (translational) motion for each particle, a direct account for the effect of the particles on the gas flow is possible, and often an account for particle-particle collisions with simplified models is performed. A typical example is the direct computation of the fractional efficiency based on the particle's trajectories. Big advantages are a possible optimization of the separator geometry (e.g., with the aim of a low pressure drop and a high separation efficiency) and the description of deposits and abrasion. The fact is, however, that these benefits goes hand in hand with a time consuming and expensive design approach. This is especially true for predicting the separation efficiency in cyclones, since the structure of turbulence in strongly swirling flows requires specialized turbulence models (e.g., LES, or Reynolds stress models) that are significantly more time consuming to evaluate. Nowadays, such a design approach is often cheaper than experiments, due to the decreasing cost for computers and the availability of open-source CFD software.

3.8 Economy of dust separators

This chapter deals with the influence of dust separators on the economy of automatic biomass heating plants. The content of this chapter is provided by the work of Nussbaumer[14]. He collected data of heating plants from 100 to 2000 [kW] and described the influences on investment and heat production costs. Nussbaumer[14] calculated the total heat production with the following assumptions.

interest rate for capital cost	5.0	[% p.a.]
payback time for hardware	15	[a]
payback time for buildings	30	[a]
operation of heating plants	2000	[h/a]
life time of filters for fabric filters (before filter replacement)	5	[a]
fuel price for wood chips at the gate	3.0	[Euro Ct./kWh]
fuel price for light fuel oil	6.0	[Euro Ct./kWh]

All following estimations of costs exclude restrictions of operation or fuel types. Figure 64 shows the specific investment costs for heat production plants. The costs for plants with electrostatic precipitators are higher than the costs for plants with fabric filters. Similar trends are shown in Figure 65 with the increase of total investment. The median difference of the increases is approximately 9 [%] between both separator types.
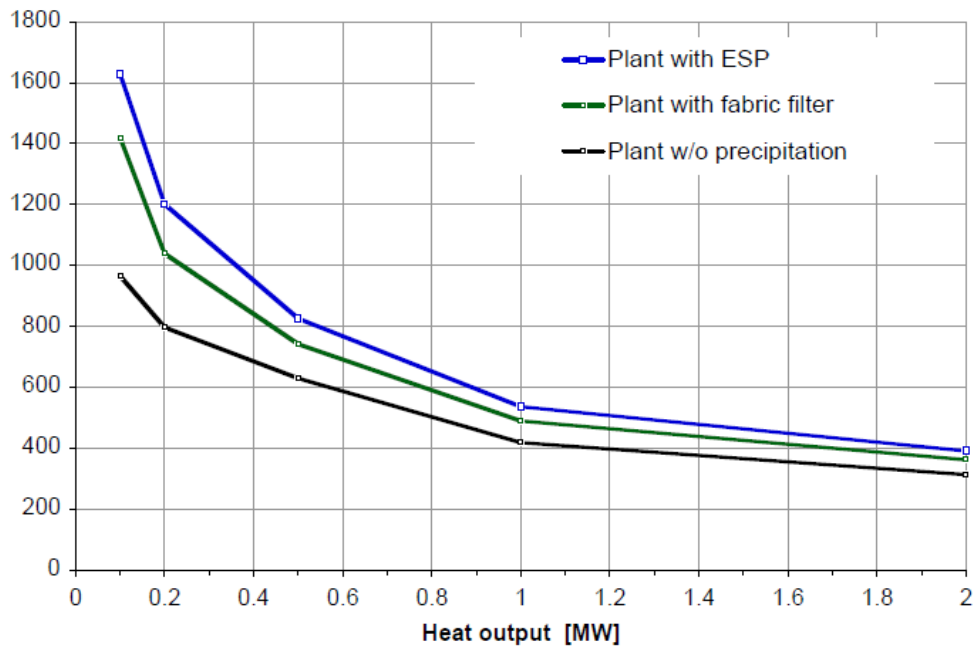
Figure 64: Specific investment costs [€/kW] for hardware (without building)[14]
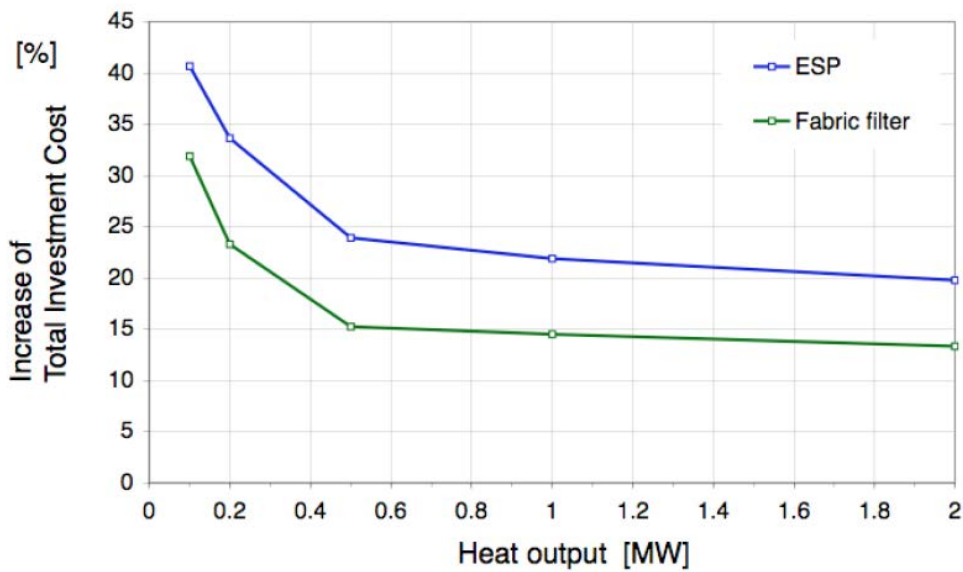
Figure 65: Increase of total investment costs for hardware[14]

Figure 66clearly describes the higher investment costs of an electrostatic precipitator compared to a fabric filter. The relation to the costs of the building and the techniques are also shown.
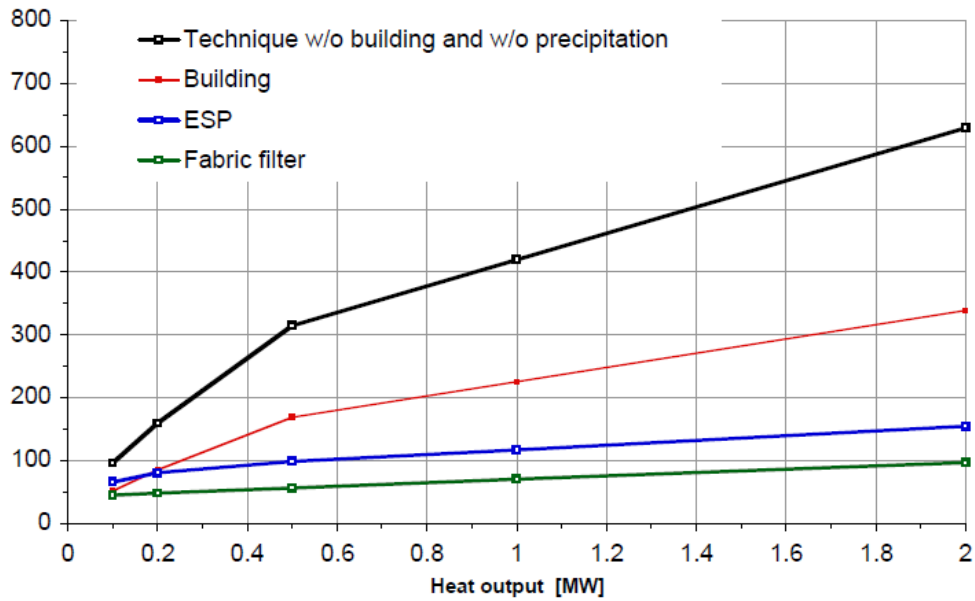
Figure 66: Investment costs for hardware, building, electrostatic precipitator and fabric filter[14]

Figure 67 and Figure 68 indicate the increase of heat production costs by an electrostatic precipitator or a fabric filter. A comparison of both filter types shows the high investment costs and the low operation costs of an electrostatic precipitator as well as the lower investment costs and the high operation costs of a fabric filter. Both total cost curves are similar with slightly higher costs for electrostatic precipitator. The sensitivity of fabric filters to moist gases make the electrostatic dust separation more practicable, because moist fuels are often used.
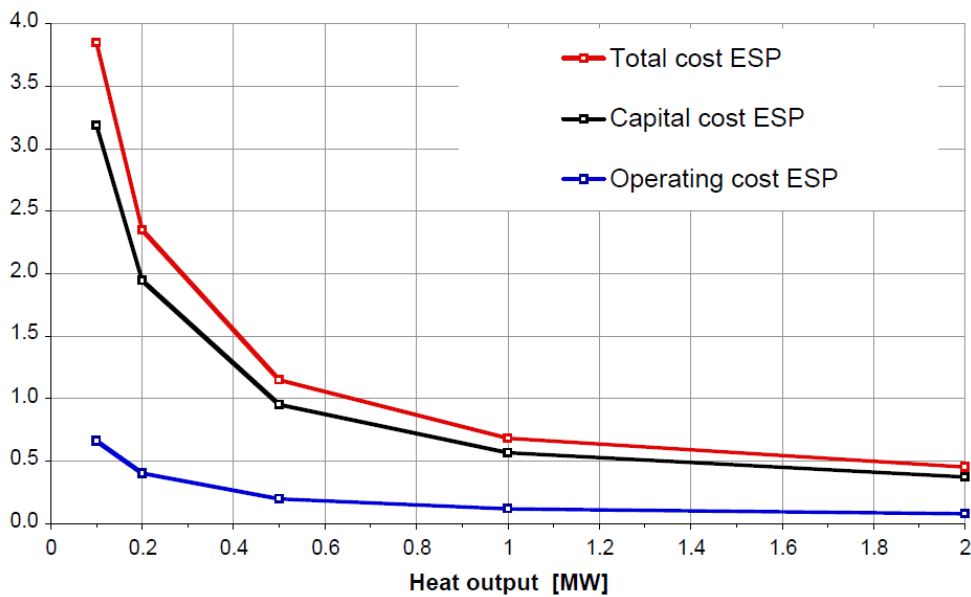
Figure 67: Increase of heat production cost by an electrostatic precipitator in [Euro Ct./kWh][14]
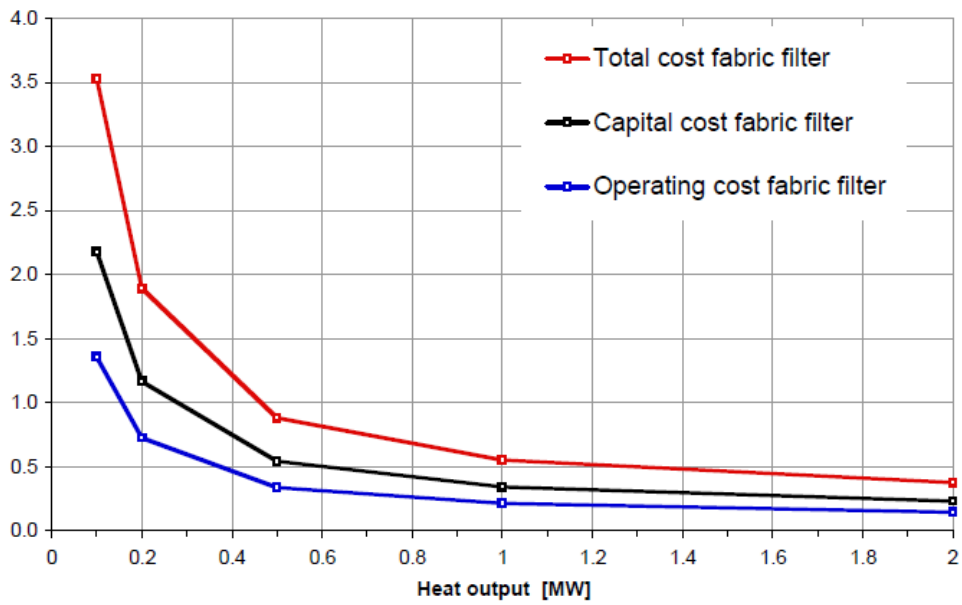
Figure 68: Increase of heat production cost by a fabric filter in [Euro Ct./kWh][14]

The total heat production costs are pictured in Figure 69. This figure also contains a curve for light fuel oil. Figure 70 shows the percentage increase of the heat production costs. Detailed values are listed in Table 13.
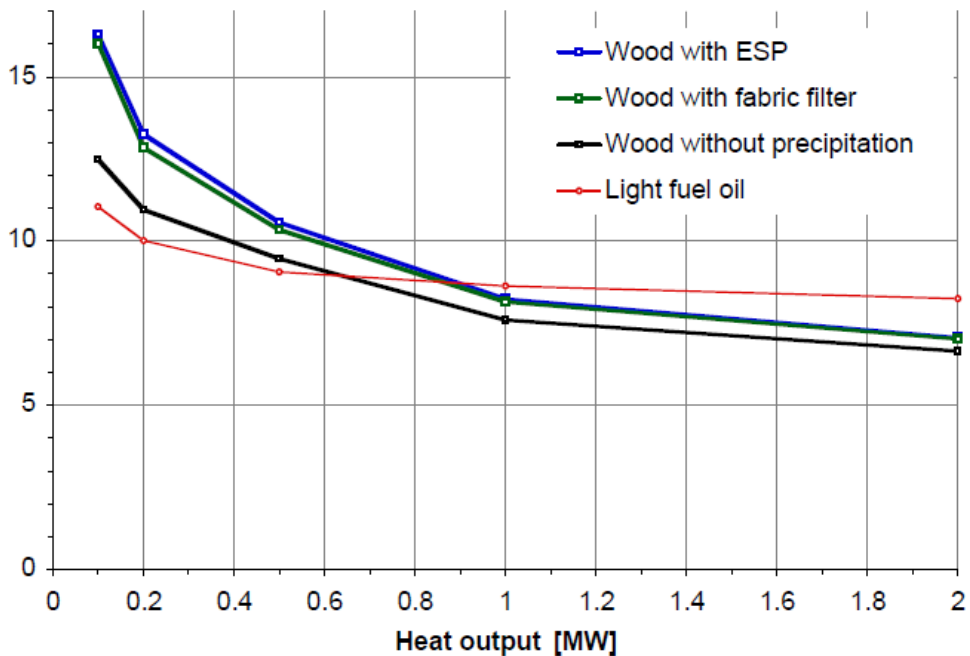
Figure 69: Total heat production cost for light fuel and for wood[14]
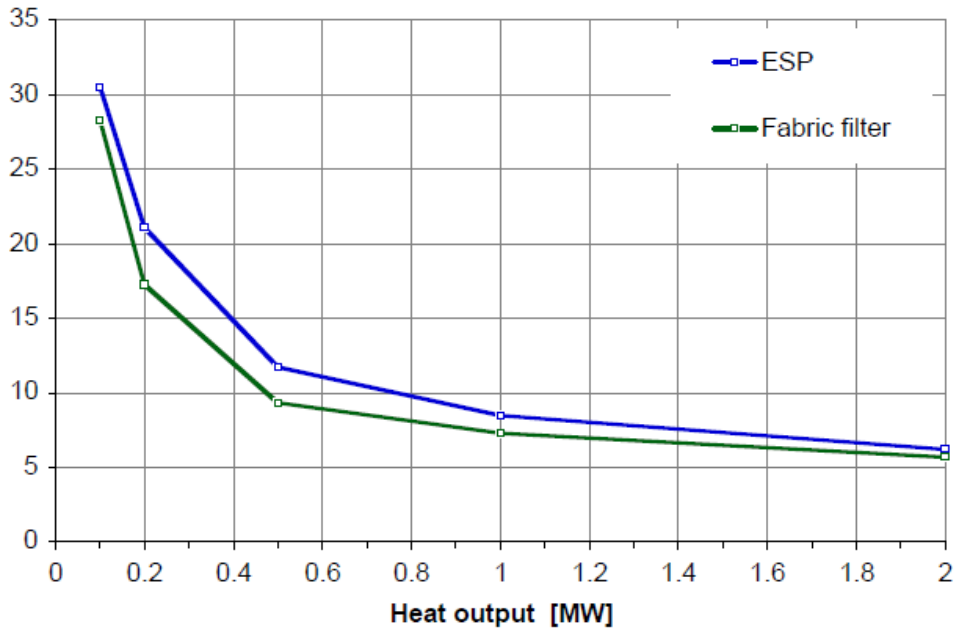
Figure 70: Percentage increase of the heat production cost[14]

Table 13: Percentage increase of the heat production costs in detail[14]

heat output	fabric filter	electrostatic precip.
[kW]	[%]	[%]
100	6	6
200	7	8
500	9	12
1000	17	21
2000	28	30

Dust separation for biomass heating plants with a boiler capacity of 200- 2000 [kW] is affordable in case higher quality requirement exists in the design process and a constant operation is provided. A fabric filter provides a better choice than an electrostatic precipitator in case the plant heat output is lower than 500 [kW]. This is because the investment and operation costs of a fabric filter in this dimension are lower than the costs of a comparable electrostatic precipitator.

4 Concept study of a new dedusting process for biomass plants

The result of the work of Singh and Shukla[8] describes that a high removal efficiency of small particles requires a combination of techniques and improved hybrid solutions. This is an approach which can be useful for general design methods and applications. In the field of biomass dedusting there are many unknown variables that make a design process so difficult. The most important variables are the dust properties and the desired separation processes.

4.1 Future Prospects

A dust separator only impairs the efficiency of the whole plant. The prices for fossil energy are too low[78] and dust separation requires a high percentage of investment costs. Due to regional differences with regard to limit values for dust emissions, every plant is designed to achieve the minimal requirements. The demand for large biomass combustion plants is rapidly declining. High energy outputs will be realized in plant systems with two or more smaller combustion units. These systems have a better partial load behaviour, and a lower probability of defects. Frequent operation under partial load reduces the lifetime of a plant. Optimization of inexpensive dust separators, cost-optimization of common dust separators and an overall view of the plant are the most promising approaches in the field of dust separation for the future.

Optimization of inexpensive dust separators

A centrifugal dust separator consists of a simple sheet metal body and several control engineering elements. In case of a simple cyclone is able to achieve the emission limit, an electrostatic filter is no longer required. Fireproof filter systems with a low pressure drop do not need other dust separators, e. g. a cyclone, as a spark arrestor. The aim of this approach is to optimize cyclones or simple filter systems to a self-sufficient operation.

Cost-optimization of common dust separators

A second way is the cost-optimization of common dust separators, by making their production process less costly, reduce material costs, as well as their application. The product range should be kept small and suitable to performance parameters like mass flow and dust loading. Dust separators should be produced in high volumes with a rigid automated production to achieve lower specific costs of each separator. With this consideration, a dust separator with the same performance parameters can be used for a coal, pellet and wood chip combustion.

Overall view of the plant

The most promising approaches are an overall view of the plant and an inclusion of all potential side processes. An efficient dust separation starts with the fuel, is supported by the combustion, takes place in a perfectly matched separator and ends with the recycling of escaping flows.

5 Conclusions

State of the art in the field of dust separation of biomass combustion plants are cyclones, especially multicyclones to handle the high volumetric flow rates of flue gas, electrostatic precipitators, and in some cases filters. Filters are not commonly used because the high pressure drop results in higher operating costs. Gravitational dust separators are not applicable in the field of biomass combustion. Types of combined gravity and centrifugal dust separators are unconsciously used in heat exchanger and flow redirection systems after the biomass furnace.

The often used combination of a cyclone and an electrostatic precipitator emerges also in this thesis as the most promising method for dust separation in biomass combustion. A cyclone can be designed as a single cyclone or a multicyclone to reduce the dust concentration to less than 100 [mg/Nm³] for typical fuels and < 150 [mg/Nm³] for problematic fuels. The second separation stage takes place in an electrostatic precipitator to the required clean gas concentration (10-62.5 [mg/Nm³] depending on the country). This combination allows a manageable product range for the manufacturer of biomass combustion plants, because only the final separator performance needs to be adapted to the local requirement. Also, a two-stage separation approach provides enough flexibility for the plant operator to react to changes in the fuel or stricter future regulations. Another advantage is the achievable separation of fine dust particles with a size down to 0.01[μm]. This advantage allows the easy achievement of future changes of dust emission limits.

The selection of a suitable dust separation method is primarily based on empirical methods, rather simple design equations and literature data. Dust properties vary with the fuel, combustion and the mode of operation. This makes an efficient design without empirical information difficult. An ideal approach to develop new separators is a fundamental groundwork study, a detailed dust analysis of the combustion problem, and finally measurements in a pilot plant. The design and the scale up should be supported by a CFD simulations to achieve maximum separation efficiency at the lowermost pressure drop. Furthermore, a geometric optimization is only possible by CFD, e.g., for cyclones, where single-phase simulations have become a standard tool in industry. Unfortunately, at the current development stage CFD simulations cannot accurately predict grade efficiency curves with reasonable expense. This is because modelling of (i) turbulent flow and dispersion, (ii) agglomeration and adhesion of particles, (iii) thermo- and turbophoretic effects, as well as (iv) flow details near walls require (expensive) highly-resolved simulations, or are simply infeasible due to missing particle parameters. A recommendation is to use CFD simulations for the optimization of pressure drop and flow distribution (e.g., for

multicyclones), and use rapid-prototyping methodology (e.g., 3D printing) on a pilot scale to assess separation efficiency of CFD-based designs.

An often underestimated point of the separator design is the dust analysis. The particle size distribution of the flue gas changes drastically with the fuel type. Particles with a lower diameter (< 10 [µm]) are more difficult to separate than particles with a larger diameter (> 10 [µm]). The particle distribution gives information on the amount of small and big particles. In the case that the amount of particles consists primarily out of big particles, a cyclone could be enough to achieve the required dust limits. Dust limits < 20 [mg/Nm³] can only be achieved by filters or an electrostatic precipitator. Filter and electrostatic precipitator often have problems with high temperatures and the size of the separator increases with amount of flue gas to be handled. In this case a cyclone is an ideal pre-separator for a high dust loadings and flying sparks.

Furthermore, an efficient and economic dust separation exists if related effects of the dedusting performance are considered. These effects are (i) the influence of changing temperatures, (ii) gas flow rates, (iii) flue gas humidity, and (iv) other parameters (e.g., particle composition, or morphology). For example, the adhesive strength between dust particles increase with the humidity of the flue gas due to capillary forces. In the case of well-defined process conditions, the design of a plant customized dust separator is possible. Unfortunately, this often requires expensive pilot-scale experiments. In such a way, operation problems can be solved already in the design stage.

The most promising components for optimization are the separator geometry, the flow inlet and outlet, the dust outlet and the process parameters. An optimization of these components require a well-known flow situation and defined dust properties. The separation efficiency can by increased with simple guiding plates or longer inlet pipes, e.g., to reduce the turbulence level. A suitable dust outlet to the separator is especially beneficial to a higher separation efficiency. A CFD simulation is often helpful, and, as detailed above, recommended for single-phase studies of fluid dynamical problems in biomass combustion plants.

All in all a detailed design process and enough information of the process is required to achieve an efficient, economic and well-working dust separation.

6 Nomenclature

Latin symbols

A_{Cu} ....Factor for Cunningham correction [ ]

A_{sr} ....Material constant of the specific electric resistance []

a_c ....Centrifugal acceleration [m/s²]

a_{pc} ....Separation distance of a particle [m]

a_p ....Particle acceleration [m/s²]

B ....Particle flexibility [m²/s]

B_G ....Parameter for the fabric permeability [m]

b_{ci} ....Width of the cyclone inlet [m]

C ....Constant [ ]

c^* ....Mass load in the discharge chamber [kg/m³]

c_{clean} ....Mass load of clean gas [kg/Nm³]

c_d ....Mass load of dust [kg/Nm³]

c_l ....Critical mass load of dust in the cyclone inlet, $c_{iv} = \left(-\frac{3k_B \cdot T}{m_I} \right)^{1/2}$ [kg/Nm³]

c_{iv} ....Parameter of ion velocity [m/s]

c_{raw} ....Mass load of raw gas [kg/Nm³]

c_s ....Mass load of the separated dust [kg/Nm³]

c_w ....Flow resistance coefficient [ ]

D_M ....Diffusion coefficient of molecular diffusion [m²/s]

d^* ....Critical diameter of separation in a cyclone [m]

d_c ....Capillary diameter [m]

d_{Cap} ....Distance correlation of height fluctuation for capillary forces [m]

d_{do} ....Diameter of the dust outlet [m]

d_e^* ....Critical diameter of wall separation in a cyclone [m]

d_p ....Particle diameter, Stokes diameter [m]

d_{sp} ....Diameter of a smooth particle [m]

d_{rp} ....Diameter for determination of particle roughness [m]

d_{vc} ....Diameter of the vortex cone [m]

d_{vf} ....Diameter of the vortex finder [m]

E ....Electrical field strength [V/m]

E_{crit} ....Critical electrical field strength [V/m]

e ....Elementary charge $e = 1.602 \cdot 10^{-19}$ [A·s]

F ....Force [N]

F_A ....Adhesive force [N]

F_B ....Buoyant force [N]

F_{Co} ....Coulomb force [N]

F_{Cel} ....Coulomb force in an electrostatic precipitator [N]

F_G ....Gravitational force [N]

F_R ....Resistance force of a single particle [N]

F_{RCu} ....Resistance force with Cunningham correction [N]

F_{VdW} ....Van der Waals force [N]

Fr_i ....Cyclone Froude number []

f ....Charge density, $f = n^* \cdot e$; $\frac{f}{e} \approx 10^8$ [Ions/m³]

g ....Gravity [m/s²]

H_s ....Height of the separator [m]

H_a ....Hagen number [ ]

$h\overline{\omega}$ ....Lifshitz-van der Waals constant[J]

h_c ....Total height of the cyclone [m]

h_e ....Height of the cyclone inlet [m]

h_i ....Height of the separation chamber in a cyclone [m]

h_{se} ....Distance between the spray electrodes[m]

i ....Spray current [A]

i_1 ....Spray current (related to 1 [cm]) [A/cm]

K_D ....Permeabillity size [m²]

k_B ....Constant of Boltzmann, $k_B = 1.38 \cdot 10^{-23}$ [J/K]

k_{icg} ....Influence factor of the cyclone inlet on the clean gas [%]

k_{ocg} ....Influence factor of the cyclone dust outlet on the clean gas [%]

k_{ps} ....Constant of the pore structure []

k_{rv} ....Constant of the radial velocity [1/s]

k_s/r_a ....Relative wall roughness [ ]

L_c ....Length of the capillary [m]

L_{icg} ....Length of the inlet pipe [m]

L_s ....Length of the separator [m]

l_{Cap} ....Scale of height deviation for capillary forces [m]

l_p ....Particle length [m]

l_{gm} ....Mean free path length of gas molecules [m]

l_s ....Separation length of a particle [m]

M_{clean} ....Mass flow of clean gas [kg/s]

M_d ....Mass flow of dust at aero dispersions [kg/s]

M_{raw} ....Mass flow of raw gas [kg/s]

M_s ....Mass flow of separated dust [kg/s]

m ....Coefficient of the wire surface []

m_p ....Particle mass [kg]

m_I ....Ion mass [kg]

N_c ....Number of capillaries per area [1/m^3]

n ....Constant []

n_V ....Number of particles at the standard volume [1/Nm³]

n^* ....Number of charges [1/m³]

Δp ....Pressure drop [Pa]

Δp_{ft} ....Total pressure drop of the filter [Pa]

Δp_{ct} ....Total pressure drop of the cyclone [Pa]

Δp_{ci} ....Pressure drop of the cyclone inlet [Pa]

Δp_{csc} ....Pressure drop of the cyclone separation chamber [Pa]

Δp_{cvf} ....Pressure drop of the cyclone vortex finder [Pa]

q ....Partial charge [A·s]

R ....Amount of residue [Mass.%]

R_{eff} ....Effective pore radius [m]

Re ....Reynolds number, $(\varrho \cdot v \cdot D)/\mu$ []

Re_R ....Reynolds number of the cyclone []

Re_P ....Particle Reynolds number []

r ....Radius [m]

r_p ....Particle radius [m]

r_a ....Outer radius of the cyclone [m]

r_{ae} ....Radius of the dust separation chamber in an electrostatic precipitator [m]

r_e ....Inlet radius of the cyclone [m]

r_i............................Radius of the vortex finder [m]

r_{ie} ....Radius of the spray electrode [m]

r_m ....Mean radius of the cyclone, $r_m = \sqrt{r_a \cdot r_i}$ [m]

ΔR_{clean} ....ΔR in the clean gas [Mass.%]

ΔR_{raw} ....ΔR in the raw gas [Mass.%]

ΔR_s ....ΔR for the separated dust [Mass.%]

S ....Area, surface [m²]

S_c ....Capillary surface [m²]

S_f ....Filter surface [m²]

S_{flow} ....Surface subjected to the flow [m²]

$S_{R,sp}$ ....Inside area of the cyclone inlet region [m²]

S_R ....Total inside surface of the cyclone [m²]

S_i ....Cross section of the cyclone inlet [m²]

S_{vf} ....Cross section of the vortex finder [m²]

s_0 ....Distance between adhesive bodies [m²]

s_p ....Distance between spray electrode and a plate (seperation electrode) [m]

s_f ....Filter thickness [m]

T ....Temperature [K]

t ....Time [s]

t_c ....Time constant, $t_0 = \frac{1}{\pi} \cdot n^* \cdot e \cdot u_{ion}$ [s]

U ....Voltage [V]

U_i ....Initial voltage [V]

u_a ....Velocity at r_a [m/s]

u_e ....Velocity at r_e [m/s]

u_i ....Velocity at r_i [m/s]

u_{ion} ....Ion mobility [m/V·s]

u_m ....Mean velocity, $r_m = \sqrt{u_a \cdot u_i}$ [m/s]

V ....Volume flow [m³/s]

V_{cap} ....The total amount of fluid present per particle fluid [m³]

V_{clean} ....Volume flow of clean gas [Nm³/s]

V_{raw} ....Volume flow of raw gas [Nm³/s]

V_{sc} ....Volume of the separation chamber [m³]

V_{sec} ....Secondary flow in a cyclone [m³/s]

v_{ax} ....Axial gas velocity [m/s]

v_c ....Velocity in the capillaries [m/s]

v_g ....Gas velocity [m/s]

w_h ....Horizontal particle velocity [m/s]

w_E ....Migration velocity in the vicinity of the wall [m/s]

w_p ....Settling velocity of a particle [m/s]

w_r ....Radial settling velocity of a particle [m/s]

w_t ....Tangential settling velocity of a particle [m/s]

w_z ....Axial settling velocity of a particle [m/s]

v_{vf} ....Mean gas velocity in the vortex finder [m/s]

x, y, z ....Coordinates [m]

X_0 ....Upper limit of a particle class [m]

X_l ....Lower limit of a particle class [m]

Z ....Multiplier of the gravity force in a centrifugal field [ ]

z_s ....Coordinate z of the intersection between r_a and r_1 [m]

z_0 ....Coordinate z at the beginning [m]

Greek symbols

α_{icg} ....Angle of the cyclone inlet [°]

α_{pc} ....Angle of particle contact [°]

α_{cc} ....Constriction coefficient []

α_{sr} ....Material constant of the specific electric resistance []

β_c ....Relative inlet width []

η_t ....Total separation efficiency [ ]

η_f ....Fractional separation efficiency [ ]

η_{iv} ....Separation efficiency of the inner vortex [ ]

η_{vf} ....Separation efficiency of the vortex finder [ ]

η_0 ....Approximately separation efficiency of filter effects [ ]

μ ....Dynamic viscosity [Pa·s]

$\Delta\rho$ ....Difference of density, $\Delta\rho = \rho_s - \rho_g$ [kg/m³]

ρ_g ....Gas density [kg/m³]

ρ_s.............................Solid density, Particle density [kg/m³]

ρ_e ....Specific electric resistance [Ω·mm²/m]

σ_{pg} ....Surface tension particle-gas [Pa]

σ ....Charge density (surface based) [A·s/m²]

γ ....Euler constant, $\gamma = 0.5772$ [Pa]

δ_b ....Blade angle [°]

δ_{dc} ....Penetration depth of charge [m]

ε..............................Void ratio [ ]

ε_0 ....Constant of induction [A·s/V·m]

ε_r ....Dielectric constant [ ]

ε_{Str} ....Void ratio of the streak [ ]

ε_{wa} ....Angle between conical wall and cyclone axis [°]

Γ ....Surface tensionof capillary fluid [Pa]

λ_s ....Wall friction coefficient (gas with dust) [ ]

λ_s ....Wall friction coefficient (gas without dust) [ ]

ω ....Angular velocity [1/s]

φ ....Calculation angle of a combined gravity and centrifugal dust separator [°]

7 References

[1]   M. Barth, Mechanische Staubabscheider, Die Stärke. 28 (1976) 315–322.

[2]   U.W. Bundesministerium für Land- und Forstwirtschaft, Anpassung der
        Emissionsgrenzwerte für Biomasse-Wärmeerzeugung, Wien, 2014.
        http://www.umweltfoerderung.at/uploads/_infoblatt_neue_grenzwerte_b_biomasse.pdf
        (accessed August 20, 2015).

[3]   Rechtsinformationssystem des Bundes, Feuerungsanlagen - Verordnung, 2014.
        https://www.ris.bka.gv.at/GeltendeFassung.wxe?Abfrage=Bundesnormen&Gesetzesnum
        mer=10007873 (accessed August 20, 2015).

[4]   N. und R. Bundesministerium für Umwelt, Erste Allgemeine Verwaltungsvorschrift zum
        Bundes-Immissionsschutzgesetz (Technische Anleitung zur Reinhaltung der Luft - TA
        Luft), 2002. http://www.taluft.com/taluft20020730.pdf (accessed August 12, 2015).

[5]   W. Gigl, E. Langer, Stellungnahme zum aktuellen Vorschlag der Europäischen
        Kommission für eine Richtlinie des Europäischen Parlaments und des Europäischen Rates
        zur Begrenzung der Emissionen bestimmter Luftschadstoffe aus mittleren
        Feuerungsanlagen,   2013.   http://www.carmen-
        ev.de/files/festbrennstoffe/VDBH_CARMEN_Stellungnahme_EU-Directive_.pdf
        (accessed August 20, 2015).

[6]   S. Bundesrat, Luftreinhalteverordnung - LRV, (2010) 38–54.
        http://www.admin.ch/opc/de/classified-compilation/19850321/index.html   (accessed
        April 24, 2014).

[7]   M. Canè, Quadro generale degli impianti a combustione - Biomasse Combustibili, 2013.
        http://salute.regione.emilia-romagna.it/documentazione/convegni-e-seminari/seminario-
        201cimpianti-a-biomasse-in-emilia-romagna-aspetti-autorizzativi-e-di-controllo201d-
        bologna-1-2-ottobre-2012.-gli-
        interventi/13QuadrogeneraleimpiantiacombustioneM.Can.pdf (accessed July 2, 2015).

[8]   R. Singh, A. Shukla, A review on methods of flue gas cleaning from combustion of biomass, Renew. Sustain. Energy Rev. 29 (2014) 854–864.

[9]   G. Payer, T. Kogler, R. Kulter, D. Bleiberschnig, Bilanzierungsprogramm Biomasse 17.1, KBE Kärntner Bioenergie Engineering und Consulting GmbH, Wolfsberg, 2015.

[10]   T. Brunner, I. Obernberger, J.J.H. Brouwers, Z. Preveden, Efficient and economic dust separation from flue gas by the rotational particle separator as an innovative technology for biomass combustion and gasification plants, in: C.A.R.M.E.N (Ed.), Eur. Bioenergy Conf., Rimpar. Germany, Würzburg, 1998.

[11]   N. Machan, Korngrößenverteilungen von Flugaschen aus Biomassefeuerungen und deren Einflussfaktoren, MS Thesis, University of Technology Graz, 1998.

[12]   K.A. Christensen, The formation of submicron particles from the combustion of straw, Ph.D. Thesis, Technical University of Denmark, Lyngby, 1995.

[13]   T. Lind, T. Valmari, E. Kauppinen, J. Latva-Somppi, Fractionated heavy metal separation in biomass combustion and gasification plants, in: I. Obernberger, J. Dahl (Eds.), Fractionated Heavy Met. Sep. Biomass Combust. Gasif. Plants, Six Mon. Prog. Report, JOULE III Proj. No. JOR3-CT950001, Eur. Comm. DG XII, Brussels, Belgium, 1997.

[14]   T. Nussbaumer, Overview on Technologies for Biomass Combustion and Emission Levels of Particulate Matter, Swiss Federal Office for the Environment (FOEN), Zürich, 2010.   http://www.citepa.org/old/forums/egtei/Nussbaumer_EGTEI-Report_final.pdf (accessed August 14, 2015).

[15]   W.   Batel,   Entstaubungstechnik,   Springer-Verlag,   Berlin,   Heidelberg,   1972. doi:10.1007/978-3-642-49194-8.

[16]   H. Robel, P. Vogel, W. Berger, R. Berndt, D. Brandt, S. Conrad, et al., Apparate zur Staubabscheidung, in: Verfahrenstechnische Berechnungsmethoden - Tl. 3 Mech. Trenn. Fluider Phase, VCH Verlagsgesellschaft, Weinheim, 1985: pp. 247–410.

[17]   M. Sommerfeld, Bewegung fester Partikel in Gasen und Flüssigkeiten, in: VDI Wärmeatlas, VDI e.V., Berlin, Heidelberg, 2013. doi:10.1007/978-3-642.

[18] C. Oseen, Neue Methoden und Ergebnisse in der Hydromechanik, Akadem. Verlagsgesellschaft, Leipzig, 1927.

[19] L. Schiller, A. Naumann, Über die Grundlegenden Berechnungen bei der Schwerkraftaufbereitung, VDI Zeitung. 77 (1933) 318–320.

[20] I. Langmuir, K. Blodgett, American Air Force Report 4518, 1946.

[21] F. Schytil, Wirbelschichttechnik, Springer, Berlin, Göttingen, Heidelberg, 1961.

[22] E. Cunningham, On the Velocity of Steady Fall of Spherical Particles through Fluid Medium, Proc. R. Soc. London. A 83 (1910) 357–365.

[23] C.N. Davies, Aerosol Science Vol. 1102, Academic Press, London/New York, 1966.

[24] C.N. Davies, Definitive equations for the fluid resistance of spheres, Proc. Phys. Soc. 57 (1945) 259.

[25] W. Lewis, E. Gilliland, W. Bauer, Characteristics of fluidized particles, Ind. Eng. Chem. 41 (1949) 1104–1117.

[26] R.C. Senior, J.R. Grace, Integrated particle-collision and turbulent diffusion model for dilute gas-solid suspensions, Powder Technol. 96 (1998) 48–78.

[27] H. Wang, G. Qiu, Investigation of the gas-solid flows in a circulating fludisied bed with multi-cyclone separators by electrical capacitance tomography, (2013) 1–5.

[28] W. Ranz, Technology Report No. 8, January 1st., Univ. Illinios. Engng. Expt. Station., 1953.

[29] J. Townsend, Electricity of gases, Clarendon Press. Oxford. (1915) 376.

[30] I. Wilson, The deposition of charged particles in tubes with reference to the human lung, J. Colloid Sci. 2 (1947) 271.

[31] W. Foster, Deposition of unipolar charged aerosols particles by mutual repulsion, Brit. J. Apply. Phys. 10 (1959) 206.

[32] N. Fuchs, The mechanics of aerosols, Pergamon Press. Oxford. (1964).

[33] J. Pich, Zur Theorie der elektrostatischen Zerstreuung monodisperser Aerosole, Staub. 22 (1962) 15–17.

[34] K. Whitby, B. Liu, The electrical behaviour of aerosols, in: C. Davies (Ed.), Aerosol Sci., Academic Press, London/New York, 1966: p. chapter 3.

[35] H. Schubert, Handbuch der Mechanischen Verfahrenstechnik, Wiley-VCH, 2003.

[36] H. Krupp, Particle adhesion. Theory and experiment, Adv. Colloid Interface Sci. 1 (1967) 111–139.

[37] T.C. Halsey, A.J. Levine, How Sandcastles Fall, Phys. Rev. Lett. 80 (1998) 3141.

[38] W. Kottler, H. Krupp, H. Rabenhorst, Adhesion of electrically chargde particles, Z. Abgew. Phys. 24 (1968) 219–223.

[39] H. Lowe, D. Lucas, The physics of electrostatic precipitation, Brit. J. Apply. Phys. 24 (1953) 540–547.

[40] G. Zebel, Coagulation of Aerosols, in: C.N. Davies (Ed.), Aerosol Sci., Academic Press, London/New York, 1966.

[41] A.C. Hoffmann, L.E. Stein, Gas Cyclones and Swirl Tubes - Principles, Design and Operation, Springer-Verlag Berlin Heidelberg, 2008.

[42] U. Muschelknautz, Zyklone zum Abscheiden fester Partikel aus Gasen, in: VDI (Ed.), VDI Wärmeatlas, 10th ed., Springer Berlin Heidelberg, Berlin, Heidelberg, 2010: p. Lcd 1–12.

[43] M. Trefz, Die verschiedenen Abscheidevorgänge im höher und hoch beladenen Gaszyklon unter besonderer Berücksichtigung der Sekundärströmung, VDI Fortschritt-Berichte. VDI Verlag. 3 (1988).

[44] J. Hejma, Einfluss der Turbulenz auf den Abscheidevorgang im Zyklon, Staub-Reinh. Luft. 31 (1971) 290–295.

[45]   S. Obermair, G. Staudinger, Einfluss der Feststoffaustragungsgeometrie auf die Abscheidung im Gaszyklon, Chemie Ing. Tech. 73 (2001) 203–207.

[46]   K. Schmidt, Physikalische Grundlagen und Prinzip des Drehströmungsentstaubers, Staub. 23 (1963) 491–501.

[47]   H. Klein, Entwicklung und Leistungsgrenzen des Drehströmungsentstaubers, Staub. 23 (1963) 501–509.

[48]   H. Klein, Drehströmungs-Entstaubungsverfahren, Wirkungsweise und Einsatz, Keram. Z. 11 (1968) 479–484.

[49]   K. Parker, Electrical Operation of Electrostatic Precipitators, IEE power , Institution of Engineering and Technology, London, 2007.

[50]   Whitehead, Dielectric phenomena - Electrical discharges in gases, part I: Experimental laws of corona, Ernest Benn Ltd., London, 1927.

[51]   W. Sproull, Corona quenching - Its significance in electrical in electrical precipitation, J. Air Pollut. Control Assoc. 13 (1963) 617–621.

[52]   M. Pauthenier, M. Moreau-Hanot, La charge des particules spheriques dans un champ ionise, J. Phys. 3 (1932) 590–613.

[53]   H. Rohmann, Methode zur Messung der Größe von Schwebeteilchen, Z. Phys. 17 (1923) 253.

[54]   H. White, Particle charging in electrostatic precipitation, AIEE Trans. 70 (1951) 1186–1191.

[55]   J. Böhm, Verzögerung der Aufladung von Teilchen in einem Elektrofilter, Staub-Reinh. Luft. 28 (1968) 270–273.

[56]   P. Arendt, H. Kallmann, Über den Mechanismus der Aufladung von Nebelteilchen, Z. Phys. (1926) 421–441.

[57]   R. Ladenburg, Elektrische Gasreinigung (Elektrofilter), in: A. Eucken, M. Jacob (Eds.), Der Chemie Ing., Akademische Verlagsgesellschaft., Leipzig, 1934.

[58]   N. Troost, A new approach to the theory and operation of electrostatic precipitators for use on pulverised-fuelfired boilers, Proc. IEE. 101 (1954) 369.

[59]   K. Darby, D. Heinrich, Konditionierung der Rauchgase von Kesselanlagen zur Verbesserung des Abscheidegrades von Elektrofiltern, Staub-Reinh. Luft. 26 (1966) 464–468.

[60]   K. Schrader, Verbesserung des Abscheidegrades von Elektroentstaubern durch SO3-Einblasung in die Rauchgase, Mitt. Vereinig. Großkesselbes. 48 (1968) 430–436.

[61]   H. Eishold, Der elektrische Staubwiderstand im Elektrofilter, Arch. Hüttenwes. 3 (1961) 221–224.

[62]   W. Deutsch, Bewegung und Ladung der Elektrizitätsträger im Zylinderkondensator, Ann. Phys. 68 (1922) 335–344.

[63]   D. Heinrich, Vergleichende Betrachtung über den Einfluß von Teilchengröße, Höhe des Abscheidegrades, Gasgeschwindigkeit und Leistungsaufnahme auf die Abscheidewirkung von Elektrofiltern, Staub. 23 (1963) 83–91.

[64]   A. Jaworek, T. Czech, E. Rajch, M. Lackowski, Laboratory studies of back discharge in fly ash, J. Electrostat. 64 (2006) 326–337.

[65]   T. Nussbaumer, A. Lauber, Formation mechanisms and physical properties of particles from wood combustion for design and operation of electrostatic precipitators, in: 18th Eur. Biomass Conf. Exhib., ETA-Florence, Lyon, 2010. http://www.researchgate.net/publication/229018338_Formation_mechanisms_and_physical_properties_of_particles_from_wood_combustion_for_design_and_operation_of_electrostatic_precipitators (accessed August 18, 2015).

[66]   S. Beer, Entwicklung und Test einer Elektrofilteranlage für kleine Biomasseheizkessel, Fachhochschule Amberg-Weiden, Amberg, 2004. http://www.oth-aw.de/fileadmin/user_upload/Professoren/Beer/Artikel_Banz_2004.pdf (accessed August 1, 2015).

[67]   R. Frey, Grundlagen der Staubabscheidung - Einfluss der Partikeleigenschaften, in: 9. Holzenergie-Symposium, Von Roll Umwelttechnik AG, Zürich, 2006: p. 35.

http://www.holzenergie-symposium.ch/Dokumente/Referate/05 Frey.pdf (accessed July 4, 2015).

[68] T. Nussbaumer, Stand der Technik und Kosten der Feinstaubabscheidung für automatische Holzfeuerungen von 100 kW bis 2 MW, Abteilung Luftreinhaltung des Kantons Thurgau, 2006. http://www.verenum.ch/Publikationen/TN_FSabscheider_2006_V2.pdf (accessed July 3, 2015).

[69] T. Nussbaumer, Feinstaub aus Holzfeuerungen, Verenum, Zürich, 2011. http://www.verenum.ch/Publikationen/TNHKGTFeinstaub.pdf (accessed July 3, 2015).

[70] J. Kozeny, Über kapillare Leitung des Wassers im Boden, in: Ber. Akad. Der Wissenschaften 136, Mathem. Naturwiss. Abt., Wien, 1929: pp. 271–360.

[71] P. Carman, Flow of gases through porous media, Butterworths, London, 1956.

[72] R. Sullivan, K. Hertel, The flow of air through porous media, J. Appl. Phys. 11 (1940) 761.

[73] I. Obernberger, T. Brunner, Zwischenbericht zum Projekt - Der rotierende Partikelabscheider als innovative Technologie zur Staubabscheidung in Biomassefeuerungen, BIOS-Bioenergiesysteme and Kohlbach AG, Graz, 1997.

[74] R. Brökeland, Technische Verfahren zur Staubabscheidung bei Festbrennstoffanlagen, in: Arbeitstagung "Technik Im Gartenbau," C.A.R.M.E.N., Rehburg-Loccum, 2002. http://www.carmen-ev.de/infothek/publikationen/140-untergeordnete-beitraege (accessed February 1, 2015).

[75] R. Von Turegg, Richtige und effiziente Staubabscheidung - Technologien und Potentiale, VDI Bericht 1319 - Thermische Biomassenutzung. Tagung Sal (1997) 167–198.

[76] J. Podliński, J. Dekowski, J. Mizeraczyk, D. Brocilo, K. Urashima, J.S. Chang, EHD flow in a wide electrode spacing spike-plate electrostatic precipitator under positive polarity, J. Electrostat. 64 (2006) 498–505. doi:10.1016/j.elstat.2005.10.004.

[77] S. Radl, Script to the lecture Particle Technology II, University of Technology Graz, Graz, 2014.

[78]   I. Obernberger, Stand und Entwicklung der Verbrennungstechnik, in: VDI Bericht 1319 - Thermische Biomassenutzung - Tech. Und Realis., VDI Verlag GmbH, Düsseldorf, 1997: pp. 47–80.

[79]   R. Miller, Kofil dust filtration - filter media, Slovenske Konjice, Slovenia, 2015. http://www.kofil.com/index.php?language=ang&s=dust2 (accessed April 2, 2015).

8 Appendix A – centrifugal dust separator

8.1 Typical dimensions of a centrifugal dust separator

Table 14: Dimensions of cyclones with a high separation performance[16]

Size	Flow rate		d_A	Single assembly			Mass	Multiple assembly			Mass
				h_1	e_1	h_5		h_1	e_1	h_5	
	[m³/s]	[m³/h]	[mm]	[mm]	[mm]	[mm]	[kg]	[mm]	[mm]	[mm]	[kg]
25	0.25	900	450	2395	340	280	100	2675	620	560	105
32	0.32	1152	500	2610	375	315	115	2925	690	630	120
40	0.40	1440	560	2860	415	355	175	3215	770	710	180
50	0.50	1800	630	3375	460	400	240	3725	810	750	250
63	0.63	2268	710	3705	510	450	285	4055	860	800	295
80	0.80	2880	800	4045	560	500	405	4395	910	850	415
100	1.00	3600	900	4745	620	560	555	5085	960	900	570
125	1.25	4500	1000	5175	690	630	665	-	-	-	-
160	1.6	5760	1120	5675	770	710	795	-	-	-	-

Size	a	b	d2	d3	d6	e2	e3	e4	e5	h2	h3	h4	h9
	[mm]	[mm]	[mm]	[mm]	[mm]	[mm]	[mm]	[mm]	[mm]	[mm]	[mm]	[mm]	[mm]
25	90	224	236	250		225	250	140	163	450	1120	1630	
32	100	250	265	280	500	250	280	160	183	500	1250	1810	485
40	112	280	300	315		280	315	180	206	560	1400	2020	
50	125	315	335	355		315	355	200	230	630	1600	2290	
63	140	355	375	400	710	355	400	225	258	710	1800	2570	685
80	160	400	425	450		400	450	250	293	800	2000	2860	
100	180	450	475	500		450	500	280	328	900	2240	3200	
125	200	500	530	560	1000	500	560	315	365	1000	2500	3560	985
160	224	560	600	630		560	630	355	412	1120	2800	3980	

Table 15: Dimensions of a cyclone pre-separator[16]

Size	Flow rate		h_4	h1	e1	h5	a	b	d2	d3
	[m³/s]	[m³/h]	[mm]	[mm]	[mm]	[mm]	[mm]	[mm]	[mm]	[mm]
100	1.00	3600	750	3670	590	530	180	450	450	500
125	1.25	4500	850	4040	660	600	200	500	500	560
160	1.60	5750	950	4615	730	670	224	560	560	630
200	2.00	7200	1060	5045	810	750	250	630	630	710
250	2.50	9000	1180	5770	910	850	280	710	710	800
315	3.15	11350	1320	6320	1010	950	315	800	800	900
400	4.00	14400	1500	7270	1120	1060	355	900	900	1000
500	5.00	18000	1700	7290	1240	1080	400	1000	1000	1120

Size	d6	e2	e3	e4	e5	h2	h3	h4	hg	Mass
	[mm]	[mm]	[mm]	[mm]	[mm]	[mm]	[mm]	[mm]	[mm]	[kg]
100	800	375	450	250	315	750	1600	2410	730	408
125	800	425	500	280	350	850	1800	2710	730	472
160	1000	475	560	315	392	950	2000	3010	935	601
200	1000	530	630	355	440	1060	2240	3360	935	718
250	1250	600	710	400	495	1180	2500	3740	1180	928
315	1250	670	800	450	550	1320	2800	4180	1180	1127
400	1600	750	900	500	628	1500	3150	4710	1500	1461
500	1600	850	1000	560	700	1700	3550	5310	1500	1787

9 Appendix B – Filter

9.1 Filter materials

Table 16: General fibre characteristics of Kofil filter media[79]

fibre generic term	density [g/m³]	cont. operating temp. [°C]	max short duration temp. [°C]	moisture regain [%]
polyester	1.38	150	160	0.4
acrylic (homopolymer)	1.15	125	140	1
meta aramid	1.38	180	200	4
polypropylene	0.91	90	100	0.1
PTFE	2.30	250	260	0
polyphenylene sulphide	1.37	190	230	0.6
polyimide	1.41	240	260	3

Table 17: Chemical resistance of Kofil filter media[79]

fibre generic term	Strong acids	weak acids	strong alkalis	weak alkalis	solved agents	hydrolysis	oxidation
polyester	+++	+++	+	++	+++	+	++++
acrylic (homopolymer)	+++	+++	+++	+++	+++	+++	+++
meta aramid	++	+++	+++	+++	+++	++	+++
polypropylene	++++	++++	++++	++++	++++	++++	+++
PTFE	++++	++++	++++	++++	++++	++++	++++
polyphenylene sulphide	+++	+++	++	++	+++	++++	+
polyimide	+++	+++	++	+++	+++	+++	++

10 Appendix C – Rotational particle separator

10.1 Experimental results for hardwood

Table 18: RPS results for hardwood[73]

wood chips (hardwood)		full load		partial load	
Date		07.05.97	15.05.97	07.05.97	07.05.97
fuel water content	[mass.% dry fuel]	21	23.5	25	25
energy output	[kW]	1451	1132	1048	961
combustion temp.	[°C]	957		932	868
flue gas temp. at RPS inlet	[°C]	270		225	208
flue gas velocity	[m/s]	11.64	10.7	7.01	6.3
O2-content at the wet flue gas	[Vol.%]	5.6	6.8	6.1	6.3
flue gas humidity	[Vol.%]	13.7	13.1	14.2	14.0
particle size distribution before the RPS					
	X_l	X_u		load	
	[µm]	[µm]	[mg/Nm³]	[mg/Nm³]	[mg/Nm³]	[mg/Nm³]
	8.000	16.000	0.00	0.00	1.39	1.39
	4.000	8.000	1.87	0.00	0.00	1.39
	2.000	4.000	0.00	1.99	1.39	0.00
	1.000	2.000	0.00	0.00	1.39	2.77
	0.500	1.000	1.87	0.00	1.39	2.77
	0.250	0.500	9.36	7.96	19.50	23.57
	0.125	0.250	44.94	47.76	52.93	52.69
	0.065	0.125	13.11	13.93	9.75	4.16
	total		71.16	71.64	87.76	88.75
dust past the RPS [mg/Nm³ dry flue gas, 13 Vol.% O2]		98.0	53.0	98.0	101.0

10.2 Experimental results for softwood

Table 19: RPS results for softwood[73]

wood chips (softwood)			full load		partial load	
date			11.04.97	25.04.97	29.04.97	29.04.97
fuel water content	[mass.% dry fuel]		20	40	50	50
energy output	[kW]		1244	815	550	400
combustion temp.	[°C]		825	676	638	605
flue gas temp. at RPS inlet	[°C]		250	236	185	140
flue gas velocity	[m/s]		13.76	12.2	6.75	4.57
O_2-content at the wet flue gas	[Vol.%]		5.8	8.8	8.0	7.7
flue gas humidity	[Vol.%]		13.3	14.9	18.7	19.1
particle size distribution before the RPS						
	X_l	X_u		Load		
	[µm]	[µm]	[mg/Nm³]	[mg/Nm³]	[mg/Nm³]	[mg/Nm³]
	8.000	16.000	1.10	1.47	0.00	0.00
	4.000	8.000	3.30	0.00	1.17	0.00
	2.000	4.000	0.00	1.47	0.00	0.00
	1.000	2.000	3.30	2.95	0.00	0.00
	0.500	1.000	3.30	0.00	1.17	0.00
	0.250	0.500	4.41	1.47	2.34	4.07
	0.125	0.250	20.93	16.22	18.72	9.77
	0.065	0.125	7.71	7.37	2.34	2.44
	total		44.06	30.96	25.74	16.28
dust past the RPS [mg/Nm³ dry flue gas, 13 Vol.% O2]			30.3	33.0	29.0	22.0